Doctoral thesis

USC
UNIVERSIDADE
DE SANTIAGO
DE COMPOSTELA

Structural characterization of recombinant mammalian prions

Alejandro Manuel Sevillano Mantas

Santiago de Compostela
2016

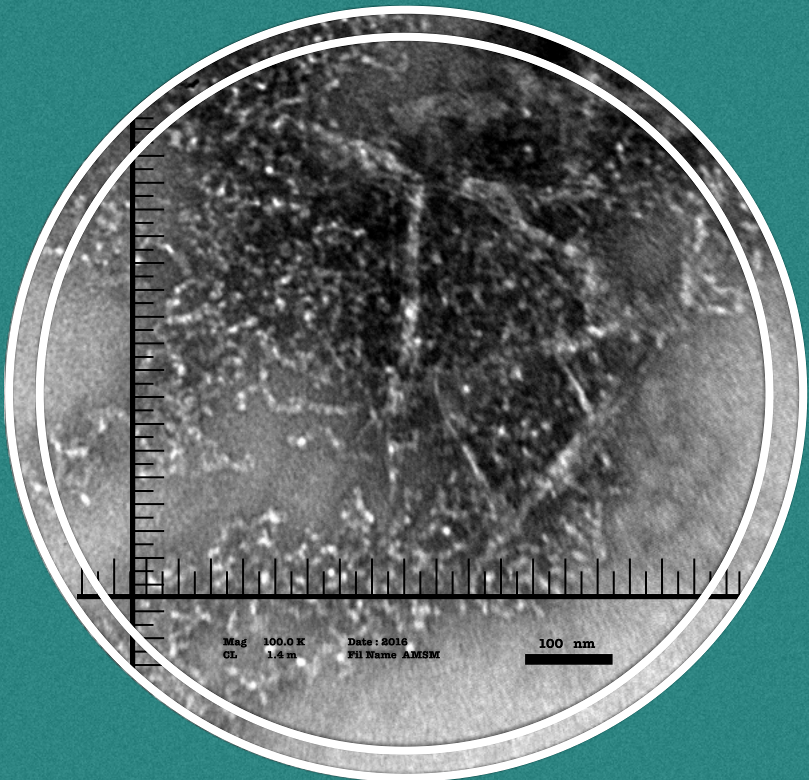

Universidad de Santiago de Compostela

Center for Research in Molecular Medicine and Chronic Disease (CiMUS)

Departamento de Medicina

Structural characterization of recombinant mammalian prions

Tesis Doctoral/ Doctoral Thesis
Director: Dr. Jesús Rodríguez Requena.

Alejandro Manuel Sevillano Mantas.

Santiago de Compostela, 2016.

CiMUS
Center for Research
in Molecular Medicine and
Chronic Diseases

USC
UNIVERSIDADE
DE SANTIAGO
DE COMPOSTELA

Center for Research in Molecular Medicine and Chronic Disease (CIMUS)

El Dr. Jesús Rodríguez Requena, Pofesor Contratado Doctor de la Universidad de Santiago de Compostela

CERTIFICA:

Que el presente trabajo titulado “Structural characterization of recombinant mammalian prions” presentado por D. Alejandro Manuel Sevillano Mantas, para optar al grado de Doctor por la Universidad de Santiago de Compostela, ha sido realizado bajo su dirección en el CIMUS y reúne los requisitos exigidos por la normativa vigente para ser valorada por la comisión correspondiente.

Y para que así conste a los efectos oportunos, se firma el presente documento.

En Santiago de Compostela, a 13 de Abril de 2016.

Fdo: Dr. Jesús Rodríguez Requena.

Alejandro Manuel Sevillano Mantas is the recipient of an Campus Vida pre-doctoral fellowship

This work has been carried out in CIMUS Biomedical Research Institute

Agradecimientos/ Acknowledgements

No puedo negar que esta sección aún siendo de las que más ganas tenía de escribir, es de las más difíciles, pues no quisiera olvidarme de ninguna persona que ha sido cómplice de esta experiencia que ya llega a su fin. Han sido más de 4 años de duro trabajo y que sin la ayuda de mucha gente, estoy convencido de que todavía seguiría a la deriva. Durante estos años he podido aprender, trabajar, compartir, reír, disfrutar, frustrarme, avanzar... en definitiva, he podido vivir una experiencia inolvidable rodeado de múltiples personas. Gracias a todos y os pido disculpas de antemano si me olvido de alguno.

En primer lugar me gustaría agradecer el apoyo institucional a la Universidad de Santiago de Compostela y más concretamente al Campus Vida por concederme la beca que me ha permitido realizar esta tesis doctoral. Gracias a ella, he podido formarme tanto profesional como personalmente.

En segundo lugar, a mi director de tesis, Jesús R. Requena no sólo por darme la oportunidad de realizar esta tesis doctoral, sino por su dirección, asesoramiento, consejos, ánimos e inagotable paciencia. Muchas gracias por enseñarme tantas cosas.

No puedo dejar sin mencionar a mis compañeros de laboratorio que marcaron mi inicio en esta andadura, gracias Ester y Adriana, marcasteis el camino a seguir. A mis compañeros que durante este tiempo estuvieron compartiendo conmigo las aventuras de laboratorio y alguna que otra cerveza; gracias Álex R, Shamim, Sofía, Keshav y Caterina por vuestra ayuda y apoyo tanto dentro como fuera del laboratorio. A los compañeros del SSL7, Irene, María y en especial a Isaac y Paula, por todos esos momentazos vividos juntos. A los compañeros que pasaron un corto periodo de tiempo, Neelam, Emma, Mateo, Isa y Carla, breve pero intensa fue vuestra visita, gracias chicos por vuestra ayuda. Con un especial cariño me gustaría agradecer tanto a Sonia, Carmen como a Daniela por el apoyo incondicional, ánimo, cariño y amistad que me habéis dado durante esta etapa. A la gente del CiMUS con la que he compartido tantas horas de conversaciones, risas y consejillos, Ruth, Mari, Shiara, Xoana, Esther, Lorena, Ester, Cris, Iñaki... Muchas gracias a todos por todos esos momentos compartidos.

No me puedo olvidar de toda la gente que trabaja entre bambalinas; personal de limpieza, personal de asuntos económicos, en especial a Mari Luz porque gracias a ella el mundo económico y burocrático se reduce al mínimo. A Bernardo, responsable del animalario, cuya ayuda y cobertura con los bichos ha sido crítica para la realización de esta tesis. A Susana y Raquel por su asesoría técnica y ayuda. En general muchas gracias a todos los que forman parte de los servicios comunes de la USC, CiMUS y IDIS cuya labor es imprescindible para el buen funcionamiento de todo.

Esta tesis no podría haberse realizado sin la experiencia bilbaína, por ello, me gustaría agradecer a Joaquín Castilla por haberme acogido en su laboratorio y por haberme hecho sentir como uno más en ese grupo de grandes personas que forman parte del PrionLab del CIC-BioGUNE. Nagore, Maite, Patricia, Jorge, Chafik, Vanessa y Hasier (gracias por hacerme un hueco como okupa en el famoso piso-patera) muchas gracias a todos. También me gustaría agradecer tanto a Saioa como a Natalia por el apoyo, ánimo y consejos tanto en lo personal como en lo laboral, durante y después de esa estancia.
Me gustaría también agradecer a todas aquellas personas con las que he colaborado estos años, gracias por vuestro ayuda y asesoramiento para la realización de este trabajo.
Muchas gracias a todos.

A un modo más personal me gustaría agradecer a todas aquellas personas que indirectamente me han ayudado a la culminación de esta etapa y que sin ellos seguramente hubiera sido más duro.

En este aspecto, quisiera agradecer a Carlos Fernández, Maestro y amigo. Gracias por acogerme en tu casa, hacerme participe y protagonista de ese proyecto personal tuyo llamado Taiki-do. Gracias a ello mi inicio y mi estancia en Santiago ha sido mucho más fácil desde que entré a formar parte de la familia Vitalia, donde no sólo encontré un espacio para entrenar sino que su filosofía de Escuela me caló desde raíz y donde pude conocer a otro gran Maestro, Marcial y a mis hermanos de armas Abel, Xan, Raúl, Pablo, Imir, Ghato, David, Dani, Casti, Noe, Neira, Javi, Oscar y un laaargo etc, sois fieros adversarios dentro del tatami y amigos incondicionales fuera de él.

Cómo olvidarme de la gente con la que compartí piso, Gael, Carol, Lupa, Sofía, muchas gracias por vuestra acogida y por vuestra amistad, me hicisteis sentir como en casa. Y qué decir de la gente de Rúa do Vilar, centro de largas conversaciones, risas, cumpleaños y cualquier evento deportivo-festivo, acompañados siempre con la mejor música "Mix-Moncho" que se pueda tener... gracias Ben, Moncho, Leo, Saleta, Carlos, Diego, Fonk, Fredo, Caro, Jose y a todos los que habéis estado a mi lado durante esta preciosa etapa.

A mis amigos y compañeros de Espeleología, Iago, Miguel, Rosi, Antón, Ana... por tan buenos momentos dentro y fuera de las cuevas.

A mis amigos del "Descansa" Peter, Ángel CJ., David, Dani, Kike, Ángel A., qué os voy a decir, lleváis a mi lado toda la vida, muchas gracias chicos por todo.

A mis amigos del Aries-Team, Pablo, Rober, Carlos y Jordi... no podía perder esta oportunidad para agradeceros todo lo que habéis hecho por mí.

A mi familia por su infinito apoyo, por haberme acompañado durante esta experiencia, por vuestras visitas, consejos, fuerzas, ánimos, cariño...Tíos, primos, primas, Josito, Martita (sois muchos para mencionaros uno a uno)... no hay palabras para expresar toda la gratitud que os debo, muchas gracias familia. En especial, me gustaría mencionar a dos pequeñajos que más me han extrañado durante estos años, a mis sobrinos María y Gonzalo, bella y bestia, nunca os cansáis de ver a vuestro "Tito" y de hacerle tan feliz. Gracias pequeñajos.

A una persona muy especial, que se ha convertido en parte indispensable durante la tesis. Gracias Laura, por estar a mi lado todos los días de estos últimos años, has compartido conmigo los mejores y menos buenos momentos (porque gracias a ti, nunca han habido malos, sino menos buenos), gracias por todo esa paciencia, consejos, alegrías y por toda la ilusión compartida conmigo para que este proyecto viera la luz, me has dado mucha fuerza, energía y un apoyo infinito. Muchas gracias peque. Como olvidarme de Fran, José, Carliños y Florinda, por esas risas,

buenos momentos, ayuda, cariño y por ese pollo con patatas que es fuente de mi devoción y que me ha servido para recargar las pilas más de una vez. Muchas gracias a todos por vuestro apoyo y ánimo. Lola (la perra más bonita del mundo), a ti te tengo que agradecer que has estado estos meses aguantándome como una campeona, tuviera el humor que tuviera, no has dejado de buscar que jugara contigo.

No quería terminar esta sección sin mencionar a las personas más importante de mi vida. A Mis padres... muchas gracias por vuestro ejemplo de lucha y perseverancia, por creer en mí y por ese aliento de ánimo que cada día me habéis dado. Gracias papá, por esos consejos que son voz de la experiencia. Gracias mamá, no has dejado que me rindiera, me has mantenido siempre con los pies en el suelo. Me gustaría deciros que sin vosotros no hubiese conseguido nada, todo lo que tengo y he conseguido es gracias a vosotros, no dejéis de luchar y de dar ejemplo.

A todos.

A mis padres

A mi familia

A Laura

...Decidí aprender hacerme yo la maleta para poder vivir... (Extremoduro)

...de te fabula narratur (Horacio)

Resumen

Caracterización estructural de los priones recombinantes de mamífero.

Las Encefalopatías Espongiformes Transmisibles (EETs), también conocidas como enfermedades priónicas, son un grupo de trastornos neurodegenerativos mortales que son causados por la forma patogénica de la proteína prion PrP^{C}, denominada PrP^{Sc}. Las enfermedades priónicas afectan a diferentes especies de mamíferos incluyendo el hombre y se caracterizan por una amplio rango de manifestaciones clínicas que comprenden ataxia, demencia, parasteis, paraplejia e insomnio. En la histopatología realizada en cerebros de animales afectados por priones se pueden observan; perdida neuronal, acumulación de agregados de PrP^{Sc}, espongiosis, vacuolación y astrogliosis.

La replicación de los priones se produce mediante la conversión de la proteína prion PrP^{C}, hacia su isoforma patogénica PrP^{Sc}. Aunque se conoce que este proceso se debe a una reorganización estructural post-traduccional, el mecanismo molecular que gobierna dicha reorganización es desconocido.

La estructura primaria de las proteínas PrP^{C} y PrP^{Sc} es idéntica. La secuencia primaria de la proteína PrP de ratón, proteína en la que se centra este trabajo, contiene 254 aminoácidos. Tras varias modificaciones post-traduccionales, la proteína PrP^{C} es anclada a la membrana plasmática de las células mediante la proteína de anclaje GPI (por su nombre en ingles; glycophosphatidilinositol) en forma de una proteína más corta de 209 aminoácidos (numerada como 23-231). Posee dos sitios de

N-glicosilación (N_{180} y N_{196}) y un enlace disulfuro entre las posiciones Cys_{178}-Cys_{213}. No se han observado diferencias covalentes entre PrP^C y PrP^{Sc}, la única diferencia entre ambas es conformacional, son isoformas. Ambas proteínas tienen un peso molecular de 33-35 KDa.

La proteína PrP^C, por su parte, es una proteína monomérica. Su solubilidad en medios acuosos ha permitido la aplicación de técnicas de alta resolución, como la Resonancia Magnética Nuclear y Cristalografía de rayos X, para su determinación estructural. La estructura tridimensional de la PrP^C, en grandes rasgos, contiene tres hélices-α, y dos hojas-ß cortas.

La reorganización estructural de la PrP^C hacia la isoforma patogénica PrP^{Sc}, conlleva la adquisición de nuevas propiedades físico-químicas. Estas nuevas propiedades, provocan que la PrP^{Sc} se encuentre en forma multimérica, bien formando estructuras organizadas en forma de fibras amiloides, o bien en forma de agregados amorfos. Su intratable insolubilidad en medios acuosos e incluso en algunos detergentes imposibilita la utilización de las técnicas de RMN y cristalografía de rayos X para su determinación estructural. Sin embargo, un amplio número de técnicas instrumentales han proporcionado una valiosa información sobre la estructura de la PrP^{Sc}. A diferencia de la PrP^C, la PrP^{Sc} es parcialmente resistente a la digestión de la enzima Proteinasa-K (PK). El uso de esta enzima ha permitido identificar el núcleo resistente de la PrP^{Sc}, que de un tamaño aproximado de 27-30 KDa (PrP27-30), mantiene la naturaleza infecciosa de la forma no digerida. Los estudios de espectroscopía infrarrojos de transformada de Fourier (FTIR) han mostrado que la estructura secundaria de la PrP^C se compone en gran medida por hélices-α, mientras que la estructura de la PrP^{Sc} se compone únicamente por hojas-ß y elementos no estructurados como giros, lazos o elementos desordenados. La microscopía electrónica se ha aplicado tanto para la observación de las fibras amiloides en extractos purificados de cerebros como en el estudio estructural de los cristales bidimensionales de PrP27-30 obtenidos a partir de cerebros de hámster Sirio infectados con PrP^{Sc}. También se han empleado estudios de espectrometría de masas acoplado al intercambio de hidrógeno/deuterio en el estudio de la estructura de la PrP^{Sc}.

La elucidación de la estructura de la PrP^{Sc} sigue siendo uno de los mayores retos de las investigaciones sobre priones. Las bases moleculares de la biología de la proteína priónica (PrP) como el mecanismo molecular de replicación y agregación, la barrera de especie y la patogénesis de la neurodegeneración, no serán entendidos hasta que la estructura esté resuelta.

A lo largo de los años, a raíz de la información obtenida en diversos estudios, han surgido numerosos modelos teóricos para la estructura de la PrP^{Sc}. Sin embargo, ninguno de ellos ha logrado recapitular todas las restricciones obtenidas por los diferentes datos experimentales, por lo que a día de hoy no hay un modelo único. La búsqueda de un modelo único que recoja todas las restricciones estructurales, sigue siendo uno de los mayores retos en las investigaciones de priones. Actualmente, los modelos más aceptados son; el modelo PIRIBS, acrónimo procedente de su nombre en inglés, Parallel In-Register ß-Sheet, sugiere que la fibras de PrP^{Sc} están formadas por un único protofilamento, en el que las moléculas de PrP^{Sc} se encuentran paralelamente apiladas en registro a lo largo del eje fibrilar. Los autores de este trabajo sugieren que en cada monómero el plegamiento de las hojas-ß se realiza de tal manera que ocupa una simple capa o piso dentro de la fibra amiloide de PrP^{Sc}. El modelo ß-solenoide, en contraposición con el modelo PIRIBS, conserva la idea de que cada fibra está constituida por dos 2 protofilamentos. Este modelo sugiere que cada molécula de PrP^{Sc} está constituida por el replegamiento de las hojas-ß adquiriendo una conformación de ß-solenoide de múltiples pisos. Cada monómero de PrP^{Sc} está superpuesto en registro, con el siguiente.

Teniendo en cuenta ambos modelos, una parte de este trabajo se ha centrado en aportar nuevas evidencias que puedan ayudar a consolidar uno de estos modelos para definir la estructura de la PrP^{Sc}.

Además del núcleo clásico de PrP^{Sc} resistente a PK (~90-230), la PrP^{Sc} tiene un núcleo interno resiste a PK que se expande entre las posiciones 152-230. Este núcleo interno resiste a la digestión de PK en un estado de desplegamiento parcial reversible inducido por guanidina. Basándonos en esto, es factible pensar que si las fibras de PrP^{Sc} están constituidas por monómeros cuya conformación es en forma de multi-pisos de láminas-ß, como sugiere el modelo ß-solenoide, el tratamiento con Gn/HCl y posterior incubación con PK, provocaría que las fibras amiloides de PrP^{Sc}, perdieran su organización fibrilar debido a la digestión de la mitad amino terminal ~90-151, ya que esta mitad actuaría como "base" en cada monómero desintegrado. Si por el contrario, las fibras de PrP^{Sc} están formadas por unidades planas, tal como sugiere el modelo PIRIBS y ocurre en las fibras amiloides de proteína PrP recombinante de hámster, el tratamiento de éstas con un guanidina y posterior incubación con PK conllevaría, de la misma manera que en el caso anterior, a la digestión de la mitad amino terminal ~90-150, sin embargo, la estructura fibrilar permanecería intacta. Para comprobar esta hipótesis, la proteína nativa PrP^{Sc} carente de GPI (GPI-anchorless PrP^{Sc}) se trató con diferentes concentraciones de Gn/HCl con el fin de conocer qué concentración conduce a un desplegamiento parcial de PrP^{Sc}. Tras obtener dicha concentración, las muestras incubadas con Gn/HCl, se trataron con PK con el fin de obtener el núcleo interno resiste a PK. Las imágenes obtenidas mediante TEM han mostrado que dicho tratamiento conlleva a que las fibras de PrP^{Sc} se desarmen, mientras que la proteína recombinante PrP, cuya mitad N-terminal es más flexible que la mitad C-terminal y por tanto más accesible a la digestión con PK, mantiene su arquitectura fibrilar original tras digerir con PK. Este resultado no demuestra que la proteína nativa PrP^{Sc} posee una estructura tipo solenoide, pero sí demuestra que la estructura descrita por el modelo PIRIBS no puede ser aplicada a proteína PrP^{Sc} derivada de cerebro.

Por ello, este estudio aporta una novedosa información que puede servir para elegir el modelo ß-solenoide como el modelo más plausible para representar la estructura de PrP^{Sc}.

A pesar de que el material PrP nativo resulta el más idóneo para el estudio estructural, la ausencia de un método que genere una purificación 100% homogénea, así como la imposibilidad de usar en este material en las técnicas de RMN y cristalografía de rayos X, ha provocado el auge de la utilización de material recombinante, mucho más versátil y cuya producción y purificación es relativamente más sencilla. La generación de la proteína recombinante PrP conlleva un amplio abanico de posibilidades a la hora de usar un gran número de técnicas para el estudio de PrP^{Sc} con mayor resolución. La posibilidad de marcar los residuos con material isotópico, permite la identificación de éstos mediante RMN. La sustitución de ciertos aminoácidos permite estudiar la implicación de éstos en diferentes procesos que atienden a la naturaleza de la PrP^{Sc}. No obstante, para un apropiado uso de las proteínas recombinantes, es necesario que adquieran la naturaleza priónica de la PrP^{Sc}.

En la literatura, se han descrito diversos trabajos referentes a la obtención de proteínas recPrP que adquieren la naturaleza priónica de la PrP^{Sc}, sin embargo no muchos lo han logrado. En un primer lugar, el resultado de la simple incubación de la proteína recPrP con un homogeneizado de cerebro procedente de hámster infectados, generaron una proteína recPrP mal plegada que recapituló algunas de las características de la PrP^{Sc}, como resistencia a PK, formación de agregados e insolubilidad. Sin embargo, los altos tiempos de incubación observados en los animales inoculados con recPrP mal plegado, acompañado de la falta de signos de enfermedad priónica, indican que este tipo de proteína carecía de infectividad, característica esencial de la naturaleza del prion PrP^{Sc}.
El siguiente intento de generar material recombinante infeccioso consistió en la modificación química de las condiciones de incubación de recPrP con PrP^{Sc}. El conjunto de proteínas recPrP mal plegadas, surgidas en ese estudio fueron inoculadas en animales que sobre-expresan altas tasas de PrP^{C}. A pesar de que se observaron signos de enfermedad, presumiblemente priónica, los altos tiempos de incubación de estos inóculos generaron la duda de si estos signos fueron debidos a la característica infecciosa del material recPrP o bien por la alta tasa de sobre-expresión de PrP^{C}, tal como se observaba en otros animales que sobre-expresan PrP^{C}.
A lo largo de la década del 2000, se llevó a cabo una serie de estudios que propiciaron la aparición uno de los mayores hitos en la obtención de material infeccioso generado *in vitro*. Los autores de este estudio, consiguieron mediante la incubación de PrP^{C} y PrP^{Sc} procedente de homogeneizados de cerebro y durante diversos ciclos de sonicación, una proteína mal plegada que recapitulaba la naturaleza priónica de la proteína nativa PrP^{Sc}. Este material generado *in vitro* mediante la técnica

llamada PMCA (por su nombre en inglés: Protein Misfolding Cycling Amplification), compartía propiedades bioquímicas e infecciosas con la PrP^{Sc} derivada de cerebro. El periodo de incubación observado en animales inoculados con este material, era similar al observado en animales inoculados con el prion silvestre, de igual manera, el material obtenido *in vitro* compartía con el material derivado de cerebro, su resistencia a la digestión con PK y capacidad de formación de agregados. Esto permitió establecer a la técnica PMCA como una técnica pionera en la generación de priones *in vitro*. Una vez consagrada esta técnica para generar priones *in vitro*, surgieron una serie de estudios con el fin de elucidar qué elementos básicos son requeridos para la conversión de la PrP a la forma patogénica PrP^{Sc}. En este aspecto, uno de los hitos más importantes en la investigación de priones, fue el desarrollo de una nueva versión de la PMCA. En esta nueva versión, se estableció que las moléculas de RNA y el lípido sintético POPG actúan como cofactores esenciales de la conversión *de novo* de la proteína recombinante de ratón $recPrP_{23\text{-}230}$. La proteína $recPrP^{Sc}$ surgida de varios ciclos de sonicación, recapituló las características nativas del prion nativo.

Teniendo en cuenta este hallazgo, la otra parte de este trabajo se centra en el estudio de las características estructurales de la $recPrP^{Sc}$. Para ello, se expresó la proteína recombinante de ratón $recPrP_{23\text{-}230}$. Una vez purificada y replegada en columna, la proteína $recPrP_{23\text{-}230}$ se sometió a la conversión hacía su forma malplegada, usando el sistema de recPMCA descrito para la obtención de la $recPrP^{Sc}$. Para confirmar que las $recPrP_{23\text{-}230}$ adquiridas tras la reacción de recPMCA poseen la infectividad propia del prion nativo PrP^{Sc}, se realizó un bioensayo en el que se inoculó con dicho material a animales transgénicos denominados tga20. Tras comprobar que uno de los inóculos generó el desarrollo de la enfermedad priónica en estos animales, éstos se sacrificaron para posteriormente proceder a la extracción del cerebro con el fin de realizar el análisis histopatológico y bioquímico. En la histopatología realizada a estos cerebros, se pudo encontrar los marcadores típicos de enfermadas priónicas. A su vez y de forma paralela, los cerebros se analizaron por WB con el fin de identificar la presencia de PrP PK-res (PrP resiste a la digestión de PK). Primero, se realizó un homogeneizado de cerebro que posteriormente se incubó con PK. Los resultados de WB confirmaron la presencia de PrP PK-res.

Una vez comprobado la naturaleza priónica de la recPrP^{Sc}, se procedió su caracterización estructural. Para ello, basándonos en el estudio realizado previamente de la proteína silvestre GPI-anchorless PrP^{Sc} se eligió como técnica analítica la espectrometría de masas de los péptidos surgidos de la proteólisis limitada.

La proteólisis limitada es una técnica muy útil para elucidar características estructurales de la PrP^{Sc}. Consiste en grandes rasgos en limitar la acción proteolítica de las enzimas proteasas con el fin de conocer los parámetros conformaciones característico, como la exposición de los aminoácidos a la superficie, flexibilidad e interacciones locales. Los enlaces peptídicos dentro de las hojas-ß son resistentes a la digestión proteolítica, mientras que los enlaces peptídicos localizados dentro lazos o giros pueden ser cortados. Por lo tanto esta técnica proporciona información exhaustiva del enlace peptídico con respecto al plegamiento de la proteína, permitiendo localizar las áreas más flexibles y las posibles hojas-ß.

En la literatura hay numerosos estudios que utilizan la proteólisis limitada para averiguar información sobre la proteína priónica, PrP^{Sc}. El tratamiento con la enzima no específica PK muestra que la PrP^{C} es complementare sensible a la proteólisis y que la PrP^{Sc} es parcialmente resistente, produciendo un núcleo resistente a PK de peso molecular 27-30 y que como se ha mencionado con anterioridad, mantiene la infectividad de su forma no-digerida. La longitud de este núcleo depende de la especie de la PrP, para el caso del ratón; ~90-231. Por tanto, se puede concluir que la PrP^{Sc} está constituida por dos dominios: El domino N-terminal, lábil y desestructurado, fácilmente digerida por la PK y un dominio globular C-terminal organizado, que según se ha podido establecer está únicamente constituido por hojas-ß unidas entre sí por elementos no estructurados como lazos o giros, que son escindidos por la PK. Otros estudios utilizando esta técnica han demostrado la existencia de una fracción de PrP, sensible a la digestión con PK, llamada $sPrP^{Sc}$. Esta fracción, también infecciosa, comparte muchas características básicas estructurales con la PrP PK-res. Otros estudios basados en la proteólisis limitada de PrP^{Sc}, han mostrado que diferentes cepas de priones poseen una resistencia a PK ligeramente diferente. Por ello se ha sugerido la existencia de una arquitectura básica entre las diferentes las cepas con matices diferenciales.

Por otro lado, en los estudios que anteceden a los experimentos realizados en esta tesis, se demostró la utilidad de combinar proteólisis limitada y espectrometría de masas (MS) para obtener de información estructural sobre PrP^{Sc} de hámster y de ratón. En ambos estudios se llegó a la conclusión de que el dominio C-terminal está formado por hebras-ß, intercaladas con tramos no estructurados como lazos o giros, sensibles a PK.

Más concretamente el estudio realizado sobre la PrP^{Sc} de ratón; GPI-anchorless PrP^{Sc} ha mostrado un mapa de susceptibilidad a PK que engloba a las regiones 116-118, 133-134, 141, 152-153, 162, 169 y 179, sugiere que estas regiones corresponden lazos y giros, mientras que los cortes en las posiciones 81, 85 y 89 señalan la frontera entre los dominio C-terminales estructurados y el N-terminal desestructurado de la PrP^{Sc}. Este mapa de susceptibilidad a PK, por tanto, permite la identificación de tramos de hebras-ß con constituyen la columna vertebral "cross-ß" de la PrP^{Sc}.

Siguiendo con las mismas bases para los estudios de la PrP^{Sc} de hámster y ratón, se procedió al estudio de las características estructurales de la $recPrP^{Sc}$ mediante el uso de la proteólisis limitada acoplada a MS. Para ello, la $recPrP^{Sc}$ tras ser digerida con PK en condiciones limitantes, fue sometida al análisis por electroforesis en geles de tricina-SDS, que permite resolver los péptidos de menor tamaño, con una mayor resolución que con el uso de geles convencionales de glicina-SDS. Con el objetivo de tener una visión global, los péptidos surgidos de la digestión con PK fueron teñidos con la tinción Sypro-Ruby, que permite la detección de péptidos con mayor sensibilidad que el hasta ahora usado, Azul de Coomassie. Se pudo observar diversas bandas que comprendan un peso molecular entre ~16 KDa hasta 3,5 KDa. El análisis por MS, permitió conocer la masa de los péptidos surgidos. En primer lugar, la muestra digerida con PK, fue analizada por ESI-TOF, técnica que proporciona una elevada exactitud de las masas. Se observaron tres picos cuyas masas exactas son: 9513; 9399 y 8184, que corresponden con los péptidos N_{152}-S_{230}; M_{153}-S_{230} y Y_{162}-S_{230} respectivamente. Sin embargo, los péptidos menos abundantes no se pudieron observar debido a la alta concentración de Gn/HCl empleada y la dificultada de eliminar dicho agente caotrópico sin perder cantidad de muestra. Como alternativa, la muestras digerida con PK se analizó por MALDI-TOF, donde se pudieran identificar múltiples picos de masas 13428, 11859, 11380, 10985, 10514, 9504, 9393, 8179, 6092, 3655, 3048 KDa que coinciden con las bandas correspondientes a los péptidos resistentes a PK, identificadas con el uso de tres anticuerpos tras la inmuno-transferencia. El tamaño de estos fragmentos resistentes corresponden a cortes en las posiciones 116, 134, 138, 141, 145, 152, 153, 162, 179, 201, 206 expandiéndose hasta la posición 230. Los resultados obtenidos en este estudio coinciden con las áreas susceptibles a la digestión con PK encontradas en la GPI-anchorless PrP^{Sc}; 116, 134, 141, 152, 153, 162 y 179, además se pudo observar varios puntos de corte adicionales, que se encuentran dentro de las zonas no estructuradas, lazos o giros, definidas en GPI-acnhorless PrP^{Sc}; 138, 145, o bien definen una nueva zona no estructurada centrada en el extremo carboxi-terminal, dichos puntos de corte son: 201, 206. Adicionalmente se han identificados picos de masas 9510, 8658, 6525, 2482 que corresponden a fragmentos doblemente truncados 96-178, 103-178, 91-151 y 134-178 respectivamente.

El estudio de proteólisis limitada fue ampliado con el estudio de tratamiento de $recPrP^{Sc}$ con PK a tiempos crecientes de incubación, en el que se observa un decrecimiento de intensidad en algunas de las bandas, mientras que otra permanece constante. Esto indica por un lado, que la banda mayoritaria y más resistente a PK es la correspondiente a 152/153-230 y por otro, que los fragmentos procedentes de la digestión de PK no provienen de diferentes subpoblaciones de $recPrP^{Sc}$, sino que por el contrario, son generados por el corte en zonas más sensibles de una $recPrP^{Sc}$ de mayor longitud (sin digerir).

En resumen, este estudio muestra que el $recPrP^{Sc}$ infeccioso, generado por recPMCA, exhibe propiedades bioquímicas que sugieren que su arquitectura es similar a la PrP^{Sc} derivada de cerebro. Además, aunque con algunos matices, parece que la rec PrP^{Sc} posee una mezcla de propiedades estructurales de las cepas de PrP^{Sc} "clásicas" y "atípicas". Este prometedor resultado sugiere la idea de que la $recPrP^{Sc}$ es un buen modelo de la PrP^{Sc} de cerebro y puede ser usado como un herramienta excelente para estudios estructurales futuros, como por ejemplo en el uso de RMN.

Para concluir, el trabajo aquí presentado, se centra en el estudio estructural de la proteína PrP^{Sc}. Por un lado, usando como fuente de estudio la proteína derivada de cerebro, PrP^{Sc} sin GPI, se ha aportado una novedosa información que puede ayudar a la elección de uno de los modelos representantes de la estructura de la PrP^{Sc}. Por otro lado, se ha generado la proteína recombinante PrP^{Sc} como fuente de estudio estructural. La información obtenida sugiere que tanto la $recPrP^{Sc}$ como la PrP^{Sc} sin GPI, comparten una arquitectura similar, por lo que la $recPrP^{Sc}$ podría convertirse en un buen modelo para futuros estudios de PrP^{Sc}.

Summary

Structural characterization of recombinant mammalian prions

Prion Diseases or Transmissible Spongiform Encephalopathies, are a group of deadly neurodegenerative disorders that are caused by the pathogenic protein PrP^{Sc}. The prion diseases that affect humans are Kuru, Creutzfeldt-Jakob Disease (CJD), Gerstmann-Sträussler-Scheinker Syndrome (GSS) and Fatal Familiar Insomnia (FFI). Prion Diseases are not exclusive to human, other species are very susceptible to develop this fatal neurodegenerative disorder; scrapie that affects sheep and goats, the Transmissible Mink Encephalopathy (TME) that was observed in wild mink as well as in farm animal, the Chronic Waste Disease (CWD) that also affect wild and farm cervids, like elk or deer, the Feline Spongiform Encephalopathy (FSE) that affects domestic cats or zoo animals and the Bovine Spongiform Encephalopathy, also known as mad cow, responsible of the epidemic farm disaster that affected thousands of cattle in the UK and whole Europe during the 80's and 90's.

The central event of the prion diseases is the conformational conversion of the PrP^{C} into the pathogenic isoform PrP^{Sc}. The molecular mechanism of the prion replication, molecular basis of the prion biology, the species barrier and the pathogenesis of the neurodegeneration will not be understood until the structure of the

PrP^{Sc} is solved. Because of that, elucidating the structure of the PrP^{Sc} is one major challenge in the prion research.

Nowadays, two proposed models have been highlighted for the structure of the PrP^{Sc}. The PIRIBS model suggests that PrP^{Sc} amyloid fibers are made by a single protofilament where each monomer is parallel in register stacked along the fibrillar axes and argues that PrP^{Sc} monomers are flat, with rPrP amyloid-like β-strand rich cores extending up to position ~90. In contrast, the ß-solenoid model suggest that each single PrP^{Sc} is formed by the folded of ß-strands in 4-rungs ß-solenoid architecture. In contrast to the PIRIBS model, the ß-soleonoid model argues that the fibers are made by two intertwined protofilament.

The classical PK core of the PrP^{Sc}, that span from ~90 to C-terminus, has been reported in plenty of studies. Besides this classical core, the PrP^{Sc} has an inner PK-resistant core that span from ~152-230. This inner "super-resistant" core resists partial, reversible unfolding induced by guanidine. Based on that, it is feasible to think that if PrP^{Sc} is formed by multi-layer of ß-strands, PK-treatment of partially unfolded PrP^{Sc} fibers should necessarily result in their complete disassembly, as the N-terminal "base" of each monomer disintegrates. In contrast, if PrP^{Sc} monomers are flat, fibers would persist after such treatment, as seen when rPrP fibers are treated with PK under conditions that preserve their C-terminal ß-strands rich core, which remain stacked.

In this work, the brain derived GPI-anchorless PrP^{Sc} fibers, were treated with increased concentration of Gn/HCl until partial unfold. After guanidine partial unfolding treatment, fibers were digested with PK to destroy the N-terminal half. After guanidine treatment and PK digestion, the resulted PK resistants PrP^{Sc} were analyzed by western blotting and visualized by negative stain TEM.

The results obtained show virtually complete disassembly of partially unfolded PrP^{Sc} fibers after PK treatment, whereas the rPrP remained its fibrillar architecture. These results support a multi-rung, rather than flat, architecture of the PrP^{Sc} monomers.

Since the development of a method that allows the generation of prions *in vitro*, some studies that have been focused on the understanding of molecular conversion mechanism of PrP^{C} to PrP^{Sc}, go through the use of synthetic PrP^{C}, in which the introduction of all kind of modifications can help to explain the molecular mechanism that governs the conversion into the PrP^{Sc}. In this context, one of the most important events in the prion field was the development of a recPMCA, where the production of the recombinant amyloid generated under sonication cycles recapitulates the nature of wild type prions.

The second goal of this work is to generate a $recPrP^{Sc}$ that recapitulates the nature of the PrP^{Sc} and to use this synthetic prion for structural studies. For that purpose, the recombinant mouse PrP23-230 was bacterially expressed and then purified using a HisTrap Column. During the purification, the immobilized protein was refolded and then eluted using a gradient of imidazole. The refolded recPrP23-230 was collected in different fractions and subsequently, each fraction was submitted to conversion into the misfolded $recPrP^{Sc}$ form by several rounds of recPMCA. Due to the fact that the misfolded recPrP shows different infectivity rates (non infectious or infectious), to verify the infectivity of the misfolded forms obtained after recPMCA, a bioassay was performed using a set of transgenic mice. Mice were inoculated with different misfolded PrP_{23-230}. Only one of the misfolded PrP_{23-230} generated by recPMCA resulted infectious in all the mice inoculated. This recPrP^{Sc} was used for structural studies.

Substantial evidence suggests that PrP^{Sc} is a 4-rung β-solenoid, and that individual PrP^{Sc} subunits stack to form amyloid fibers. Recently, limited proteolysis was used to map the β-strands and connecting loops that conform the PrP^{Sc} solenoid. Using high resolution SDS-PAGE followed by epitope mapping and mass spectrometry, it was possible to identify positions ~116/118, 133-134, 141, 152-153, 162, 169 and 179 (murine numbering) as Proteinase K (PK) cleavage sites in PrP^{Sc}. Such sites define loops and/or borders of β-strands, and help to define the threading of the β-solenoid.

This approach was extended to recombinant PrP^{Sc} obtained by recPMCA. Limited proteolysis in combination with the MS analysis, allowed the identification of several PK-resistant peptides. The ESI-TOF analysis identified the peaks with the masses: 9513; 9399 y 8184 correspond to the peptides N_{152}-S_{230}; M_{153}-S_{230} y Y_{162}-S_{230}. Alternatively, MALDI-TOF analysis identified peaks with the masses 13428, 11859, 11380, 10985, 10514, 9504, 9393, 8179, 6092, 3655, 3048 KDa, that correspond to cleavages of the PK at 116, 134, 138, 141, 145, 152, 153, 162, 179, 201, 206. The results obtained in this study are in agreement with the susceptible sites, previously described in the GPI-anchorless PrP^{Sc}, 116, 134, 141, 152, 153, 162 y 179, that are placed within unstructured sequences with the additional nicks at 201, 206, that might describe a new loop located at the end of the C-terminal domain. Furthermore, there were observed additional peaks with the masses; 9510, 8658, 6525, 2482 that correspond to the doubly-truncated fragments 96-178, 103-178, 91-151 y 134-178.

In summary, this study shows that the infectious recPrP^{Sc} generated *in vitro* by the recPMCA, exhibits biochemical properties that suggest that the architecture of recPrP^{Sc} is similar to that brain-derived PrP^{Sc}. These promising results suggest that the $recPrP^{Sc}$ is a good model for the brain-derived PrP^{Sc} and can be a very good tool for structural studies.

Resumo

Caracterización estrutural de prións recombinantes en mamíferos.

As enfermidades causadas por prións ou Encefalopatías Esponxiformes Transmisibles son un grupo de desordes neurodexenerativos mortais, causados pola proteína patóxena PrP^{Sc}. As enfermidades causadas por prións en humanos son o Kuru, a enfermidade de Creutzfeldt-Jacob (CJD), o síndrome de Gersmann-Sträussler-Scheinker (GSS) e o Insomnio Familiar Fatal (FFI). Estas enfermidade priónicas non son exclusivas en humanos, xa que outras especies son moi susceptibles de desenvolver estes trastornos. Así, aparece o *scrapie* en ovellas e cabras, a Encefalopatía Transmisible das Martas (TME), que foi observada tanto nas martas salvaxes como en animais criados en granxas, a Enfermidade Crónica Debilitante (CWD), que afecta a cérvidos, como alces ou cervos, a Encefalopatía Esponxiforme Felina (FSE), que dáse nos gatos domésticos e tamén nos zoolóxicos, e a Encefalopatía Esponxiforme Bovina, coñecida como o mal das vacas tolas, responsable das epidemias que afectaron a milleiros de reses gandeiras no Reino Unido nas décadas dos 80 e 90.

O proceso fundamental das enfermidades causadas por prións e o cambio conformacional da proteína normal PrP^{C} cara a forma patóxena PrP^{Sc}. Nin o mecanismo molecular de replicación do prión, nin as bases biolóxicas da molécula, e tampouco as especies afectadas e a súa dexeneración neurolóxica serán resoltos completamente ata que a

estrutura da PrP^{Sc} sexa revelada. Por esta razón, dilucidar a estrutura da PrP^{Sc} preséntase coma o maior reto na investigacións en prións.

Na actualidade, hai dous modelos propostos para PrP^{Sc}. O primeiro modelo, PIRIBS, suxire que as fibras do PrP^{Sc} están formadas por un único protofilamento, no que as moléculas de PrP^{Sc} atópanse paralelas ó longo dun eixo fibrilar, e o pregamento das follas-ß ocupa unha única capa dentro da fibra amiloide de PrP^{Sc}. No modelo ß-solenoide, en cada molécula de PrP^{Sc} as follas- ß préganse formando un ß-solenoide de 4 pisos. Así, neste modelo as moléculas apílanse unhas por riba das outras, e, en contraposición ó suxerido polo modelo PIRIBS, as fibras do PrP^{Sc}, están formadas por dous protofilamentos que se entrecruzan.

Ademais do núcleo clásico de PrP^{Sc}, resistente a PK (~90-230), hai outro núcleo, interno, que se expande entre as posicións ~152-230, e resiste a dixestión de PK nun estado de despregamento parcial reversible inducido pola guanidina. Baseándonos nesto, é posible pensar que si as fibras de PrP^{Sc} están constituídas por monómeros cuxa conformación é de folla- ß, o tratamento con PK provocaría a perda da organización fibrilar pola dixestión da metade n-terminal, xa que esta metade actuaría como base en cada monómero desintegrado. Caso contrario, se as fibras están formadas por unidades planas, como suxire o modelo PIRIBS, o tratamento con guanidina e posterior incubación con PK, deixaría a estrutura fibrilar intacta.

No presente traballo, a proteína GPI-anchorless PrP^{Sc} tratouse con diferentes concentracións de Gn/HCl, para coñecer cando se produce un despregamento parcial, e a continuación se trataron con PK, para dixerir a metade n-terminal. Os resultados foron analizados pola técnica de western-blott e visualizados nun TEM.

As imaxes obtidas mostran que tras o tratamento descrito anteriormente, as fibras PrP^{Sc} desármanse, polo que o modelo PIRIBS non se adecúa os resultados.

Desde que se desenvolveu o método que permite a xeración de prións por cultivo *in vitro,* algúns estudos que se centraron no coñecemento dos mecanismos de conversión de PrP^{Sc}, fixérono a través de PrP^{C} sintéticos, nos cales a introdución de todo tipo de modificacións axudaron a explicar o mecanismo molecular que goberna o cambio cara o PrP^{Sc}. Neste contexto, unha das achegas máis importante no campo de estudo de prións foi o desenvolvemento dun recPMCA, mediante ciclos de sonicación dende tipos salvaxes de prións.

O segundo fito na investigación priónica, e a xeración de $recPrP^{Sc}$ que recolle as características das PrP^{Sc} e o uso destes prións sintéticos para estudos estruturais. Para levalo a cabo, comprobouse a expresión en ratos de $PrP_{23\text{-}230}$, purificado usando unha columna HisTrap. Durante a purificación, a proteína foi tratada cun gradiente de imidazol. A molécula $recPrP_{23\text{-}230}$ foi recollida en diferentes fraccións e cada fracción presentada para a conversión a $recPrP^{Sc}$ en varios ciclos de recPMCA. Debido ó feito de que $recPrP^{Sc}$ mostre diferentes rangos infecciosos (dende non infectivo a infectivo), para verificar a infectividade das formas obtidas, foi realizado un bioensaio usando ratos transxénicos. Estes ratos foron inoculados con $PrP_{23\text{-}230}$ diferentes, e so unha destas moléculas resultou infectiva en todos os ratos inoculados. Foi esta molécula a usada para os estudos estruturais posteriores.

Hai evidencias substanciais que suxiren que esta PrP^{Sc} correspondese cunha conformación solenoide, e as distintas subunidades dispóñense en fibras amiloides. Mediante o uso de SDS-PAGE de alta resolución, seguido dun mapeo e unha espectometría de masas, foi posible identificar as rexións 116/118, 133-134, 141, 152-153, 162, 169 and 179 do PrP^{Sc}. como sitios susceptibles a PK. Parece ser que estas zonas en concreto correspóndense con lazos e xiros, e axudan a definir o trazado do solenoide.

Estes resultados estendéronse os PrP^{Sc} obtidos mediante recPCMA, mediante o uso dunha proteólise limitada acoplada a MS, para proceder á identificación dos péptidos que se obteñen da dixestión de PK. A posterior análise ESI-TOF deu tres picos de masas: 9513; 9399 e 8184 KDa, que corresponden cos péptidos N_{152}-S_{230}; M_{153}-S_{230} e Y_{162}-S_{230} respectivamente. Na análise por MALDI-TOF, os picos foron múltiples: 13428, 11859, 11380, 10985, 10514, 9504, 9393, 8179, 6092, 3655, 3048 KDa, que coinciden con cortes nas posicións posicións 116, 134, 138, 141, 145, 152, 153, 162, 179, 201, 206. Estes datos coinciden coas áreas susceptibles á dixestión con PK definidos coa GPI-acnhorless PrP^{Sc} 116, 134, 141, 152, 153, 162 y 179, e definen unha nova zona de corte nos puntos 201, 206, centrada no extremo c-terminal. Adicionalmente, identificáronse novos picos de masas a 9510, 8658, 6525, 2482, correspondentes a fragmentos dobremente truncados 96-178, 103-178, 91-151 y 134-178 respectivamente.

Resumindo, este estudo mostra que o $recPrP^{Sc}$ infeccioso, xerado por recPMCA, exhibe propiedades bioquímicas que suxiren unha arquitectura similar á PrP^{Sc} do cerebro. Este prometedor resultado propón a idea de que $recPrP^{Sc}$ é un bo modelo da PrP^{Sc} do cerebro e unha extraordinaria ferramenta para estudos estruturais futuros.

Table of contents

Chapter 1

Introduction

The Transmissible Spongiform Encephalopathies (TSE), also known as Prion Diseases, are a group of deadly neurodegenerative disorders that are caused by the pathogenic form of the prion protein PrP, termed PrP^{Sc}. The prion diseases that affect humans are Kuru, Creutzfeldt-Jakob Disease (CJD), Gerstmann-Sträussler-Scheinker Syndrome (GSS) and Fatal Familiar Insomnia (FFI). The Prion diseases are not exclusive to humans many other species are very susceptible to develop this fatal neurodegenerative disorder; scrapie affects sheep and goats, the Transmissible Mink Encephalopathy (TME) was observed in wild mink as well as in farm animals, the Chronic Wasting Disease (CWD) also affects wild and farm cervids, like elk or moose, the Feline Spongiform Encephalopathy (FSE) affects domestic cats or zoo animals and the Bovine Spongiform Encephalopathy, also known as "mad cow disease", responsible for the epidemic farm disaster that affected thousands of cattle in the United Kingdom and in the whole of Europe during the 80's and 90's. The molecular mechanism by which the host-encoded cellular prion protein PrP^{C} is converted into the aberrant isoform PrP^{Sc} is still unknown. This rearrangement leads to the accumulation of aggregates of the misfolded PrP^{Sc} conformers in the brain.This molecular mechanism governs the self-perpetuating process by which the PrP^{Sc} recruits and templates the PrP^{C} misfolding into a new PrP^{Sc} molecule and results in the central event in the prion diseases. The TSE have a broad range of clinical manifestations like ataxia, dementia, paresthesia, paraplegia, insomnia or abnormal behavior. The histopathology observed in the brain of the sick animals is characterized by the finding of astrocytic gliosis, widespread arthropathy, neuronal loss, vacuolation, spongiform change and PrP amyloid accumulation (Figure 1.1).

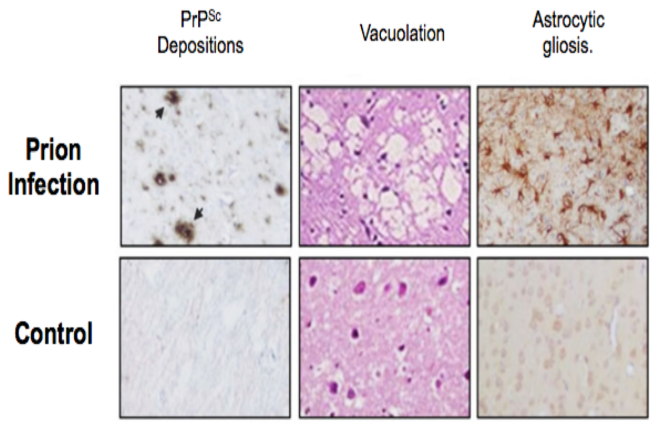

Figure 1.1. Abnormalities observed in the brain of the affected individuals of TSE. Accumulation of PrP^{Sc} deposits wasdetermined by anti-PrP antibodies. Hematoxylin and eosin staining are used to evaluate the vacuolation. Astrogliosis is detected by the use of anti-GFAP antibodies. (Figure adapted from Soto and Satani) (1)

The first steps to characterize the scrapie agent.

The infectious nature of the scrapie was first recognized in 1935 in an experimental procedure that consisted in the intraocular inoculation in a healthy ewe with the spinal cord from an infected ewe. The discovery of the fact that this agent could be transmitted between individuals of the same species relighted the interest of the contemporary researchers for the unusual properties of this agent and consequently several studies arose to elucidate its etiology.

In 1954, Sigurdsson introduced the concept of the “slow virus” in a attempt to explain the large incubation time that the infected animals took to develop the clinical signs of scrapie (2). However, the lack of inflammatory response -a common feature in all virus infectivity- and the remarkable resistance to virus inactivation were used as an argument against the hypothesis that the agent responsible for scrapie was a slow virus (3, 4).

Up till that moment, it was thought that infectivity was due to the existence of an organism that harbored nucleic acid (NA). However, a new infectivity concept emerged from the hypothesis of Griffith who suggested that the infectious agent of the scrapie could be a protein (5). In the earlier years of the 80's, the first morphological evidence of this agent was described by Merz and colleagues, who obseverded particles with a rod morphology which led them to suggest that the scrapie agent might be a “slow-virus”, they described this agent as filamentous virus (6). On the other hand, given the number of evidences showing that the scrapie agent contained a protein that was required for the infectivity, Stanley Prusiner proposed the term Prion (Proteinaceous Infectious Particle) to distinguish this small particle that lacks nucleic acid and causes TSE from the viruses, plasmid or viroids (7). One year later from the Merz studies, Prusiner and colleagues purified the PK-resistant fragment of the PrP^{Sc}, the PrP27-30 (named for its molecular weight). The authors observed that this PK-resistant peptide shared morphological features with those virus-like filaments observed by Merz (6) after visualization by Electron Microscopy (EM) (8). According to the morphology observed the authors named these fibers as prion rods and furthermore, the authors suggested that this prion rods might be amyloid (8) (Figure 1.2).

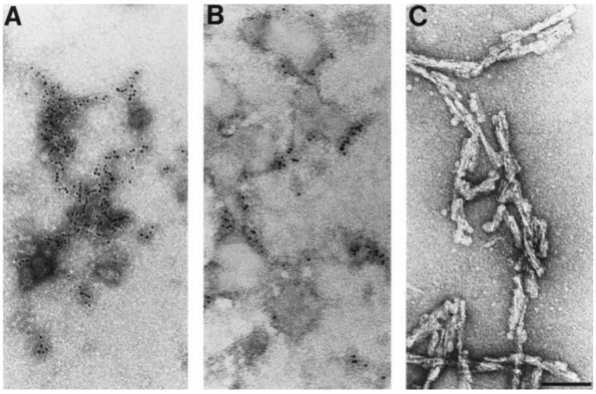

Figure 1.2. Transmission Electron Microscopy of prion proteins after negative staining and inmunogold-lageling. A) PrP^{C}. **B)** PrP^{Sc}. **C)** Prion rods composed by the PK-resistant PrP27-30. (Bar 100 nm.) Image adapted from Prusiner *et al.* (8)

The PrP27-30 purification near to homogenization allowed the NH_2-terminal amino acid sequences were determined by the Edman degradation. These milestones led to the identification of the PrP-cDNA clones from hamster and mouse PrP and allowed Weismann and collaborators to establish that PrP is encoded by a chromosome gene (PRNP) that is expressed in the brain of healthy animals (9-11). Furthermore, the unchanged levels of mRNA observed in the course of the scrapie infection led to the identification of the host protein PrP^{C}, a protein with 33-35 KDa (9, 11).

The cellular prion protein, PrP^{C}

The PRNP gene is located in the short arm of the chromosome 20 and encodes the prion protein or PrP, a protein composed of approximately 254 amino acids. PrP is synthesized in the rough endoplasmic reticulum and is transported to the cell surface through the Golgi apparatus. During its biosynthesis, PrP is subjected to several kinds of post-translational modifications. Proteolytic cleavage at position 22 (mouse PrP numbering) leads to the removal of the 22 amino acids located at the N-terminus. Another kind of modification is the N-glycosylation at the Asn-180 and Asn-186. Consequently, the PrP results in three bands after electrophoretical separation on SDS-PAGE, correspond to the variable non-, mono-, and di-glycosylation forms of PrP. Finally, the prion protein is attached to the cell surface by the glycophosphatidyl inositol moiety (GPI) that replaces the 23 C-terminal amino acids. All these modifications define the final PrP^C protein, with a molecular weight of around 33-35 KDa (209 amino acids) depending on the glycosylation state (Figure 1.3A).

The PrP^C structure has been solved by the means of NMR and the X-ray crystallography (12, 13) and mainly contains a flexible disordered N-terminal tail that spans from the residues 23 to 124. Five copies of the same amino acids sequence named octarepeats (OR); PHGGGWGQ, are located within this sequence. The central region of the PrP^C is formed by a globular domain that is spanning from the amino acid 124 to 228, where two cysteines are located at 178 and 213, forming a single disulphide bond. Finally, the C-terminal domain (229-231) is an unstructured region that is attached to the cell membrane by the GPI-anchor (Figure 1.3B).

Defining the PrP^C function/s might help to understand the TSEs. However, the structural characterization of the PrP^C the physiological function of PrP^C is still unclear. Over the last few years, several studies have tried to elucidate several processes attending to the nature of the PrP^C.

A recent study demonstrated that the OR binds with cooper and other divalent cations such as zinc or nickel, forming a complex that is associated with metal homeostasis or several other functions like neuroprotection against either apoptosis or oxidative stress (14). Although there are several pieces of evidence related to the importance of the PrP^{C}-metal complex formation, its funtion is still unclear.

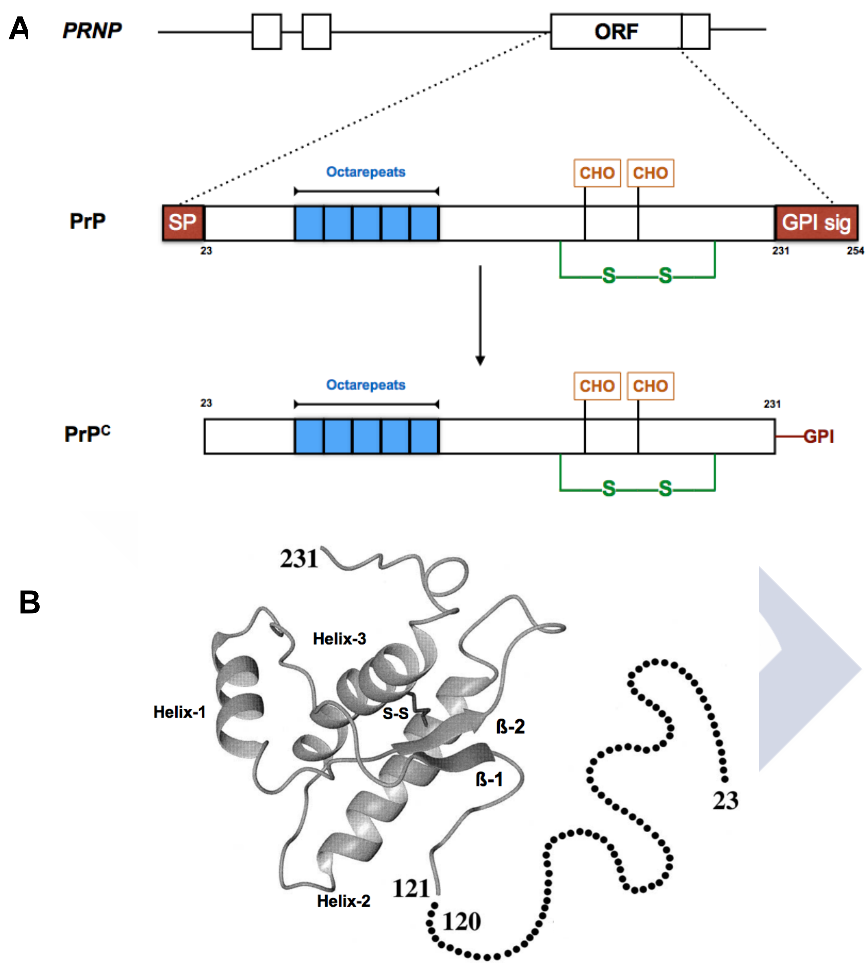

Figure 1.3. **The prion protein A)** The *Prnp* ORF encodes a protein of 254 residues, which during its biosynthesis is shortened to 209. Primary sequence of the PrP and the prion protein PrP^{C}. **B)** Mouse PrP^{C} (23-231) structure based on the NMR restraints. The globular domain (124-228) contains three α-helices (144-154; 172-193; 200-227) and two stranded anti-parallel ß-sheets (129-131; 161-163). The disulphide bond (S-S) joining the Helix-1 and Helix-3 is represented by a black line. The 23-120 N-terminal segment represented by dots is unstructured (12).

Moreover, several functions that the PrP^{C} can execute were proposed, which encompass a broad range of physiological processes like growth and neuron differentiation (15), synaptic plasticity (16, 17) and cell signaling (18, 19) as well as its function as NMDA receptor modulator (20) and myelin maintenance (21).

The PrP^{C} is converted into the pathogenic form PrP^{Sc} by structural rearrangement

The central event of the prion diseases is the conformational conversion of the PrP^{C} into the pathogenic isoform PrP^{Sc}. Elucidating the molecular mechanism that governs this structural transformation is the essential event of the prion diseases. Whereas the polypeptide chains of the prion protein PrP^{C} and the prion PrP^{Sc} are identical, their secondary structure is different. Experimental procedures based on the Circular Dichroism (CD) and Fourier Transition Infrared (FTIR) showed that the PrP^{C} is formed by 40% α-helix and a little amount of ß-sheets, while the PrP^{Sc} contain substantially more ß-sheet structure. Results were erroneously interpreted to suggest that PrP^{Sc} was formed by 30% of α-helix and more than 40% of ß-sheets and disordered elements (22-24). However, a recent reassessment of the FTIR spectra, the data at 1660 cm^{-1} attributed to α- helices was reinterpreted when the same signal was obtained in a recPrP sample that is completely devoid of α-helices.

This rearrangement allows the PrP^{Sc} to acquire new features, mainly characterized by the formation of large aggregates, insolubility and resistance to proteinase K digestion. This mechanism must involve a template process whereby the pre-existing molecules of PrP^{Sc} direct the refolding of PrP^{C} into a nascent PrP^{Sc} with the same conformation of the earlier PrP^{Sc}. This concept in which the structural conformation changes, supports the "protein only" hypothesis postulated to explain that the unique agent responsible for the prion diseases is PrP^{Sc} (25).

Although the prion replication comes about by the self-perpetuating through PrP^{C} conversion, the precise mechanism is still unknown.

According to the "protein-only" hypothesis, the PrP^{C} conversion into PrP^{Sc} must go through the interaction of PrP^{C} and PrP^{Sc}, through the formation of a PrP^{C}/PrP^{Sc} complex and consequently, through somehow the final PrP^{Sc} conformation. There are two proposed models to explain how the final PrP^{Sc} conformation is conformed (Figure 1.4).

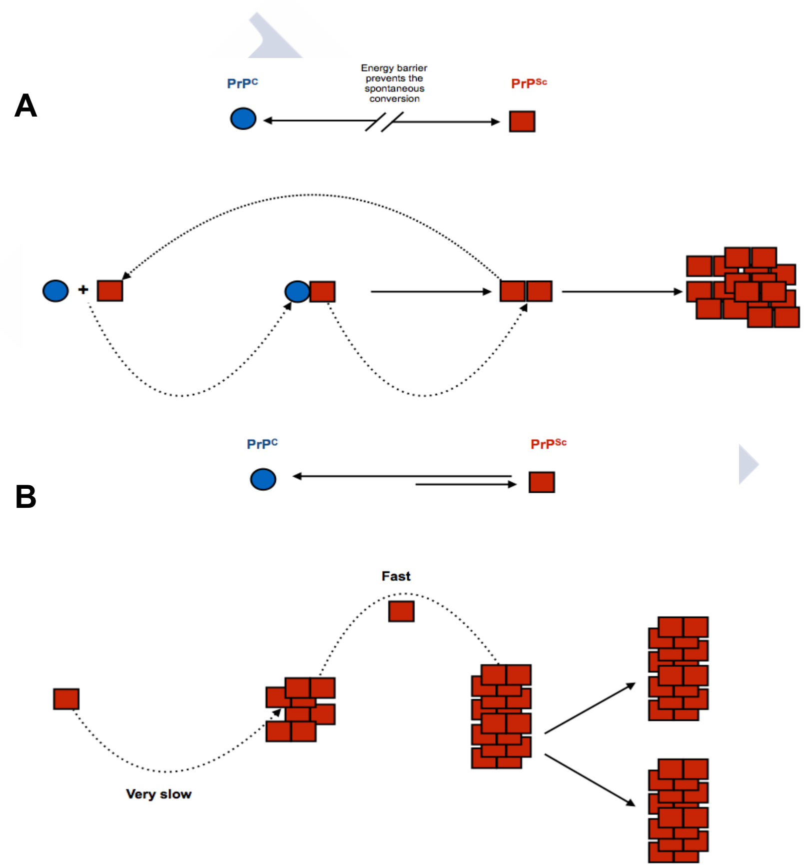

Figure 1.4. Proposed mechanisms for the PrP^{C} conversion to PrP^{Sc}. A) Template-directed model. **B)** Seeded nucleation model.

-***Template-directed refolding model***: It postulates that the PrP^{C} spontaneous conversion into PrP^{Sc} is prevented by a high-energy barrier. In the case of prion infection, the molecules of PrP^{Sc} interact with the PrP^{C}, forming the complex PrP^{C}/PrP^{Sc}. The PrP^{Sc} acts as template for the conversion PrP^{C} and subsequently forms the homodimer PrP^{Sc}/PrP^{Sc} (26) (Figure 1.4A).

-***Seeded nucleation model***. Molecules of PrP^{C} exist in a thermodynamic equilibrium with the PrP^{Sc} molecules. In the case of a healthy individual, the equilibrium would be displaced to the PrP^{C} conformation, causing the monomers of the PrP^{Sc} to be less stable. However, in the disease state, the PrP^{Sc} conformation promotes the formation of high-ordered aggregates of the PrP^{Sc}, which stabilize the PrP^{Sc} conformation and then the equilibrium shifts to the PrP^{Sc} formation (26) (Figure 1.4B).

Both models are theoretical plausible, and both could explain the conformational transformation that takes place in the infected host. However, the ability of the prions to infect one host in particular and not any other is determined by the transmission barrier. Two models have arisen over the last years in order to explain some features of the transmissible PrP^{Sc} state (Figure 1.5).

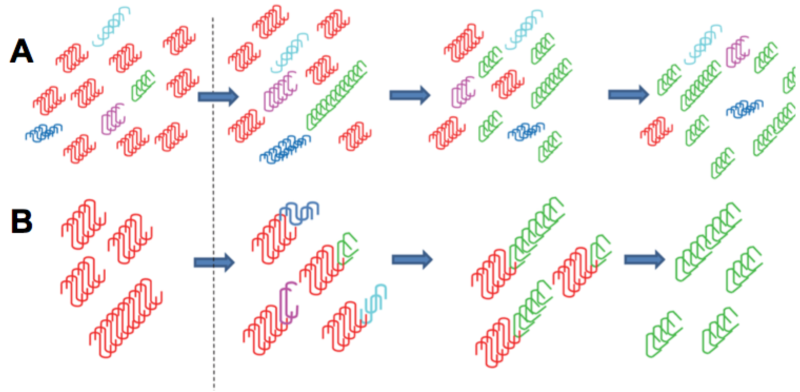

Figure 1.5. Schematic representation of the two alternative hypotheses on prion replication. A) The "cloud" hypothesis proposes that the prion strain consist in an heterogenous pool on PrP^{Sc} isoforms or variants where exists a major (red) or minor (various color) variants. Changes in the replication environment might provide selective advantages for a minor variant leading to transformation of the PrP^{Sc} population. **B)** The deformed templating model postulates that the diverse structural variant are generated as a result of changes in replication environment via numerous PrP^{Sc}-dependent trial-and-error seeding events. A newly generated variant that fits better that parent PrP^{Sc} to the altered environment replaces the original PrP^{Sc} variant. Figure adapted from Makarava *et al*. (27).

-*The cloud hypothesis*. It postulates the existence of a heterogeneous pool formed by individuals of PrP^{Sc}. The PrP^{Sc} molecule whose structure fits best with the host PrP^{C}, receives selective advantages to replicate. This notion implicates that the prion strains exhibit conformational plasticity and are subject to transformation when exposed to new replication environments (27) (Figure 1.5A).

-*Deformed templating.* It postulates that the changes in the replication environment play an important role, imposing a selective pressure in the generation of new PrP^{Sc} variants. Even if the PrP^{Sc} template does not correspond/fit to the host PrP^{C}, it can seed new PrP^{Sc} variants via deformed template. Whereas under these environments the new PrP^{Sc} variant might not be effective in replicating, a variant could fit well with new environments. Therefore, the changes in the replication environment force the conformational diversity of the PrP^{Sc} pool and select the best-fit variant for that environment (27) (Figure 1.5B).

Whatever mechanism governs the PrP^{C} conversion into PrP^{Sc}, this new aberrant conformation implies the acquisition of new physiological properties. The PrP^{Sc} conversion is followed by the aggregation of the monomers in different areas of the brain and each form of TSE manifestation is characterized by neuropathology changes, including vacuolation, astrocytic gliosis and PrP deposition (Table 1-I).

The Transmissible Spongiform Encephalopathies.

In animals, the first case of TSE was described in the 18th century. The English shepherds observed that the imported Merino Spanish Sheep were affected by any agent that produced abnormal behavior in their sheep, characterized by excessive licking, altered gait and intense compulsive scrape against the fences (28). This complaint was named as scrapie by the shepherds and it is also known by some other names; *tembladera* (Spanish) *la tremblante* (French), *traberkrankheit* (German) or *rida* (Icelandic) (29).

Unfortunately, other species are very susceptible to develop this fatal neurodegenerative disorder; the Transmissible Mink Encephalopathy (TME) was observed in wild mink as well as in farm animals, the Chronic Waste Disease (CWD) also affects wild and farm cervids like elk or moose (30), the Feline Spongiform Encephalopathy (FSE) affects domestic cats (31) and the Bovine Spongiform Encephalopathy (BSE) (32), also known as mad cow, responsible for the epidemic farm disaster that affected thousands of cattle in the UK and the whole of Europe during the 80's and 90's.

Table 1-I. Prion diseases of humans and animals (modified from Colby DW *et al.* (36)

Disease	Host	Mechanism of Pathogenesis
Kuru	Humans (Fore people)	infection through ritualistic cannabalism
Iatrogenic CJD	humans	infection from prion-contaminated HGH, medical equipment, etc.
Varian CDJ	humans	infection from bovine prions
Familial CJD	humans	germine mutation in the PRNP gene
GSS	humans	germine mutation in the PRNP gene
FFI	humans	germine mutation in the PRNP gene
Sporadic CJD	humans	somatic mutation or spontaneous conversion of PrP^C to PrP^{Sc}
sFI	humans	somatic mutation or spontaneous conversion of PrP^C to PrP^{Sc}
Scrapie	sheep	infection
BSE	cattle	infection or sporadic
TME	mink	infection with prions from sheep or cattle
CWD	deer, elk	infection
FSE	cats	infection with prion-contaminated bovine tissues or MBM
Exotic ungulate encephalopathy	greater, kudu, nyala, oryx	infection with prion-contaminated MBM

CJD: Creutzfeldt-Jakob Disease. GSS: Gerstmann-Sträussler-Scheinker. FFI: Fatal Familia Insomnia. BSE: Bovine Spongiform Encephalopathy. TME: Transmissible Mink Encephalopathy. CWD: Chronic Wasting Disease. FSE: Feline Spongiform Encephalopathy. HGH: Human growth hormone; MBM: Meat and Bone Meal.(38)

The first TSE in humans was described in 1920 by the neurologists Hans G. Creutzfeldt and Alfons Maria Jakob (33, 34). The authors described this disease as a neurological disorder of unknown etiology. Later this disease was coined as Creutzfeldt-Jakob Disease in honor of their discovery. The prion disease in humans may occur in three different ways: sporadic, sCJD, which represents the 85% of the CJD diseases. Inherited, iCJD: these kinds of diseases are due to some pathogenic mutation in the PRNP gene. Transmissible or variant CJD (vCJD) are caused by the external prion transmission, like iatrogenic or food contamination. Other known TSEs that affect humans are: Kuru, discovered by Gajduseck and Zigas, associated with a cannibal ritual in Papua New Guinea (35). The Gerstmann-Sträussler-Scheinker (GSS) syndrome, described for the first time in 1989, (36) characterized by an early age development (30-60 years old) and a slow progression (3-10 years). The Fatal Familial Insomnia (FFI) where the main clinical features include intractable insomnia, psychiatric symptoms and abnormal night sleep behavior, unsteady gait, difficulty swallow and sudden death (37).

All kind of TSE manifestations could be characterized by the type of signs, histopathology or the biochemistry properties of PrP^{Sc} (Table 1-I).

Defining the infectious agent, PrP^{Sc}.

As already stated, PrP^{Sc} is the pathogenic isoform of the host prion protein PrP^{C}. There are no differences in the primary structure between PrP^{Sc} and PrP^{C}. Rather, the central event of the pathogenesis on prion diseases is the conformational conversion of the PrP^{C} into PrP^{Sc}. This structural rearrangement provides the PrP^{Sc} with new chemical and physical properties. The insolubility of the PrP^{Sc} allowed the purification of the fibers/rods providing the first direct identification of the agent causing TSE (25). After the purification of either the full length (~33 KDa) or the proteinase K (PK) resistant fragment (27-30 KDa) were observed under EM (Figure 1.2). The prion rods of PrP27-30 observed share similar features with amyloids, as indicated by birefringence after Congo red staining.

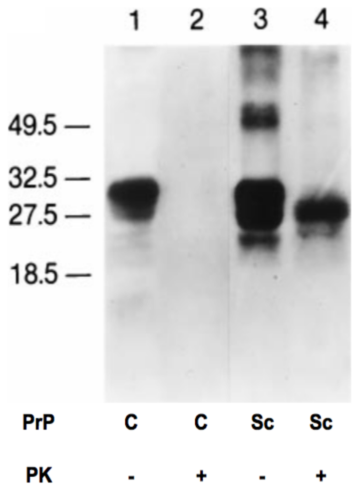

Figure 1.6. Immunoblotting of the Syriam Hamstar brain homogenates from uninfected (lanes 1-2) and prion-infected (lanes 3-4). Lanes 2 and 4 show the migration of the product from the digestion with 50µg/ml of PK. Lanes 1 and 3 were used as proteolytic digestion control. While the western blot of the hamster infected with prions showed a band PK-resistant around 27-30 KDa, no bands were observed in the western blotting from uninfected hamster. The decrease on the Molecular Weight observed in lane 4 indicated that around 67 amino acids were digested form the NH_2-teminus of the PrP^{Sc} to generate the PrP27-30. Adapted from Prusiner 1998 (25)

PrP^{Sc} is resistant to the PK digestion. The high resistance of PrP^{Sc} is correlated with the high tendency to form aggregates. Whereas the PrP^{Sc} migration in the SDS-PAGE covers a broad band of around 33-35 KDa (the non-, mono- and di-glycosilated states). PrP^{Sc} after PK digestion covers a broad band that corresponds to the PrP 27-30 KDa, indicating the existence of a truncated form of PrP^{Sc} (Figure 1.6). This truncated form retains the infectivity of the full length PrP^{Sc}, indicating that the core of the infectivity belongs to this truncated form.

Structural insight on the architecture of PrP^{Sc}.

Since the structural rearrangement of the α-helices PrP^{C} into the ß-sheet PrP^{Sc} form is considered as the central event in the infection, pathogenesis and transmissibility in the TSE diseases, resolving the structure of PrP^{Sc} is essential for elucidating this mechanism.

While the recombinant PrP, which mimics the structure of the native PrP^{C}, has been solved by NMR and crystallography (12, 13), the structure of PrP^{Sc} is poorly understood.

The heterogeneity, insolubility, even in mild detergents, and the propensity to form larger aggregates, are three intractable features that limit the use of high-resolution techniques like NMR and X-ray crystallography. Despite this limitation, a large number of indirect techniques have been used for elucidating the structure of PrP^{Sc}. Despite using this kind of techniques, a large number of experimental data could be obtained, which allowed to propose different models as well, but none of these proposed models can accommodate all of the experimental constraints (39).

Techniques applied to elucidate the structure of PrP^{Sc}

Fiber Diffraction.

One of the earliest techniques that provided substantial pieces of evidence regarding the overall fold of the amyloid fibers was the X-Ray fiber diffraction (40). Using this method, the structural information is determined based on the radiation when the sample is bombarded by X-ray. The resulting diffraction patterns indicate that some structural features are present in the fiber.

The earliest studies with X-ray fiber diffraction on the structure of PrP^{Sc} confirmed the amyloid nature of the prion rods (41). The meridional diffraction at 4,8 Å indicates the typical cross-ß structure corresponding with the distance between ß-sheet in which the hydrogen bonds run parallel to the fiber axis.

More recently, a new diffraction pattern was observed. In MoPrP 27-30 X-Ray fiber diffraction are shown several meridional reflections at 4,8; 6,4; 9,6 and 19,2 Å, (Figure 1.7). The reflection at 4,8 Å indicates the distance between of ß-sheets observed in previous studies (41), furthermore, the others were interpreted by the authors as a second, third and four repeats of the signal 4,8 Å among the fibers axes. The authors suggested that the final 19,2 Å reflection might be attributed to the the 4 ß-stranded sheets of the single molecule of PrP^{Sc} (42). In addition to this, the recPrP amyloid fibers present only a single 4,8 Å plus an equatorial reflection at 10 Å, indicating that the ß-strands are coiled/folded in a width of 10 Å. The authors suggest that the

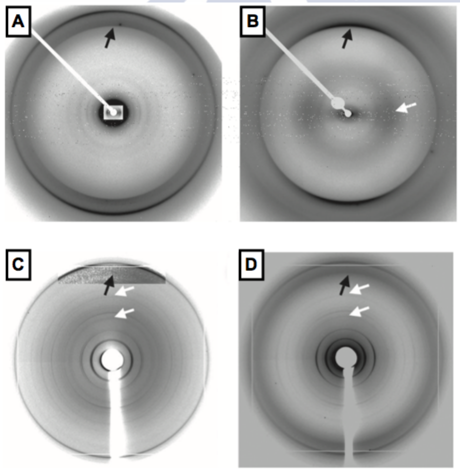

Figure 1.7. Fiber diffraction patterns of SHaPrP27-230, recSHaPrP(20-231), MoPrP27-30 and recMoPrP (89-230). The cross-ß meridional diffraction at 4,8 Å is indicated by black arrows. **A)** Diffraction from the SHaPrP27-30. **B)** recSHaPrP (90-231) shows a broad equatorial diffraction at 10,5 Å indicated by white arrow absent in SHaPrP(27-30). **C)** MoPrP27-30 (RML strain) shows a second and third orders of meridional diffraction, indicated by white arrow. These higher orders are
also observed in the synthetic prion strain, MoSP1, derived from recMoPrP (89-230) amyloid, passed twice thought Tg9949 mice. **(D).**(Images adapted from Wille *et al.* (42).

recPrP amyloid fibers are formed by single ß-stranded flats that are parallel stacked along the fiber axes separated by 4,8 Å.

Electron and atomic Force Microscopy.

The nanometer resolution that provides the Atomic Force Microscopy (AFM) and the Electron Microscopy (EM) allows the observation of many fiber characterizations, including morphology, fiber organization, twists, fiber length and width. For that reason, AFM and EM are applied in several amyloid studies. Sim and colleagues observed that the morphology of the PrP27-30 fibers from different prion strains were similar (43). Furthermore, they also observed that these fibers extended around 100-150 nm in length and were apparently formed by two intertwined protofilaments with a width of around 4-5 nm per protofilaments (Figure 1.8).

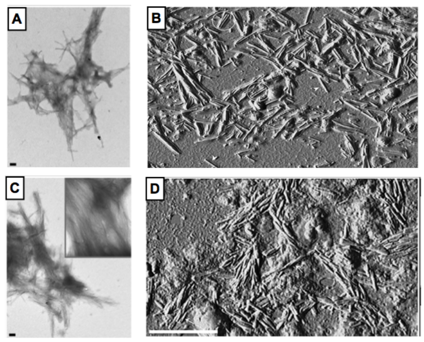

Figure 1.8. **TEM and AFM images of the prion strains 22L and RML**. The amyloid plaques formed by anchorless 22L are observed either TEM after negative staining **(A)** or by AFM **(B**). The RML anchorless fibers are also observed by negative-staining TEM **(C)** or by AFM **(D)**. The scale bar is 100 nm for TEM images and 20 nm for AFM images. Figure adapted from Sim *et al.* (43)

The PrP^{Sc} aggregates tend to polymerize in a fibrillar organization. However, that is not the exclusive organization of the PrP^{Sc} aggregates. The amorphous aggregates surrounded the PrP27-30, resulted in the formation of 2D crystal of PrP27-30 and provided a new source for the PrP^{Sc} structure study (Figure 1.9) (44). Using electron microscopy-based analysis of two-dimensional crystal of PrP27-30 Wille *et al*. discovered that some 2D crystal showing a hexagonal lattice. Through labelling with a special nano gold derivative, the authors were able to localize the periphery of the crystal subunit (Figure 1.9). Based on the findings observed in the 2D crystal of the PrP27-30 the authors concluded that to fit in a hexagonal lattice, the PrP27-30 must to be formed by parallel ß-helix. conformation.

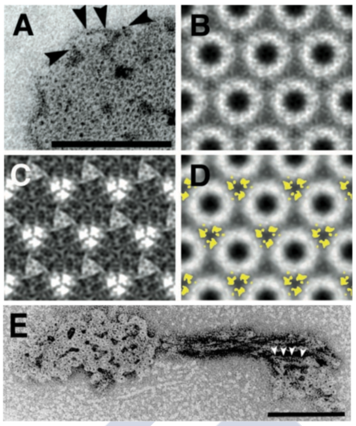

Figure 1.9. Electron microscopy images from the 2D crystals of Pr27-30. **(A)** 2D crystal of PrP27-30 stained with uranyl acetate showing tan apparent hexagonal lattice**.** **(B)** High view of a crystal after contrast transfer function and correlation-mapping and avaraging. **(C)** Substation map between unlabelled and labelled with nano gold (labelling the N-linked sugar) crystals, showing differences in lighter shades. **(D)** Projection map of the PrP27-30 with the sugar labelled outside /yellow). **(E)** Typical rod with an aggregate of crystal subutins at each end (44)

Fourier Transform Infrared Spectrometry (FTIR) and Circular Dichroism (CD).

FTIR and CD are spectroscopy techniques that provide information about the secondary structure, indicating the relative amount of α-helices and ß-strands or unstructured structures that define the protein under analysis.

FTIR and CD have been used to study the structural characterization of PrP27-30 for a long time (22-24).

In a recent experimental acquisition by the FTIR, the data at 1660 cm^{-1} attributed to α- helices was reinterpreted when the same signal was obtained in a recPrP sample that is only formed by ß-sheets. Therefore, it was concluded that the FTIR-based data do not support the presence of residual α-helices in PrP^{Sc} (45).

Hydrogen-Deuterium Exchange (H/D exchange)

Another spectroscopy technique that does not require the introduction of specific spectroscopy probes for the study of structure of PrP^{Sc} is H/D exchange coupled with Mass Spectrometry (HDXMS).

This technique is based on the ability of some hydrogens of the peptide backbone to be rapidly replaced by deuterium, which is freely in the solvent (D_2O).

This exchange depends on the status of the hydrogens. These hydrogens that participate in some hydrogen bond forming secondary structures would be replaced slower than those that are part of the unstructured region of the protein. In this regard, unstructured regions are detected by its rapid H/D exchange compared to α-helices and ß-sheets, which have slower exchangeable rates.

Taking into account the advantage of the deuterium being heavier than

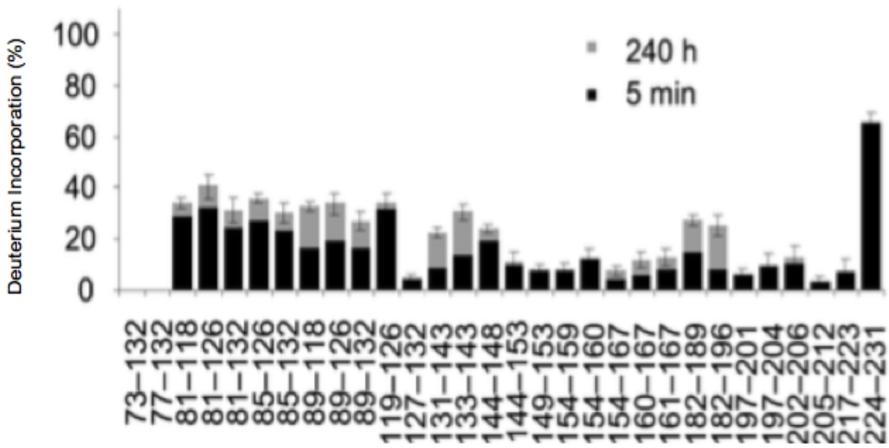

Figure 1.10. Deuterium incorporation to peptidic fragments from the GPI-anchorless mice infected with 22L prion strain. Deuterium/hydrogen incorporation was proven by 5 and 240 hour of exchange. Figure adapted from Smirnovas *et al.* (45)

hydrogen, the exchange rates are monitored by Mass Spectrometry.

According to that, the HDXMS applied to the brain derived PrP^{Sc} was used to map the ß-sheets core of GPI-anchorless PrP^{Sc} (PrP^{Sc} that lacks the membrane anchor protein GPI) (45). The authors observed that the region 80-90 to the Ct domain 231 exhibits the typical slow exchange rates of ß-sheets. Within this region, the sequence spanning from 131 to 223 exhibits particularly high degrees of protection. The stretches 80-90 to 130 and 224 to 231 exhibit less protection to H/D exchange indicating that within the ß-sheet core there are several unstructured stretches (Figure 1.10). This conclusion led to the confirmation of the idea that PrP^{Sc} consists of ß-strands connected by loops/turns.

Cryo-Electron Microscopy (Cryo-EM).

The sample is frozen at cryogenic temperature and observed under EM without sample staining. In this process, the protein is observed in the native environment providing a high resolution of the protein structure.

Recently, Vázquez-Fernández and collaborators collected cryo-EM images from the purified GPI-anchorless PrP^{Sc} fibers to study their structural features (Figure 1.11). The results obtained in this study support the hypothesis that the structure of PrP^{Sc} consists a four-rung ß-solenoid (46).

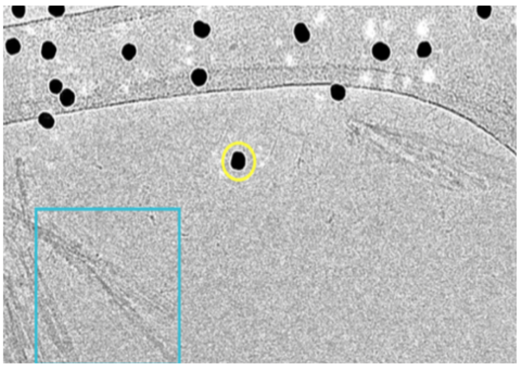

Figure 1.11. **Cryo-TEM images of the GPI-anchorless PrP^{Sc} fibers**. The fibers were observed without negative staining. The yellow circle indicates the fiduciary gold particle. These particle are added to the sample to facilitate alignment in case tomography is performed (46)

Nuclear Magnetic Resonance (NMR)

NMR is a phenomenon that occurs when the nuclei of the atoms are immersed in a static magnetic field. Each nuclei resonance is specific to the atoms and the environment where it is located. Because of that, the atoms that form the amino acids result in a specific resonance within the protein. For the study of the protein structural properties, solid-state NMR spectroscopy has become an important tool due to its precision in the resonance assignment and distance measurements among atoms (47). All together, they increase the resolution of the data collected in the study of the protein. These developments have led to the first resonance assignments of proteins and protein domains (48-50) as well as to determine three-dimensional structures (51, 52). The most successful experiment in the prion field was done by Wasmer and colleagues (53). In this study, the authors applied solid-state NMR to determine the rigid core of the yeast (*Podospera anserine*) prion Het-s and based on the resonance restraints they proposed a model of the prion-forming domain (218-289) of Het-s forming a left-handed ß-solenoid, in which each molecule is formed by two helical windings.

Chemical Cross Linking.

During the last 15 years, chemical cross-linking in combination with protein enzymatic digestion and the mass spectrometry (MS) analysis have gained importance as alternative strategies to the structural study of proteins.

The cross-linkers target specific amino acids in the protein, creating a stable covalent bond that defines structural constraints. A recent chemical cross-linkers study was used to react with the N-terminal of the PrP27-30 (54). The resulting dimers/trimers and high ordered oligomers were analyzed by MS. The authors concluded that each PrP27-30 molecule contains at least two/three monolayers that create the PrP^{Sc} architecture.

Epitope Mapping.

Epitope mapping is the experimental process to identify the binding sites of some antibodies with specific regions on the sequence of the protein. The conformational changes that involve the conversion of PrP^{C} into PrP^{Sc} were probed by the use of epitope mapping (55, 56). In epitope mapping study, the native and denatured state of PrP^{C} and PrP27-30 were studied to explore the streches accesible to bind with the antibodies. The authors observed the epitope region at the C-terminal part of both PrP^{C} and PrP27-30 was accesible to antibodies; in contrast the N-terminal domain (90 to 120) was accesible for antibodies in PrP^{C}, however this epitope was hidden in PrP27-30. The authors argued that major conformational changes underlying PrP^{Sc} formation occurs within N-terminal part of the PrP27-30 (90-120).

Surface Reactivity.

Chemical surface labeling is a method to study the accessibility of a specific region to the solvent by the reaction of specific chemicals with amino acids.

Recently, the conformation rearrangement of the PrP^{C} into PrP^{Sc} conversion was analyzed by labeling tyrosine (Tyr) residues with a chemical reagent (tetranitromethane, TNM) (57). In this study, Tyr_{225} and Tyr_{226} resulted less accessible in PrP^{Sc} compared to PrP^{C}, indicating that the rearrangement around this region goes through in a high-packed secondary structure, perhaps defined by the ß-sheet conformation.

Limited proteolysis.

Limited proteolysis is a technique that uses the proteolytic digestion by proteases under limited condition. In a first attempt, the protease digests the most exposed and flexible regions like loops and turns providing information of the specific organization in the overall of the protein.

The use of a non-specific protease like proteinase K (PK) has been used for a long time in the prion field. While PrP^{Sc} is partially resistant to PK digestion, PrP^{C} is totally destroyed after incubation with PK (Figure 1.5). The PK-resistant peptide (PK-res PrP or PrP27-30) retains the infectivity of the full length PrP^{Sc}. In addition to this, the PK-resistant cores are variable in length depending on the species, the most abundant span the residues ~90-231. Therefore, it can be concluded that the PrP^{Sc} is formed by two domains: the N-terminal domain, which is unstructured and easily degraded by PK and the C-terminal domain, which its highly ordered and partially resists the proteolytic digestion of the PK (58, 59).

Nonetheless, additional studies have demonstrated the existence of a sensitive PrP^{Sc} to PK digestion ($sPrP^{Sc}$) that shares structural and biochemical features with the PK-resistant PrP^{Sc} (PK-res PrP) (60-62). The most noticeable difference is that whereas PK-res PrP form large aggregates, $sPrP^{Sc}$ forms small aggregates.

Recently, limited proteolysis combined with mass spectrometry has been used to study the structural features of the GPI-anchorless PrP^{Sc} (63). In addition to the previously reported cleavage site (64), Vázquez-Fernández and colleagues were able to find new cleavage sites. The authors concluded that the structure of PrP^{Sc} consists of a series of high PK-resistant ß-sheet strands that are connected through loops and turns in agreement with the previous results (45).

Although the use of this kind of techniques allowed to obtain a large number of experimental data and they finally could propose some different models based on their findings, none of these models is able to accommodate all the experimental constraints.

Structural models of PrP^{Sc}

The first effort to model PrP 27-30 was carried out by Huang and collaborators. In this proposal PrP^{Sc} model, based on the combination of computational and experimental constraints, they suggest that the PrP^{Sc} is folded in 4 ß-stranded ß-sheets and 2 additional α-helices (Figure 1.12A) (65). However, the discordant interpretation is the existence of α-helices supported by the means of FTIR. As commented above, the FTIR signal at 1660 cm^{-1} has been obtained in recPrP, and is only formed by ß-sheets, therefore the α-helices cannot be interpreted as a secondary structure on the PrP^{Sc} by the means of FTIR (45).

One of the most important models comes from the studies on the 2D crystals of PrP 27-30 and the miniprion PrP106, which lacks the central part of the PrP sequence (Δ23-88; Δ141-176). The model based on 2D electron crystallography of PrP27-30 suggests that the PrP displays a central parallel ß-helix and the C-terminal regions and retains its -helical conformation (Figure 1.12B) (44). However, according to the new reinterpretation of the signal at 1660 cm^{-1} in FTIR, the existence of α-helices cannot be longer supported (*vide supra*).

Other important model arises from molecular dynamics data. The model proposed by DeMarco and colleagues suggests that the architecture of the

PrP^{Sc} consists in a spiral organization that retains the three α-helix of the PrP^{C} and extends the number of ß-sheets to four (Figure 1.12C) (66). The high proportion of α-helical structure is in conflict with the recent FTIR experimental data (*vide supra*) and the limited proteolysis data and furthermore, the model is in an absolute conflict with one experimental fact that is absolutely definitive now: that PrP^{Sc} is amyloid and has cross-ß architecture (45, 63, 67).

The next model arises from the site-labelling and EPR spectrometry analysis of the recombinant PrP amyloid, a misfolded that was reported to induce transmissible disease in mice overexpressing an N-terminally truncated form of PrP^{C} (68). Although these recombinant amyloid resulted infectious, they could harbor difference with the brain-derived prion, therefore the authors suggested that this recombinant amyloid could be an useful tool for the study of the PrP^{Sc} structure (69). In this model, within each of the PrP molecules, the amyloid core forms a single layer that is parallel stacked on the other amyloid core, where the ß-strands are in register (Figure 1.12D).

Regarding this kind of organization, the most recent model for elucidating the molecular structure of the PrP^{Sc} is the PIRIBS (Parallel In Register ß-sheets) model (70). According to the authors, the PrP^{Sc} fibers consist only of a single filament. Thus, **parallel in register ß-sheets** fold perpendicular to fiber axes, so that every PrP^{Sc} monomer consist of a single flat layer. Each one of the monomers of the PrP^{Sc} is parallel-stacked along the fiber axis (Figure 1.12E).

In contrast, the most recent model proposed by Vázquez-Fernández used a combination of EM and computational approaches to obtain new pieces of evidence in the structure of the GPI-anchorless PrP^{Sc} (46). For this purpose, the authors collected a large number of cryo-TEM images from the purified GPI-anchorless PrP^{Sc} fibers and generated their 3D structure by a helical reconstruction. According to the data collected and with the pieces of evidence based on 2D electron crystallography and X-ray fiber diffraction, the authors suggest that the structure of the PrP^{Sc} consists of stacks of 4-rung ß-solenoids (Figure 1.12F).

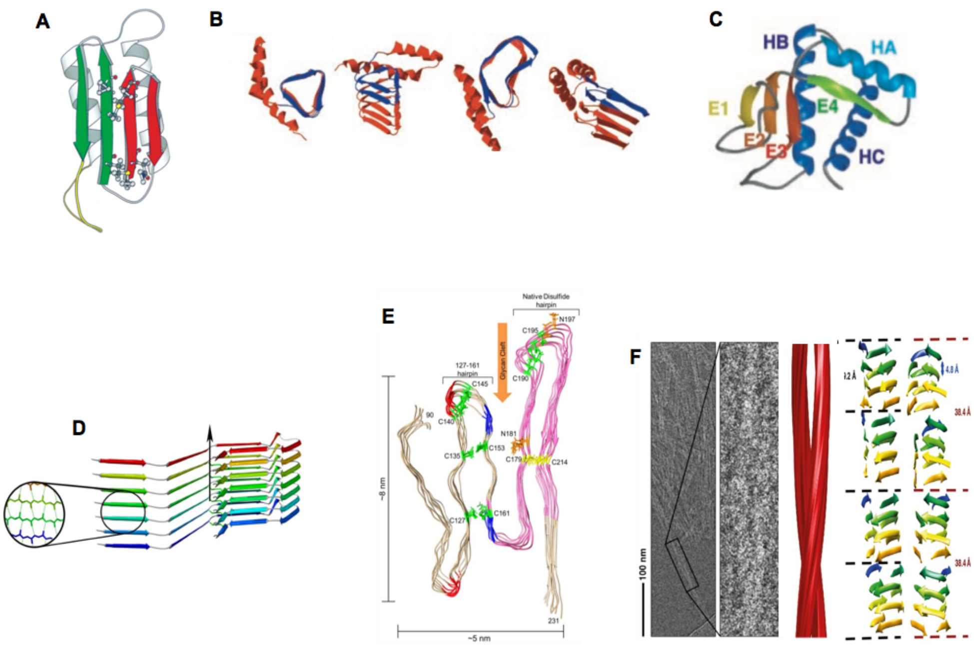

Figure 1.12. Some of the proposal models for structure of the PrP^{Sc}. A. The model proposed by Huang Z. and collaborators for the PrP^{Sc} based on the combination of computational and experimental constraints, suggested that PrP^{Sc} was folded in 4 ß-stranded ß-sheets and 2 additional α-helices. **B)** The model proposed by Wille, H and colleagues is based on the electron crystallography of the 2D crystal of PrP27-30. The structure PrP^{Sc} is folded in ß-helical conformation, where the α-helices remain after conversion. **C)** Molecular dynamics was used by Marco and collaborators to devise the ß-spiral model of the PrP^{Sc}. The structure of the PrP^{Sc} is based on the combination of 4 short ß-sheets with α-helices. **D)** Cobb *et al.* (68) used EPR spectrometry for the structural study of the recPrP amyloid. Each molecule of recPrP is formed by ß-strands that are parallel stacked in register along the fiber axis. **E)** PIRIBS model proposed by Govearman *et al.*. **F)** ß-helical model suggested by Vázquez and collaborators. The acquisitions of several constraints from X-Ray Fiber Diffraction, 2D Crystallography and reconstruction of cryo-EM images were used to propose that the structure of PrP^{Sc} consists in the stacking of 4 rungs of ß-solenoid.

Diversity of prions

One of the most fascinating phenomenon in the biology of prions is the existence of a diversity of PrP^{Sc} molecules coming from the same host. This diversty of the PrP^{Sc} is known as prion strains. The existence of the prion strains raised the question of how the "protein–only" hypothesis could explain the fact that the same amino acid sequence can play as template to form different strains of prions and how the same amino acids sequence may result in different strains of prions capable of generating different phenotypes of prion diseases in the same host. In 1991, it was shown that a subtype of prion causes different phenotypes in the same host. These features of the disease phenotype were classified depending on the symptomatology, deposit pattern of the aggregates in the brain, histopathology and cellular tropism. Later, the lesion profile and incubation time were used to classify the prion strains (71).

The "protein–only" hypothesis suggests that this diversity is given by the differences on the tertiary and quaternary structure of the PrP^{Sc}. This notion was supported by the observation of the different pattern observed in the two subtypes of prions that arose when the mink PrP^{Sc} was inoculated in the Syrian hamsters. Hamsters inoculated with the mink PrP^{Sc} developed prion diseases with different features. Biochemical analyses of the brain-derived PrP^{Sc} from each hamster revealed that after PK digestion, the electrophoretic mobility in SDS-PAGE was different (72). Given that two types of PrP^{Sc} came through from the same amino acid sequence, it was concluded that the prion strains obtained have different tertiary structures, suggesting that the refolding is different in each strain; that makes the PK accessibility different in each conformation.

The PrP^C presents three states of N-glycosylation; non-, mono- and di- form, this feature remains after conversion into PrP^{Sc}. The proportion of glycosylation could be different depending on the prion strain (73, 74). The presence of different proportion of the glycosylation pattern is another topic to be considered to define the strains.

The discovery of the two main digestion patterns has divided the prion diversity into 2 main strain groups.

Classical prion strains.

The PK digestion pattern is represented by 3 glycosylated bands with different proportions according to the prion strains.

Atypical prion strains:

The most important characterization of the atypical prion strains is the presence of smaller PK-resistant peptides that correspond to the internal fragments from the N terminal and the C- terminal of the truncated forms. The Molecular Weight (MW) observed in the western blot is usually at 8 and 6 KDa. According to this, several atypical prion strains were observed in different TSEs (75-77).

In summary, despite the absence of a nucleic acid genome, there are multiple prion strains that are observed in wild animals and can be propagated in the laboratory, (*in vivo* or/and *in vitro*), differentiated by the patterns of the diseases they produce, histopathology, and biochemical properties.

Synthetic Prions.

Over the years, the use of synthetic prions has been gaining importance in the prion field. The need to answer the question about the nature of the prion disease agent, promotes the use of the recombinant PrP (recPrP) to elucidate the protein-only hypothesis (78, 79).

Not only the protein-only hypothesis has to be solved; the use of the recPrP allows the introduction of all kind of modifications in the amino acid sequence in order to study the implication of the natural mutant of the PrP (80). It is worth to mention that to produce the recPrP a prokaryotic system that involves some questions about the production of protein is needed; which should mimic the nature of the PrP^{C}. The recPrP generated lacks the glycosylation modification that occurs naturally in the eukaryotic cells, and lacks the GPI anchor, that has been an important role in the PrP^{Sc} pathogenesis. These elements have proven to be essential or at least important factors in the PrP^{Sc} conversion (81, 82). Due to these lacks, the development of a method that mimics the conversion or recPrP into $recPrP^{Sc}$ is essentially important in prion research.

Methods to generate recombinant prions

QUICK.(QUaking Induced Conversion)

The production of high-titers of the $recPrP^{Sc}$ is essential in the prion research. Because of that, one of the methods to mimic the PrP^{C} conversion is described as QUICK, (Quaking Induced Conversion). This method, which consists in the incubation of a recPrP with a PrP^{Sc} from the brain of an animal inoculated with prions and the subsequently agitation, could replicate the PrP^{Sc} conversion after several incubations (83). Nonetheless, although this method is capable of replicating a large number or prion strains and converted into misfolded forms, and furthermore could be used to diagnosis purpose, it does not produce any recPrP that shows infectivity after being inoculated in animals (84).

PMCA (Protein Misfolded Cycling Amplification)

In the method known as Protein Misfolding Cycling Amplification or PMCA, the PrP^{Sc} is incubated with PrP^{C} and the resulting aggregates are disrupted by sonication cycles to create several units for the constant formation of PrPSc and finally, after several cycles, the PrP^{Sc} was amplified (85). Castilla and colleagues could demonstrate that the PMCA mimics the conversion of PrP^{C} into PrP^{Sc}. The resulting PK-resistant PrP shares similar biochemical and structural features with the PrP^{Sc} from brain homogenate of an inoculated hamster. In addition to this, the hamsters inoculated with the PK-res PrP formed after PMCA develop the scrapie disease with the same clinical signs and histopathology profiles as the ones inoculated with the wild type PrP^{Sc}, demonstrating that prions can be generated *in vitro* (86). Recently, the group of Jiyan Ma could generate a synthetic PrP *de novo* that recapitulates the milestones of the prion infection after the inoculation in a wild type mouse. This finding opens a new door in the prion research, providing a new tool for structural and biological studies of the agent causing TSE (79).

In summary, elucidating the PrP^{Sc} structure may help to understand the molecular basis of the biology of PrP^{Sc}, furthermore the molecular mechanism that governs the structural conversion of PrP^{C} into PrP^{Sc}, the prion replication, prion strain and the transmissible barrier will not be understand until the structure is solved.

Over the years, many studies have applied several experiment data to propose different models for the structure of the PrP^{Sc}, however none of these models is able to accommodate all the experimental constraints. Recently, two proposal models have been highlighted to become the most feasible model for the PrP^{Sc} structure. In this context, one of the aims of this work is to provide new information that may help to select one of these models for the structure of PrP^{Sc}.

In addition to the studies of the brain-derived PrP^{Sc}, the use of recombinant PrP have gained importance since its versatility at the time to produce a broad kind of study combinations, eg. the specific substitution of the amino acids may help to understand some features of the PrP biology, the introduction of isotopically labelled amino acids might be a good tool for structural studies. In this context, the development of a system that allowed to convert recPrP into the infectious misfolded form, made this technique a very attractive tool for the generation of $recPrP^{Sc}$. Based on that, the other goal of this thesis was the generation of synthetic prions and subsequently study their structural features.

References

1. Soto, C. and Satani, N. (2011) The intricate mechanisms of neurodegeneration in prion diseases. *Trends Mol Med* 17, 14-24
2. B., S. (1954) Maedi, a slow progressing pernumonia of sheep: An epizoological and pathological study. *British Vet J.* 110, 225-258.
3. Alper, T., Haig, D. A. and Clarke, M. C. (1966) The exceptionally small size of the scrapie agent. *Biochem Biophys Res Commun* 22, 278-284
4. Alper, T., Cramp, W. A., Haig, D. A. and Clarke, M. C. (1967) Does the agent of scrapie replicate without nucleic acid? *Nature* 214, 764-766
5. Griffith, J. S. (1967) Self-replication and scrapie. *Nature* 215, 1043-1044
6. Merz, P. A., Somerville, R. A., Wisniewski, H. M. and Iqbal, K. (1981) Abnormal fibrils from scrapie-infected brain. *Acta Neuropathol* 54, 63-74
7. Prusiner, S. B. (1982) Novel proteinaceous infectious particles cause scrapie. *Science* 216, 136-144
8. Prusiner, S. B., Groth, D. F., Bolton, D. C., Kent, S. B. and Hood, L. E. (1984) Purification and structural studies of a major scrapie prion protein. *Cell* 38, 127-134
9. Chesebro, B., Race, R., Wehrly, K., Nishio, J., Bloom, M., Lechner, D., Bergstrom, S., Robbins, K., Mayer, L., Keith, J. M. and et al. (1985) Identification of scrapie prion protein-specific mRNA in scrapie-infected and uninfected brain. *Nature* 315, 331-333
10. Oesch, B., Westaway, D., Walchli, M., McKinley, M. P., Kent, S. B., Aebersold, R., Barry, R. A., Tempst, P., Teplow, D. B., Hood, L. E. and et al. (1985) A cellular gene encodes scrapie PrP 27-30 protein. *Cell* 40, 735-746
11. Basler, K., Oesch, B., Scott, M., Westaway, D., Walchli, M., Groth, D. F., McKinley, M. P., Prusiner, S. B. and Weissmann, C. (1986) Scrapie and cellular PrP isoforms are encoded by the same chromosomal gene. *Cell* 46, 417-428

12. Riek, R., Hornemann, S., Wider, G., Glockshuber, R. and Wuthrich, K. (1997) NMR characterization of the full-length recombinant murine prion protein, mPrP(23-231). *FEBS Lett* 413, 282-288

13. Apostol, M. I., Perry, K. and Surewicz, W. K. (2013) Crystal structure of a human prion protein fragment reveals a motif for oligomer formation. *J Am Chem Soc* 135, 10202-10205

14. Pushie, M. J., Pickering, I. J., Martin, G. R., Tsutsui, S., Jirik, F. R. and George, G. N. (2011) Prion protein expression level alters regional copper, iron and zinc content in the mouse brain. *Metallomics* 3, 206-214

15. Steele, A. D., Emsley, J. G., Ozdinler, P. H., Lindquist, S. and Macklis, J. D. (2006) Prion protein (PrP^C) positively regulates neural precursor proliferation during developmental and adult mammalian neurogenesis. *Proc Natl Acad Sci U S A* 103, 3416-3421

16. Maglio, L. E., Perez, M. F., Martins, V. R., Brentani, R. R. and Ramirez, O. A. (2004) Hippocampal synaptic plasticity in mice devoid of cellular prion protein. *Brain Res Mol Brain Res* 131, 58-64

17. Caiati, M. D., Safiulina, V. F., Fattorini, G., Sivakumaran, S., Legname, G. and Cherubini, E. (2013) PrP^C controls via protein kinase A the direction of synaptic plasticity in the immature hippocampus. *J Neurosci* 33, 2973-2983

18. Mouillet-Richard, S., Ermonval, M., Chebassier, C., Laplanche, J. L., Lehmann, S., Launay, J. M. and Kellermann, O. (2000) Signal transduction through prion protein. *Science* 289, 1925-1928

19. Santuccione, A., Sytnyk, V., Leshchyns'ka, I. and Schachner, M. (2005) Prion protein recruits its neuronal receptor NCAM to lipid rafts to activate p59fyn and to enhance neurite outgrowth. *J Cell Biol* 169, 341-354

20. Khosravani, H., Zhang, Y., Tsutsui, S., Hameed, S., Altier, C., Hamid, J., Chen, L., Villemaire, M., Ali, Z., Jirik, F. R. and Zamponi, G. W. (2008) Prion protein attenuates excitotoxicity by inhibiting NMDA receptors. *J Gen Physiol* 131, i5

21. Bremer, J., Baumann, F., Tiberi, C., Wessig, C., Fischer, H., Schwarz, P., Steele, A. D., Toyka, K. V., Nave, K. A., Weis, J. and Aguzzi, A. (2010)

Axonal prion protein is required for peripheral myelin maintenance. *Nat Neurosci* 13, 310-318

22. Caughey, B. W., Dong, A., Bhat, K. S., Ernst, D., Hayes, S. F. and Caughey, W. S. (1991) Secondary structure analysis of the scrapie-associated protein PrP 27-30 in water by infrared spectroscopy. *Biochemistry* 30, 7672-7680

23. Pan, K. M., Baldwin, M., Nguyen, J., Gasset, M., Serban, A., Groth, D., Mehlhorn, I., Huang, Z., Fletterick, R. J., Cohen, F. E. and et al. (1993) Conversion of α-helices into beta-sheets features in the formation of the scrapie prion proteins. *Proc Natl Acad Sci U S A* 90, 10962-10966

24. Safar, J., Roller, P. P., Gajdusek, D. C. and Gibbs, C. J., Jr. (1993) Conformational transitions, dissociation, and unfolding of scrapie amyloid (prion) protein. *J Biol Chem* 268, 20276-20284

25. Prusiner, S. B. (1998) Prions. *Proc Natl Acad Sci U S A* 95, 13363-13383

26. Aguzzi, A. and Calella, A. M. (2009) Prions: protein aggregation and infectious diseases. *Physiol Rev* 89, 1105-1152

27. Makarava, N. and Baskakov, I. V. (2013) The evolution of transmissible prions: the role of deformed templating. *PLoS Pathog* 9, e1003759

28. Zabel, M. D. and Reid, C. (2015) A brief history of prions. *Pathog Dis*

29. Detwiler, L. A. and Baylis, M. (2003) The epidemiology of scrapie. *Rev Sci Tech* 22, 121-143

30. Williams, E. S. and Young, S. (1993) Neuropathology of chronic wasting disease of mule deer (Odocoileus hemionus) and elk (Cervus elaphus nelsoni). *Vet Pathol* 30, 36-45

31. Kelly, D. F., Wells, G. A., Haritani, M., Higgins, R. J. and Jeffrey, M. (2005) Neuropathological findings in cats with clinically suspect but histologically unconfirmed feline spongiform encephalopathy. *Vet Rec* 156, 472-477

32. Wells, G. A., Scott, A. C., Johnson, C. T., Gunning, R. F., Hancock, R. D., Jeffrey, M., Dawson, M. and Bradley, R. (1987) A novel progressive spongiform encephalopathy in cattle. *Vet Rec* 121, 419-420

33. Creutzfeldt, H. G. U ̈bereineeigenartigeherdfo ̈rmigeErkrankung des Zentralnervensystems (vorla ̈ u ge Mitteilung). Z Gesamte Neurol Psy 1920;57:1–18. *Neurol Psy*. 57, 1–18.

34. A., J. (1921) U ̈ber eigenartige Erkrankungen des Zentralnerven- systems mit bemerkenswertem anatomischem Befunde. (Spastische Pseudosklerose-Encephalomyelopathie mit dis- seminierten Degenerationsherden). *J Z Gesamte Neurol Psy* 64, 147–228.

35. Gajdusek DC, Z. V. (1959) Kuru. *AmJ Med* 26, 442–469

36. Hsiao, K., Baker, H. F., Crow, T. J., Poulter, M., Owen, F., Terwilliger, J. D., Westaway, D., Ott, J. and Prusiner, S. B. (1989) Linkage of a prion protein missense variant to Gerstmann-Straussler syndrome. *Nature* 338, 342-345

37. Medori, R., Montagna, P., Tritschler, H. J., LeBlanc, A., Cortelli, P., Tinuper, P., Lugaresi, E. and Gambetti, P. (1992) Fatal familial insomnia: a second kindred with mutation of prion protein gene at codon 178. *Neurology* 42, 669-670

38. Colby, D. W. and Prusiner, S. B. (2011) Prions. *Cold Spring Harb Perspect Biol* 3, a006833

39. Requena, J. R. and Wille, H. (2014) The structure of the infectious prion protein: experimental data and molecular models. *Prion* 8, 60-66

40. Eanes, E. D. and Glenner, G. G. (1968) X-ray diffraction studies on amyloid filaments. *J Histochem Cytochem* 16, 673-677

41. Nguyen, J. T., Inouye, H., Baldwin, M. A., Fletterick, R. J., Cohen, F. E., Prusiner, S. B. and Kirschner, D. A. (1995) X-ray diffraction of scrapie prion rods and PrP peptides. *J Mol Biol* 252, 412-422

42. Wille, H., Bian, W., McDonald, M., Kendall, A., Colby, D. W., Bloch, L., Ollesch, J., Borovinskiy, A. L., Cohen, F. E., Prusiner, S. B. and Stubbs, G. (2009) Natural and synthetic prion structure from X-ray fiber diffraction. *Proc Natl Acad Sci U S A* 106, 16990-16995

43. Sim, V. L. and Caughey, B. (2009) Ultrastructures and strain comparison of under-glycosylated scrapie prion fibrils. *Neurobiol Aging* 30, 2031-2042

44. Wille, H., Michelitsch, M. D., Guenebaut, V., Supattapone, S., Serban, A., Cohen, F. E., Agard, D. A. and Prusiner, S. B. (2002) Structural studies of the scrapie prion protein by electron crystallography. *Proc Natl Acad Sci U S A* 99, 3563-3568

45. Smirnovas, V., Baron, G. S., Offerdahl, D. K., Raymond, G. J., Caughey, B. and Surewicz, W. K. (2011) Structural organization of brain-derived mammalian prions examined by hydrogen-deuterium exchange. *Nat Struct Mol Biol* 18, 504-506

46. Vázquez-Fernández E, V. M., Cebey L, Renault L, Sevillano AM, Peters PJ, Fernández JL, Young H, Wille H, Requena JR. (2014) Recent advances towards an understanding of the structure of PrP^{Sc}.in *International Prion Congress 2014* (Chernoff, Y. O. ed., Landes Bioscience, Trieste

47. Wuthrich, K. (2001) The way to NMR structures of proteins. *Nat Struct Biol* 8, 923-925

48. Pauli, J., Baldus, M., van Rossum, B., de Groot, H. and Oschkinat, H. (2001) Backbone and side-chain 13C and 15N signal assignments of the α-spectrin SH3 domain by magic angle spinning solid-state NMR at 17.6 Tesla. *Chembiochem* 2, 272-281

49. Bockmann, A., Lange, A., Galinier, A., Luca, S., Giraud, N., Juy, M., Heise, H., Montserret, R., Penin, F. and Baldus, M. (2003) Solid state NMR sequential resonance assignments and conformational analysis of the 2x10.4 kDa dimeric form of the Bacillus subtilis protein Crh. *J Biomol NMR* 27, 323-339

50. van Rossum, B. J., Castellani, F., Pauli, J., Rehbein, K., Hollander, J., de Groot, H. J. and Oschkinat, H. (2003) Assignment of amide proton signals by combined evaluation of HN, NN and HNCA MAS-NMR correlation spectra. *J Biomol NMR* 25, 217-223

51. Castellani, F., van Rossum, B., Diehl, A., Schubert, M., Rehbein, K. and Oschkinat, H. (2002) Structure of a protein determined by solid-state magic-angle-spinning NMR spectroscopy. *Nature* 420, 98-102

52. Jaroniec, C. P., MacPhee, C. E., Bajaj, V. S., McMahon, M. T., Dobson, C. M. and Griffin, R. G. (2004) High-resolution molecular structure of a peptide in an amyloid fibril determined by magic angle spinning NMR spectroscopy. *Proc Natl Acad Sci U S A* 101, 711-716

53. Wasmer, C., Lange, A., Van Melckebeke, H., Siemer, A. B., Riek, R. and Meier, B. H. (2008) Amyloid fibrils of the HET-s(218-289) prion form a beta solenoid with a triangular hydrophobic core. *Science* 319, 1523-1526

54. Onisko, B., Fernandez, E. G., Freire, M. L., Schwarz, A., Baier, M., Camina, F., Garcia, J. R., Rodriguez-Segade Villamarin, S. and Requena, J. R. (2005) Probing PrP^{Sc} structure using chemical cross-linking and mass spectrometry: evidence of the proximity of Gly90 amino termini in the PrP 27-30 aggregate. *Biochemistry* 44, 10100-10109

55. Peretz, D., Williamson, R. A., Matsunaga, Y., Serban, H., Pinilla, C., Bastidas, R. B., Rozenshteyn, R., James, T. L., Houghten, R. A., Cohen, F. E., Prusiner, S. B. and Burton, D. R. (1997) A conformational transition at the N terminus of the prion protein features in formation of the scrapie isoform. *J Mol Biol* 273, 614-622

56. Williamson, R. A., Peretz, D., Pinilla, C., Ball, H., Bastidas, R. B., Rozenshteyn, R., Houghten, R. A., Prusiner, S. B. and Burton, D. R. (1998) Mapping the prion protein using recombinant antibodies. *J Virol* 72, 9413-9418

57. Gong, B., Ramos, A., Vazquez-Fernandez, E., Silva, C. J., Alonso, J., Liu, Z. and Requena, J. R. (2011) Probing structural differences between PrP(C) and PrP(Sc) by surface nitration and acetylation: evidence of conformational change in the C-terminus. *Biochemistry* 50, 4963-4972

58. Bolton, D. C., McKinley, M. P. and Prusiner, S. B. (1982) Identification of a protein that purifies with the scrapie prion. *Science* 218, 1309-1311

59. McKinley, M. P., Bolton, D. C. and Prusiner, S. B. (1983) A protease-resistant protein is a structural component of the scrapie prion. *Cell* 35, 57-62

60. Safar, J., Wille, H., Itri, V., Groth, D., Serban, H., Torchia, M., Cohen, F. E. and Prusiner, S. B. (1998) Eight prion strains have PrP(Sc) molecules with different conformations. *Nat Med* 4, 1157-1165

61. Pastrana, M. A., Sajnani, G., Onisko, B., Castilla, J., Morales, R., Soto, C. and Requena, J. R. (2006) Isolation and characterization of a proteinase K-sensitive PrP^{Sc} fraction. *Biochemistry* 45, 15710-15717

62. Sajnani, G., Silva, C. J., Ramos, A., Pastrana, M. A., Onisko, B. C., Erickson, M. L., Antaki, E. M., Dynin, I., Vazquez-Fernandez, E., Sigurdson, C. J., Carter, J. M. and Requena, J. R. (2012) PK-sensitive PrP is infectious and shares basic structural features with PK-resistant PrP. *PLoS Pathog* 8, e1002547

63. Vazquez-Fernandez, E., Alonso, J., Pastrana, M. A., Ramos, A., Stitz, L., Vidal, E., Dynin, I., Petsch, B., Silva, C. J. and Requena, J. R. (2012) Structural organization of mammalian prions as probed by limited proteolysis. *PLoS One* 7, e50111

64. Sajnani, G., Pastrana, M. A., Dynin, I., Onisko, B. and Requena, J. R. (2008) Scrapie prion protein structural constraints obtained by limited proteolysis and mass spectrometry. *J Mol Biol* 382, 88-98

65. Huang, Z., Prusiner, S. B. and Cohen, F. E. (1995) Scrapie prions: a three-dimensional model of an infectious fragment. *Fold Des* 1, 13-19

66. DeMarco, M. L. and Daggett, V. (2004) From conversion to aggregation: protofibril formation of the prion protein. *Proc Natl Acad Sci U S A* 101, 2293-2298

67. Baron, G. S., Hughson, A. G., Raymond, G. J., Offerdahl, D. K., Barton, K. A., Raymond, L. D., Dorward, D. W. and Caughey, B. (2011) Effect of glycans and the glycophosphatidylinositol anchor on strain dependent conformations of scrapie prion protein: improved purifications and infrared spectra. *Biochemistry* 50, 4479-4490

68. Legname, G., Baskakov, I. V., Nguyen, H. O., Riesner, D., Cohen, F. E., DeArmond, S. J. and Prusiner, S. B. (2004) Synthetic mammalian prions. *Science* 305, 673-676

69. Cobb, N. J., Sonnichsen, F. D., McHaourab, H. and Surewicz, W. K. (2007) Molecular architecture of human prion protein amyloid: a parallel, in-register beta-structure. *Proc Natl Acad Sci U S A* 104, 18946-18951

70. Groveman, B. R., Dolan, M. A., Taubner, L. M., Kraus, A., Wickner, R. B. and Caughey, B. (2014) Parallel in-register intermolecular beta-sheet architectures for prion-seeded prion protein (PrP) amyloids. *J Biol Chem* 289, 24129-24142

71. Bruce, M. E. (2003) TSE strain variation. *Br Med Bull* 66, 99-108

72. Bessen, R. A. and Marsh, R. F. (1992) Biochemical and physical properties of the prion protein from two strains of the transmissible mink encephalopathy agent. *J Virol* 66, 2096-2101

73. Race, R. E., Raines, A., Baron, T. G., Miller, M. W., Jenny, A. and Williams, E. S. (2002) Comparison of abnormal prion protein glycoform patterns from transmissible spongiform encephalopathy agent-infected deer, elk, sheep, and cattle. *J Virol* 76, 12365-12368

74. Castilla, J., Morales, R., Saa, P., Barria, M., Gambetti, P. and Soto, C. (2008) Cell-free propagation of prion strains. *EMBO J* 27, 2557-2566

75. Tagliavini, F., Lievens, P. M., Tranchant, C., Warter, J. M., Mohr, M., Giaccone, G., Perini, F., Rossi, G., Salmona, M., Piccardo, P., Ghetti, B., Beavis, R. C., Bugiani, O., Frangione, B. and Prelli, F. (2001) A 7-kDa prion protein (PrP) fragment, an integral component of the PrP region required for infectivity, is the major amyloid protein in Gerstmann-Straussler-Scheinker disease A117V. *J Biol Chem* 276, 6009-6015

76. Gambetti, P., Dong, Z., Yuan, J., Xiao, X., Zheng, M., Alshekhlee, A., Castellani, R., Cohen, M., Barria, M. A., Gonzalez-Romero, D., Belay, E. D., Schonberger, L. B., Marder, K., Harris, C., Burke, J. R., Montine, T., Wisniewski, T., Dickson, D. W., Soto, C., Hulette, C. M., Mastrianni, J. A., Kong, Q. and Zou, W. Q. (2008) A novel human disease with abnormal prion protein sensitive to protease. *Ann Neurol* 63, 697-708

77. Pirisinu, L., Nonno, R., Esposito, E., Benestad, S. L., Gambetti, P., Agrimi, U. and Zou, W. Q. (2013) Small ruminant nor98 prions share biochemical

features with human gerstmann-straussler-scheinker disease and variably protease-sensitive prionopathy. *PLoS One* 8, e66405

78. Diaz-Espinoza, R. and Soto, C. (2010) Generation of prions in vitro and the protein-only hypothesis. *Prion* 4, 53-59

79. Wang, F., Wang, X., Yuan, C. G. and Ma, J. (2010) Generating a prion with bacterially expressed recombinant prion protein. *Science* 327, 1132-1135

80. Shirai, T., Saito, M., Kobayashi, A., Asano, M., Hizume, M., Ikeda, S., Teruya, K., Morita, M. and Kitamoto, T. (2014) Evaluating prion models based on comprehensive mutation data of mouse PrP. *Structure* 22, 560-571

81. Kim, J. I., Surewicz, K., Gambetti, P. and Surewicz, W. K. (2009) The role of glycophosphatidylinositol anchor in the amplification of the scrapie isoform of prion protein *in vitro*. *FEBS Lett* 583, 3671-3675

82. Ma, J. (2012) The role of cofactors in prion propagation and infectivity. *PLoS Pathog* 8, e1002589

83. Orru, C. D., Wilham, J. M., Vascellari, S., Hughson, A. G. and Caughey, B. (2012) New generation QuIC assays for prion seeding activity. *Prion* 6, 147-152

84. Atarashi, R., Wilham, J. M., Christensen, L., Hughson, A. G., Moore, R. A., Johnson, L. M., Onwubiko, H. A., Priola, S. A. and Caughey, B. (2008) Simplified ultrasensitive prion detection by recombinant PrP conversion with shaking. *Nat Methods* 5, 211-212

85. Saborio, G. P., Permanne, B. and Soto, C. (2001) Sensitive detection of pathological prion protein by cyclic amplification of protein misfolding. *Nature* 411, 810-813

86. Castilla, J., Saa, P., Hetz, C. and Soto, C. (2005) *In vitro* generation of infectious scrapie prions. *Cell* 121, 195-206

Chapter 2

O b j e t i v e s

I. **Provide new evidence that could help to decide between the PIRIBS and ß-soleonoid models for the PrP^{Sc} structure.**

II. **Generation of recombinant prions.**

III. **Study of the structural characterization of the recombinant prions.**

Chapter 3

PK-induced disassembly of partially unfolded PrP^{Sc} fibers supports a multi-rung architecture of PrP^{Sc} subunits.

Evidence based on solid state NMR strongly suggests that recombinant PrP (rPrP) amyloid fibers are an in-register stack of single-rung "flat" monomers, whose β-strand rich cores span from position ~160 to the C-terminus. In contrast, evidence from 2D electron crystallography, X-ray fiber diffraction and reconstruction of cryo-EM images (1) suggests that PrP^{Sc} consists of stacks of 4-rung β-solenoids. However, the recently proposed PIRIBS model (2) argues that PrP^{Sc} monomers are also flat, with rPrP amyloid-like β-strand rich cores extending up to position ~90.

Besides a proteinase K (PK) resistant core spanning ~90-230, PrP^{Sc} has an inner "super-resistant" ~152-230 core that resists partial, reversible unfolding induced by guanidine (3). Based on this it was reasoned that if PrP^{Sc} is a multi-rung solenoid, PK-treatment of partially unfolded PrP^{Sc} fibers should necessarily result in their complete disassembly, as the N-terminal "base" of each monomer disintegrates. In contrast, if PrP^{Sc} monomers are flat, fibers would persist after such treatment, as seen when rPrP fibers are treated with PK under conditions that preserve their C-terminal β-strand rich cores, which remain stacked.

To address the question whether the PrP^{Sc} fibers are formed by the stacking of single flat monomers or in contrast, they are formed by the stacking of multiple rung subunits, the effect of partially unfolding PrP^{Sc} and subsequently digesting with PK was studied. The resulting PK- resistant PrP^{Sc} samples were analyzed by western blotting using a C-terminus antibody and negative stain transmission electron microscope (TEM).

The results described in this chapter show virtually complete disassembly of partially unfolded PrP^{Sc} fibers after PK treatment, supporting a multi-rung, rather than flat, architecture of PrP^{Sc} monomers. As a corollary, PrP^{Sc} fibers would be made up of two protofilaments, as has been the general consensus based on the general appearance of negative stain TEM images, rather than a single superpleated filament, as proposed for the PIRIBS model.

The elucidation of the structure of the mammalian prion, PrP^{Sc}, continues to be a major challenge in prion research. Structural studies have been hampered by the intractable nature of this insoluble, aggregated infectious protein, which prevents the use of high resolution techniques such as NMR or X-ray crystallography (4-7). Although many different structural models of PrP^{Sc} have been proposed, none of them complies fully with the growing set of experimental structural constraints available. Therefore, it can be concluded that all of them are partially or totally inaccurate (7). One important structural feature of PrP^{Sc}, which is now widely accepted, is that its basic architecture of PrP^{Sc} fibers is that of an amyloid (7). Definitive evidence for this conclusion derives from conspicuous meridional 4.8 Å reflections detected by fiber X-ray diffraction of PrP^{Sc} samples (7, 8). Such an architecture agrees with the high content of ß-sheet secondary structure of PrP^{Sc}, detected in FTIR studies (9, 10). A large fraction of the PrP sequence (~90-230) is believed to participate in the PrP^{Sc} amyloid core, given that treatment of PrP^{Sc} with PK results in fibers whose main components are ~90-230 cores of PrP (4). Numerous negative stain TEM studies show that these fibers exhibit a width of ~10 nm, and are apparently composed of two symmetrical, intertwined protofilaments, each ~5 nm wide (4, 8, 11). Given the large length of the core, it is impossible to fit it into the relatively small cross-section of a ~5 nm wide protofilament, as in the classic architecture of amyloids such as $A\beta$ (12), in a one-layer stack (13). This lends strong support to the proposal, originally put forward by Wille *et al.* (8, 14) that PrP^{Sc} coils onto itself to form a multi-rung ß-solenoid; vertical stacking of individual ß-solenoid units would result in a narrow protofilament complying with the ~5 nm width constraint. On the other hand, extensive vertical intra- and intermolecular hydrogen bonding between ß-strands would form the amyloid cross-ß spine (Figure 3.1A). A similar architecture is adopted by the fungal prion HET-s (Figure 3.1B), whose fibers are composed of stacked 2-rung ß-

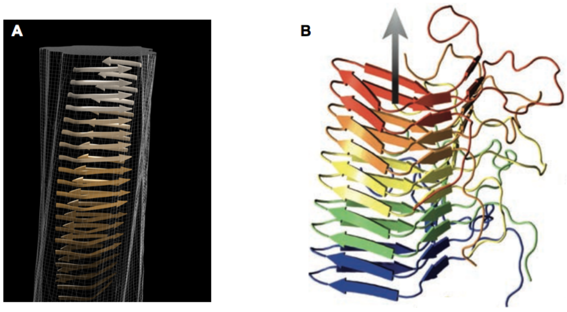

Figure 3.1.**A) Structural model of the PrP^{Sc}** from 2D electron crystallography, X-ray fiber diffraction and reconstruction of cryo-EM images constraints. The model suggests that PrP^{Sc} coils itself forming a 4-rung β-solenoid. Each PrP^{Sc} molecule is stacking along the fiber axes forming a narrow protofilament (5 nm width). proposed by Vázquez-Fernández (1) **B) Structural model of the *Podosperaanserina* fungal prion HET-s**. The prion forming domain (218-289) forms a left-handed ß-soleoind in which, each molecule forming two helical twist, a compact hydrophobia core, three salt bridges and two ladders (15).

solenoidal monomers (15).

On the other hand, Groveman *et al.* (2) have recently proposed an alternative solution to the narrow protofilament fitting problem, named the PIRIBS, (Parallel in Register ß-Sheets) model: according to these authors, PrP^{Sc} fibers do not contain two protofilaments, rather, they consist of a single, ~10 nm wide filament (2) (Figure 3.2A). Thus, each PrP^{Sc} monomer might be tightly packed, by lateral pleating, to fit into one single layer of the PrP^{Sc} fiber. Since a single filament fiber clashes with visual evidence gathered in many TEM-based studies and dozens of published images, the authors offer a plausible explanation based on the fact that the negative stain might pool in a central

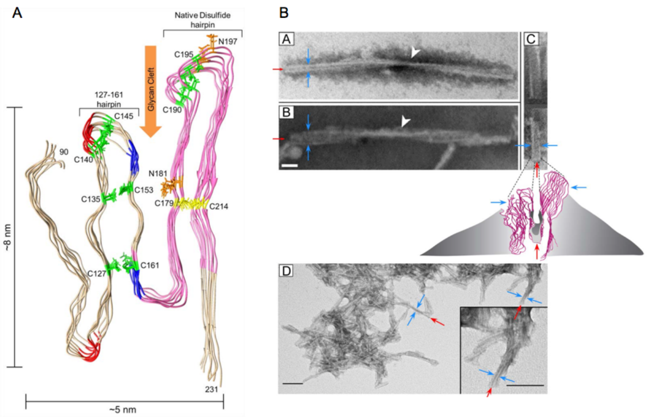

Figure 3.2. **PIRIBS model to PrP^{Sc} described by Groveman et al. (2)**. **A)** PrP^{Sc} is formed by a single monolayer of ß-sheets packed by laterally pleating in a ~10 nm narrow. ß-sheets are connected by hairpins and loops. **B)** Single protofilament forms the fibrilar state of PrP^{Sc} where the negative stain is collected into the glycan cleft.

cleft of the single, multi-pleated fiber, generating the misleading *trompe l´œil* of two protofilaments (Figure 3.2B).

In this context, the goal of the study described in this chapter is to address the question of whether the fibers are formed by the stacking of multi-rung subunits or in contrast are formed by single monomers that are stacked in a parallel in register fashion. An experimental test was designed to

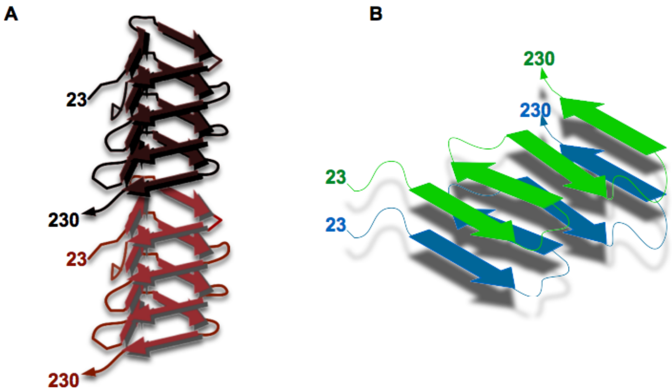

Figure 3.3. Cartoon representation of the PIRIBS and ß-solenoid models. **A**. In a **ß-solenoid** model, the polypeptide chain folds itself forming a hydrophobic core. Monomers of PrP^{Sc} is formed by the coiled forming multi-rungs of triangular or irregular cores. Each monomer stacks along the fiber axes. **B.** In **parallel in register ß-sheets** fold perpendicular to fiber axes forming a single rung of monomers, each monomer of PrP^{Sc} is stacking parallel along the fiber axes.

provide evidence which might help to make a choice between the multi-rung β-solenoid and the extensively pleated single-rung flat monomer (Figure 3.3) Kocisko *et al.* first showed that PrP^{Sc} can be partially and reversibly unfolded by treatment with Gn/HCl (3). At concentrations of guanidine that are high for a regular protein but intermediate for its extreme conformational resilience, PrP^{Sc} partially unfolds, a process that might involve changes in its secondary, tertiary and quaternary structures (3). Upon removal of the chaotropic agent, and provided that a threshold has not been crossed, partially unfolded PrP^{Sc} recovers its original PrP^{Sc} conformation and its converting activity (3). Importantly, partial unfolding renders an N-terminal portion of the characteristic (~90-230) PK-resistant core of PrP^{Sc} susceptible to degradation by PK, leaving a shorter C-terminal PK-resistant "inner core". Kocisko *et al.* performed a preliminary epitope mapping of such PK-resistant fragment, which was completed by Sajnani *et al.* and Vázquez-Fernández *et al.* (16, 17) using mass spectrometry techniques. These studies showed that the inner PK-resistant core span from position ~152/153 to the C-terminus (16, 17).

It is therefore reasonable that if PrP^{Sc} is a β-solenoid, upon Gn/HCl partial unfolding and subsequent treatment with PK, no fibers would remain. This is so because destruction of a half of its sequence must destroy necessarily one or more rungs, completely dismantling the contacts between stacked PrPSc subunits (Figure 3.4A). Therefore, persistence of fibers after such treatment would be a harsh blow to the β-solenoid proposal, and would by elimination lend support to the PIRIBS model (Figure 3.4B).

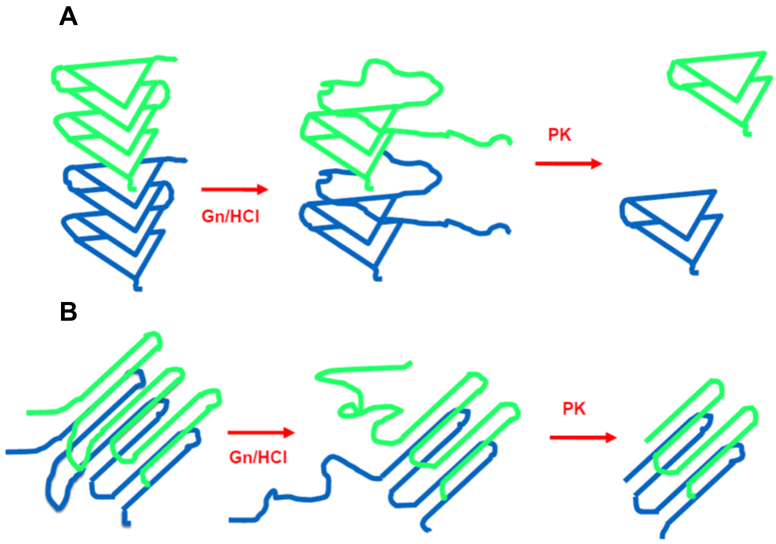

Figure 3.4. Cartoon representation of the Gn/HCl incubation and subsequent PK digestion: consequences to fiber architecture. A) Solenoid, multi-layer architecture; **B)**In register, monolayered stack architecture.

To investigate the persistence of PrP^{Sc} fibers, an experimental procedure was carried out, wherein purified GPI-anchorless PrP^{Sc} fibers were incubated with different concentrations of Gn/HCl in order to partial unfolding, as a consequence of partial unfolding, the N-terminal portion (~90-151) was exposed to PK digestion while the shorter "inner-core" ~152-230 would result resistant to proteolytic digestion (Figure 3.4). The resulting PK-resistant samples were probed with R1 and were visualized by negative stain TEM. It is important to mention that for a good yield of the analysis, the sample should contain elevated levels of PrP^{Sc}; in addition to high purity, fiber polymerization is another factor to be taken into account for the choice of the PrP^{Sc} source. Considering these factors, the transgenic mice tg44$^{+/+}$was selected for this study.

The homozygous tg44+/+ mice express PrP^C lacking the glycophosphatidylinositol (GPI) anchor. The absence of the GPI anchor leads to an abnormal glycosylation of PrP^C in endoplasmic reticulum during its post-translational modification (18, 19). In addition to this, the lack of GPI-anchor led PrP^{Sc} to accumulate in the extraneural tissue in large amyloid deposits that allows the use of centrifugation at lower speed than in a purification of PrP^{Sc} in a non-transgenic mice, these low speed avoids the sedimentation of impurities (9, 19). Clinical neurological signs appeared at 348-408 dpi (days post inoculation) with RML prions, showing higher levels of PK-res PrP than observed in the non-transgenic mice (20).

To sum up, the profile of GPI-anchorless PrP^{Sc} makes this PrP^{Sc} a good tool for the proposal study, because it is feasible to obtain from the same source, elevated levels of PrP^{Sc}, highly resistant to chaotropes like Gn/HCl (21) and purification yields/quality led to identify clearly PrP^{Sc} fibers in transmission electron microscopy (9).

Generation of homozygous GPI-anchorless PrP^C ($tg44^{+/+}$) was carried out by crossing heterozygous GPI-anchorless PrP^C ($tg44^{+/0}$) males, kindly provided by Bruce Chesebro, with wild type PrP^C (+/+) female on the background C57BL/10. Cross mating were first performed by Ester Vázquez-Fernández during her thesis studies (22) and maintained during this work (Expanded Materials and Methods, EM&M). The offspring generated were genotyped as previously indicated (20, 22) (Figure 3.5). Only mice positive to PrnpGPI-/PrnpGPI- ($tg44^{+/+}$) were used for breeding during this study.

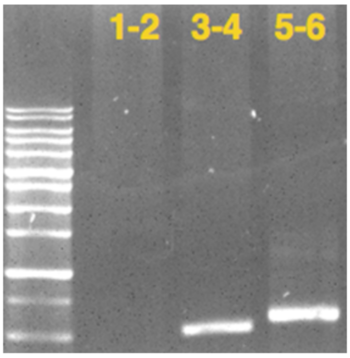

Figure 3.5.**PCR images of the genotyping of the crossbreeds**. The primers set of the null allele, Ko, (3-4) is also able to amplify the GPI-achorless transgene (PrnpGPI-) This overlapping has been observed before (22) in the case of PrnpGPI-/0 in F1 (EM&M). However, given that the possibility to confusion with PrnpGPI-/0 was avoided in the F2, the crossing was continued with safety.

GPI-anchorless-PrP^{C} mice were identified using PCR with three different oligonucleotides as well as indicated in Table 3-I of EM&M and previously reported (17, 20) (Figure 3.5). Only female homozygous GPI-anchorless mice (tg44$^{+/+}$) were inoculated at the age of 2-3 months with the prions of the Rocky Mountain Laboratory strain (RML), kindly provided by Juan María Torres, CISA, Madrid, Spain, and euthanized after 365 days post inoculation. No clinical sings were observed.

Due to the absence of clinical signs of prions diseases, the presence of GPI-anchorless-PrP^{Sc} was tested in one mouse of the RML-inoculated group. For this purpose, brain homogenization was performed in PBS at 10 % (w/v) and digested with 25µg/ml of PK for 1 hour at 37°C. Digestion was quenched by 2 mM of Pefabloc. (Figure 3.6).

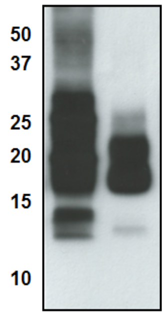

Figure 3.6. Accumulation of PrP^{Sc} in GPI-anchorless tg mice inoculated with RML. Immunoblotting was carried on using 15% SDS-PAGE and detected by 3F10 as primary antibody (epitope: 137-151) (kindly provided by JoaquínCastilla, CICBioGune, Derio, Guipúzcoa, Spain) Peroxidase-labelled (GE Healthcare Little Chalfont, UK) antimouse was used as a secondary antibody at 1:5000 dilution. (GE Healthcare Little Chalfont, UK)

Once the presence of GPI-anchorless-PrP^{Sc} was confirmed, isolation and purification of GPI-anchorless PrP^{Sc} fibers were carried on using the previously reported procedure (9) with small changes (Figure 3.7) that are detailed in EM&M.

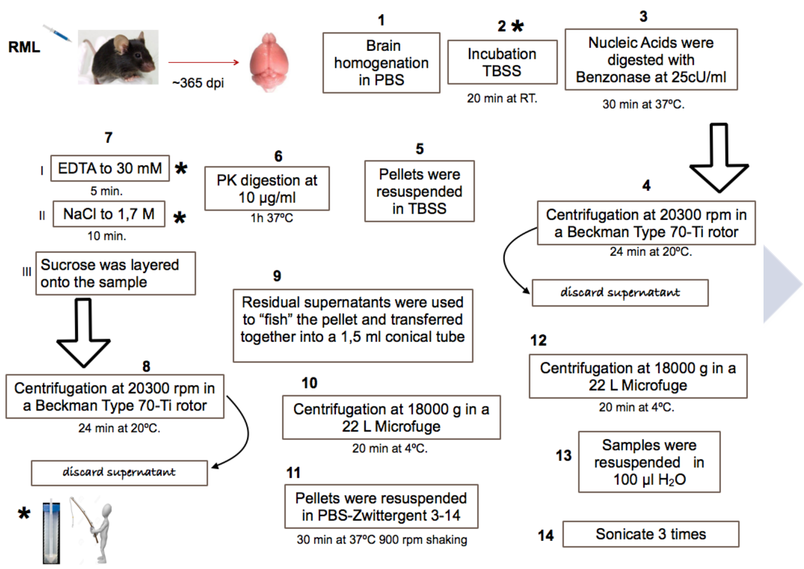

Figure 3.7.Scheme of the purification of GPI-anchorless PrP^{Sc}. Tg 44$^{+/+}$ mice were inoculated with RML prions.Brains were rinsed with PBS and prepared in 10% of PBS. Brain homogenates (BH) were adjusted to contain 50 mM of Tris-HCl, 137 mMNaCl and 2% salkosyl, (TBSS). After incubation at room temperature (RT) for 20 minutes, nucleic acids were digested with the addition of Benzonase. The sample was centrifuged at 20300 (poner g, no rpm) rpm in a Beckman Type 70 Ti-rotor. Pellets were resuspended in TBSS and incubated at 37 °C for a digestion with PK. GPI-anchorless PrP^{Sc} were pelleted in a sucrose cushion at 20300 rpm in a Beckman Type 70 Ti-rotor. Sample were "fished", and transferred into a 1,5 ml conical tube and sedimented at 20.000 rpm in a microfuge. Pellets were resupended in PBS-Zwittergent 3-14 sonicated one pulse and incubated at 30°C for 30 minutes at 900 rpm shaking. GPI-anchorless PrP^{Sc} was pelleted in a microfuge. The final GPI-anchorless PrP^{Sc} was resuspended in 100 µl of spH_2O (two conical tubes of 1,5 ml, 100µl each) and sonicated 3 times at 50% of amplitude with a probe ultrasonic homogenizer (Cole Parmer Instrument CO., Chicago, IL, USA).

Purified GPI-anchorless PrP^{Sc} fibers were subjected to biochemical analyses to assess the purity of preparations. Analysis by 15% SDS-PAGE with Coomassie and SYPRO Ruby staining showed that the preparations of purified GPI-anchoreless PrP^{Sc} were highly pure (Figure 3.8A and 8B respectively). The doublet band observed around the 17 KDa is due to the existence of a "ragged end" pattern of PK cleavage around 88-90 (17). In addition to this, negative staining samples observed by TEM showed GPI-anchorless fibers highly pure (Figure 3.8 C). Nevertheless, traces of tubulin were also observed in some purification samples (Figure 3.8 D). It is not surprising at all to find tubulin in some preparations since it is a protein that

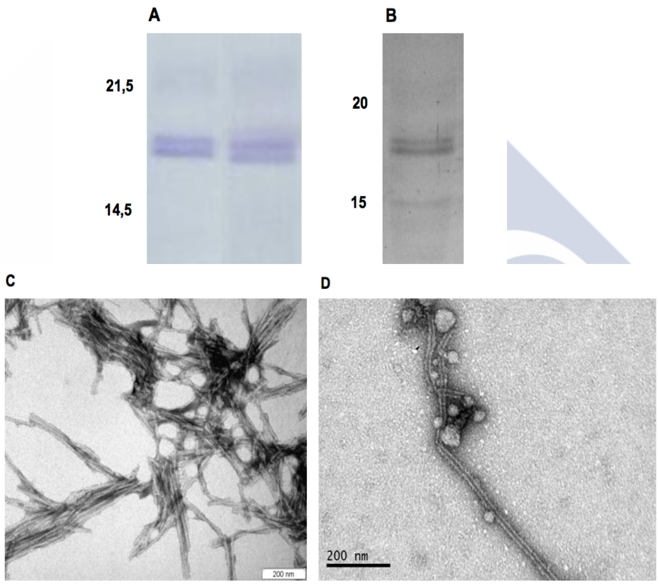

Figure 3.8.Characterization of purified GPI-anchorless PrP^{Sc}. 5 µl of sample was loaded on 15% SDS-PAGE gel. Electrophoresis was carried following the same conditions described in EM&M. Purity was assessed by staining with **A)** Coomassie and **B)** Sypro Ruby. For negative staining visualization in TEM, 10 µl of the sample was loaded into a glow-discharged gold-grids and stained with 2% of AcU as described in EM&M. **C)** Purified GPI-anchorless PrP^{Sc}. **D)** Tubulin impurities were observed in some preparations.

co-purifies with PrP^{Sc} (23).

Once the GPI-anchorless PrP^{Sc} is purified, to verify if the isolated GPI-anchorless PrP^{Sc} retains its infectivity after purification, a bioassay was performed using a set of six female wild type mice with the background C57BL/6. Mice were inoculated with purified GPI-anchorless PrP^{Sc} or with GPI-anchorless PrP^{Sc} BH and with PBS as negative control. To estimate the amount of purified GPI-anchorless PrP^{Sc} suitable for inoculation, serial dilution of the purified material was compared with 2% RML infected mice brain homogenate, which was used to inoculate WT mice and $tg44^{+/+}$ mice. The amount of total PK-res GPI-anchorless PrP is around 10 times less than RML (Figure 3.9 A, lane 1). Because of that, the inoculum used from then on was the purified GPI-anchorless PrP^{Sc} to final dilution at 1/10 in PBS-5% Glucose.

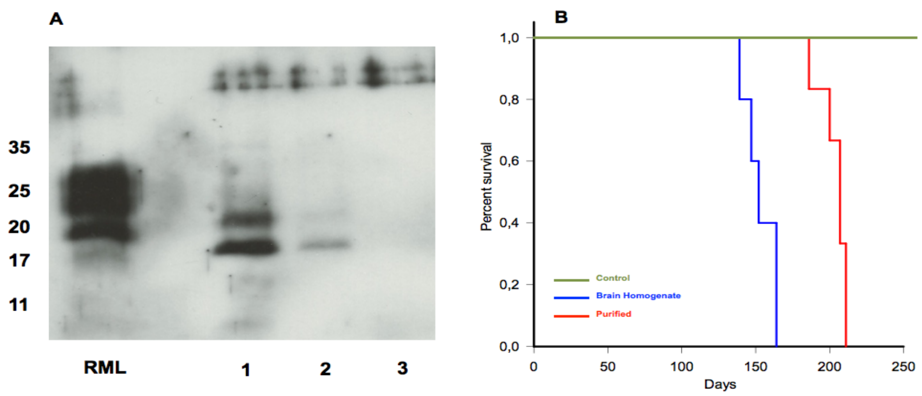

Figure 3.9. Characterization of purified GPI-anchorless PrP^{Sc}. A. Comparison of the RML inoculum and purified GPI-anchorless PrP^{Sc} varying the dilution.RML; 2% of brain homogenate from mice infected with RML, used as inoculum in the WT mice inoculation.Line 1-3; serial dilution of purified GPI-anchorless PrP^{Sc} (1/10; 1/100; 1/100 respectively). Samples were treated with 20 µg/ml of PK and probed with R1 antibody (225-230). Inoculum was performed with purified GPI-anchorless to 1/10 dilution in PBS-5% glucose. **B.** Kaplan-Meier curve plot survival of WT mice inoculated with purified GPI-anchorless PrP^{Sc} (red) (203 ±9 days inoculated with 2% GPI-anchorless PrP^{Sc} brain homogenate (BH), (blue) (153 ±10 days) and inoculated with PBS as negative control (green) (n=6, P< 0,05 Breslow-Wilcoson test)

All mice were inoculated intra-cerebrally (IC) with 20 µl of the corresponding inoculum in the right temporal lobe at the age of 6 months. All female wild type mice inoculated with purified GPI-anchorless PrP^{Sc} succumbed after 204 ± 9 days post inoculation (Figure 3.9B) and developed classical signs of prion disease as well as what was previously reported, when wild type mice were inoculated with GPI-anchorless PrP^{Sc} brain homogenate (17, 21). Mice inoculated with GPI-anchorless PrP^{Sc} brain homogenate, died after 150 days developing classical neurological signs of prion disease (20). The extended incubation time observed, is consistent with the degradation of the PK-sensitive as a consequence of the PK digestion as a part of the purification protocol, thus reducing the prion titer (24, 25). Another explanation for this increase is the nature of the purified GPI-anchorless PrP^{Sc}, which shows high levels of aggregation that are related to lower the effective titer (26, 27). Mice were humanely euthanized once the signs of prion disease appeared. For biochemical studies, brains were longitudinally cut in two halves. One of these was stored at -80ºC until use. For histopathology, the other half brain was stored in 10% formaldehyde (formalin). Brains fixed in formalin were shipped to Enric Vidal (CReSA, Barcelona, Spain) for histopathology study. Brains were sliced and treated as described in EM&M. Brains were stained with haematoxylin-eoisn (HE) to characterize the lesion profile. Deposits of PrP^{Sc} were found in mice inoculated with PrP^{Sc} (P-PrP^{Sc} or BH-PrP^{Sc}) by probing the brain sections with 2G11 primary antibody. Astrocyte activation was observed with rabbit polyclonal antibody against glial fibrillary acidic protein. Only brains from mice inoculated with PrP^{Sc} (BH-GPI anchorless PrP^{Sc}, purified GPI-anchorless PrP^{Sc}) showed spongiosis (Figure 3.10, D and

G) PK-res PrP deposits (Figure 3.10, E and H) and astroglial activation (Figure 3.10, F and I), all of them, hallmarks of prion diseases.

Brain homogenization was performed in 10 % of PBS to carry out

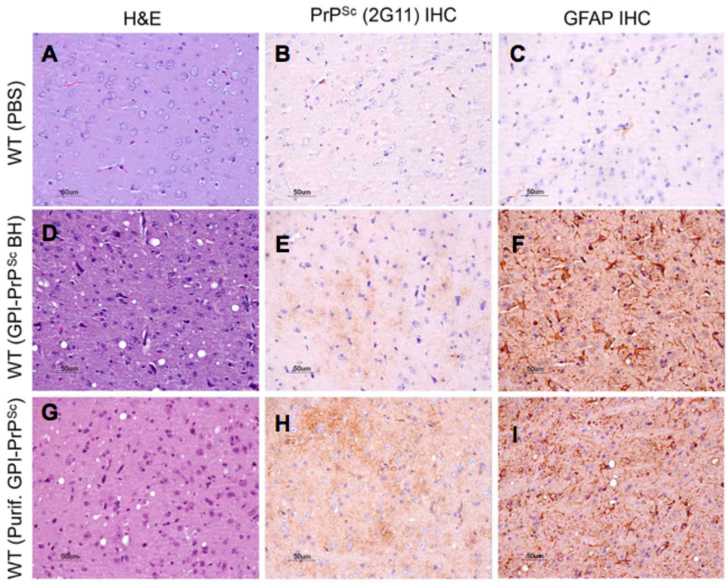

Figure 3.10. Histopathology of the brains from animals used in the bioassay inoculated with GPI-anchorless PrP^{Sc} brain homogenate and with purified GPI-anchorless PrP^{Sc}. One section was stained with hematoxylin and eosin (H&E, left), two others were analyzed via immunohistochemistry (IHC) using the anti-PrP antibody 2G11 (middle), and an antibody against the glial fibrillary acidic protein (GFAP) to reveal astroglial activation (right). Control WT mice inoculated with PBS (A to C). WT mice infected with GPI-anchorless PrP^{Sc} BH (D to F); and WT mice infected with purified GPI-anchorless PrP 27-30 (G to I). All mouse groups, except those inoculated with PBS, show spongiform change, PrP^{Sc} deposition and astroglial activation characteristic of a prion disease

biochemical analysis. To test the presence of PK-res PrP, BH was challenged by PK digestion at 25 µg/ml for 1 hour at 37^{o}C. Immunoblotting of mouse inoculated with purified GPI-anchorless PrP^{Sc} revealed the presence of PK-res PrP (Figure 3.11 lanes 6 and 7)

Once the infectivity of purified GPI-anchorless PrP^{Sc} was confirmed, the sample was used to challenge to proposal that the basic architecture of PrP^{Sc} conforms to a multi-rung ß-solenoid by assessing the persistence of fibers after PK treatment of partially unfolded GPI-anchorless PrP^{Sc} fibers.

To test the hypothesis that the digestion of the N-terminal half of the

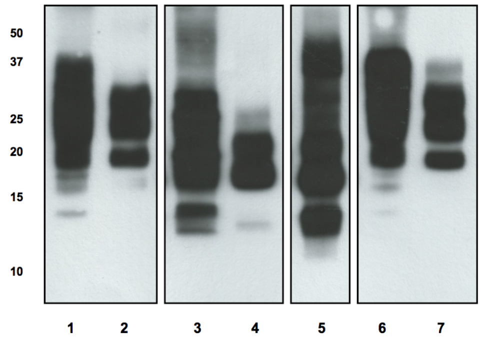

Figure 3.11. Immunoblottingof the serial passage of RML PrP^{Sc}. Western blot probed with 3F10 antibody (137-151) revealing the presence of PK-res PrP. Lines 1-2. Brain homogenate (BH) from wild type mouse inoculated with RML. Lanes 3-4. RML-infected GPI-anchorless PrP transgenic mouse BH. Line 5, purified GPI-anchorless PrP^{Sc}. Lines 6-7. BH of mouse infected with purified GPI-anchorless PrP^{Sc} with the same 1/10 dilution showed in Figure 3.9A.

protein would result in a disassembly of fibers, purified GPI-anchorless PrP^{Sc} fibers were treated with increasing concentrations of Gn/HCl and subsequently digested with PK. The resulting fibers were analyzed by immunoblotting and TEM, following the scheme represented in Figure 3.12. GPI-anchorless PrP^{Sc} fibers were treated with increasing concentrations of Gn/HCl in order to partially unfold it to a degree at which the ~90-230 PK-resistant core becomes partially sensitive to PK, with only an “inner PK-resistant core”spanning residues ~153 to 230 resist the proteolytic action of PK as well as observed previously by Vázquez-Fernández *et al.* (17). Immunoblotting was performed using R1 antibody that recognizes residues 225-230 at 1:5000 dilution (a kind gift from Anna Serban, USCF). Peroxidase-labelled anti-human antibody at 1:5000 dilution was used as secondary antibody (Figure 3.12).

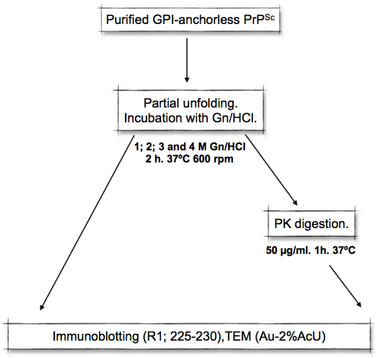

Figure 3.12. Scheme of the treatment of purified GPI-anchorless PrP^{Sc} fibers treatment. The experimental procedure is detailed in EM&M.

Treatment with 4M Gn/HCl followed by PK digestion results in a persistence of a fragment around 10 KDa of molecular width, that corresponds with the "inner PK-resistant core" fragment that spans ~153-230 (Figure 3.13). Previous studies used less amount of Gn/HCl to explore the resistance to chaotropes (3, 17). However in the latter case, an increased amount and a longer incubation in Gn/HCl (see EM&M) was needed to degrade the full length ~90-230 PrP^{Sc} leading the "inner-core" ~153-230 resistant to PK digestion.

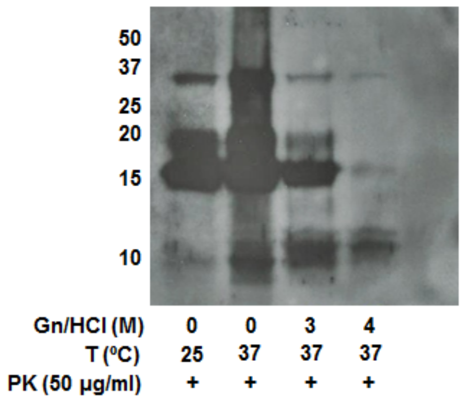

Figure 3.13.Immunoblotting of GPI-anchorless PrP^{Sc} after partial unfolding with Gn/HCl and subsequent treatment with PK. A) 0M Gn/HCl. **B)** 3M Gn/HCl. **C)** 4M Gn/HCl. A 10 kDa PK-resistant "inner core" spanning ~152-232 (18) remains after PK treatment of samples partially unfolded with 4M Gn/HCl

The samples treated with Gn/HCl and PK digestion were imaged using TEM after negative staining with 2% uranyl acetate. Gold grids were glow discharged previous to sample loading (see EM&M). To visualize the PrP^{Sc} deposited in the grids, the zones with high levels of contrast were magnified. The proportion of fibers:aggregates were estimated by the observation of the numbers of isolated fibers and aggregates in different quadrants until covering the majority of the high-contrast zones. The proportion observed in each sample is summarized in Table 3-I. A set of representative images from non-treated / treated samples is shown in Figure 3.14. The treatment of GPI-anchorless PrP^{Sc} with 4 M Gn/HCl had the effect of partially disassembling the fibers (Figure 3.14 C). While untreated samples contain ~95% of fibers vs. 5% of small aggregates (Figure 3.14 A) (Table 3-I), in the Gn/HCl treated samples the proportion of fibers to aggregates decreased to 50/50 (Figure 3.14 C) (Table 3-I). When the samples that had been incubated with Gn/HCl were further treated with 50 μg/ml of PK (Figure 3.13), very few fibers were left (Figure 3.14 D), with an estimated ratio of fibers: aggregates of 10:90 (Table 3-I). The very occasional, short residual fibers seen, would be compatible with traces of ~90-230 PK-resistant cores seen in the Western blot (Figure 3.13). In contrast, treatment with PK under the same conditions of control samples, not subjected to Gn/HCl-induced partial unfolding, resulted only in a modest destruction of fibers (Figure 3.14 A and Table 3-I).

Table 3-I. Semiquantitative assessment of fiber/disassembled aggregates in GPI-anchorless PrP^{Sc} samples

Sample	Gn/HCl (M)	PK (µg/ml)	Ration estimated “fibers:aggregates”	Relative amount of fibers
A	0	0	95:5	+++++
B	0	50	90:10	+++++
C	4	0	50:50	+++
D	4	50	10:90	+

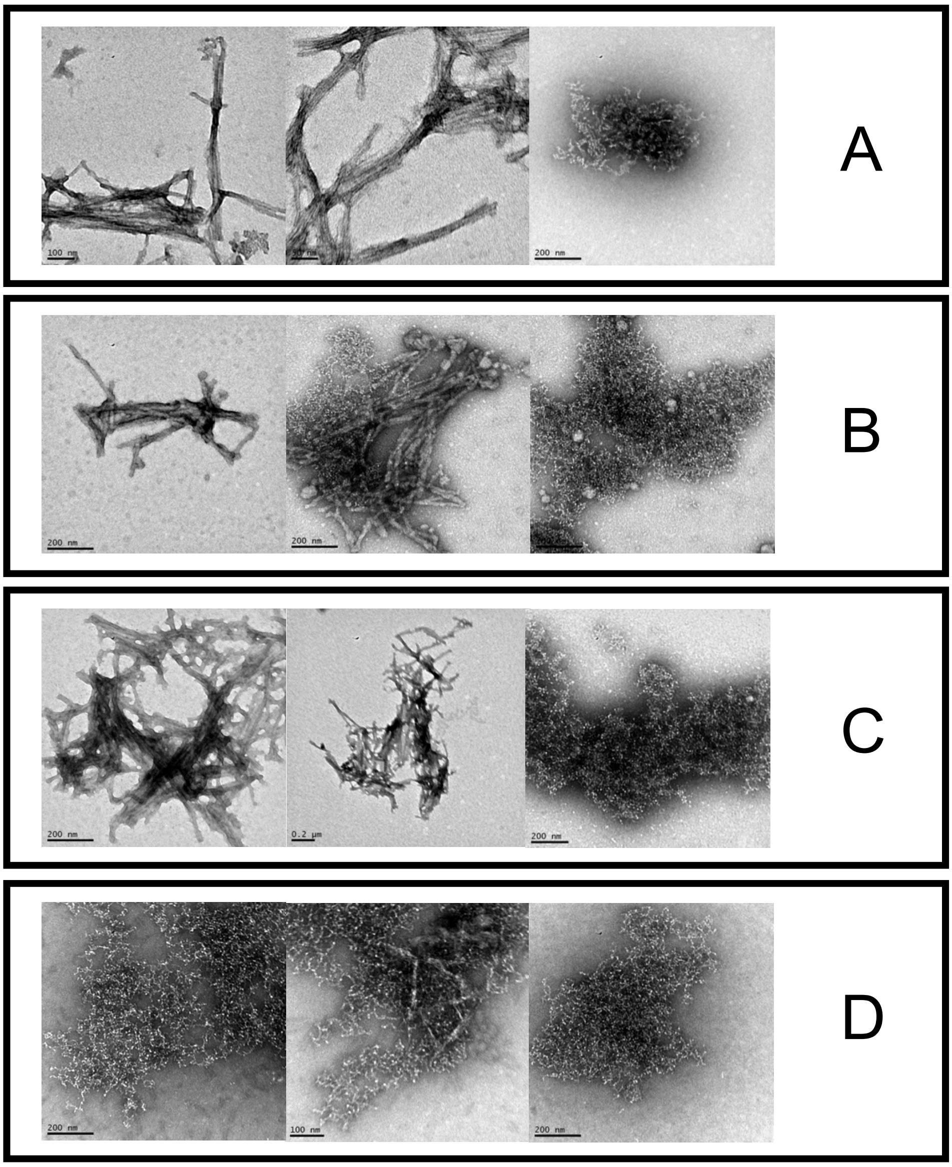

Figure 3.14. PK digestion of partially unfoded GPI-anchorless PrP^{Sc} results in virtually complete disappearance of fibers. **A**) Control samples (no Gnd/HCl/no PK); **B**) 0 M Gnd/HCl, PK digestion; **C**) 4 M Gnd/HCl alone; **D**) 4M Gnd/HCl and subsequent digestion with PK.

In recombinant PrP (rPrP) amyloids, the residues spanning 90-140 are less likely to form the core structure in PrP^{Sc} and found to be more exposed to the solvent (10, 12, 28). It is therefore not surprising that upon treatment with PK, the most abundant PK-resistant cores are 152/153–230 and 162–230 (29). Such architecture of rPrP fibrils was also supported by immunoconformational microscopy (a technique that uses an array of antibodies for recognizing specific regions, which are visualized by fluorescence microscopy) of single fibrils that showed that the epitopes within the region 90-150 were partially solvent exposed, whereas the region 162-230 was buried under native conditions and was the most resistant to the Gn/HCl-induced denaturation (Figure 3.4 B) (30). In addition to this, given that the cross-β hydrogen bonds that hold the fibers together are formed exclusively by the amyloid core, with the unfolded N-terminal regions protruding out (~90-150), the PK treatment does not destroy rPrP amyloid fibers (31) (Figure 3.4 B). For this reason, treatment with the Gn/HCl was not necessary for rPrP amyloid fibers. To test the persistence of the rPrP fibrilar architecture after PK digestion, the collaboration with Professor Ilia V. Baskakov (University of Maryland, Baltimore, USA) was sought. Prof. Baskakov performed an experimental study in which the recombinant mouse PrP23-230 was expressed and converted into the amyloid form as well as what was reported by Bochorova *et al.* (32). rPrP fibers were digested with PK at different ratios and visualized by TEM (Figure 3.15) (32).

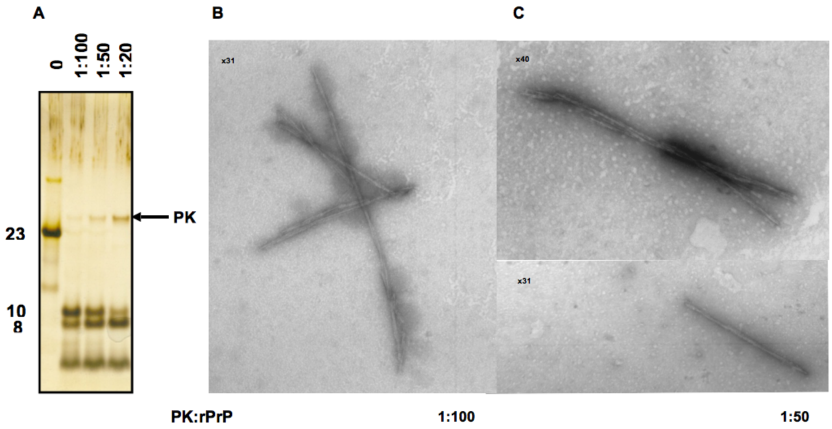

Figure 3.15.PK treatment of rPrP amyloid fibers does not affect their fibrillar integrity. A) Silver stained SDS-PAGE showing that PK treatment of rPrP amyloid fibers leaves only 10 and 8 kDa bands (aa. 152-230 and 162-230, respectively) fragments and smaller. Bocharova Protein Science**B)**negative stain TEM of rPrP amyloid fibers after PK (1:100) ; **C)** negative stain TEM of rPrP amyloid fibers after PK (1:50) (32)

Electron microscopy images (Figure 3.15 B and C) negatively stained amyloid fibrils revealed intact single fibrils suggesting that the amyloid core persists after the proteolytic digestion with PK (10-8 KDa, Figure 3.15 A) whereas the architecture of purified GPI-anchorless PrP^{Sc} fibers architecture succumbed to proteolytic digestion after partial unfolding.

It could be argued that the Gn/HCl itself has a disaggregating effect, but only a fraction of the fibers are disaggregated in the absence of a subsequent treatment with PK (Fig. 14 C and Table 3-I). Another possible explanation for the disappearance of fibers would be that even in the non-disaggregated fibers remaining after treatment with Gn/HCl, some subtle destabilization effect exists that leads to complete disaggregation upon subsequent treatment with PK. However, it is difficult to envision which kind of effect that might be. Another possibility that can explains the fact of why a portion of GPI-anchorless-PrP^{Sc} fibers disassembles in the presence of Gn/HCl is that while sharing an overall structural similarity with rPrP amyloids, GPI-anchorless PrP^{Sc} is subtly different from it, and therefore its PK-resistant ~152-230 "inner cores" are unable to sustain fibers as the equivalent amyloid cores present in rPrP amyloid fibers do; however, once more, it is difficult to envision structural differences with that effect. All things considered, the most parsimonious conclusion is that the structure of GPI-anchorless PrP^{Sc} and that of flat $rPrP^{Sc}$ are different.

Conclusions

Many models have been proposed to solve the PrP^{Sc} structure for years, however most of them are not able to comply fully with the experimental structural constraint available (7). Nevertheless, today, there are two models that argue with the majority of experimental constraints. A) **ß-soleoind model**: monomers of PrP^{Sc} coil themselves to form a multi-rung ß-solenoid. The vertical stacking of individual subunits of ß-solenoid would result in a narrow protofilament complying with the ~5 nm width constraint. Intertwined protofilaments exhibits a 10 nm of fiber width, as observed in numerous negative staining TEM studies (4, 8, 11). Reflection of 4,8Å detected by fiber X-ray diffraction of PrP^{Sc} samples (8, 33) indicates the intramolecular hydrogen bound between two ß-strands. In the model of a ß-solenoid, this distance corresponds to the distance between two rungs that running along the fiber axis. Vázquez-Fernández et al. (17) have recently used limited proteolysis to map the interspersed β-strands and connecting loops that conform the PrP^{Sc} monomers. Using high resolution tricine SDS-PAGE followed by epitope mapping, and mass spectrometry, they identified several PK cleavage sites. Such sites define loops and/or borders of β strands. The 5 nm of width that the monomers have can occupy, the 4,8 Å of the spacing between rungs and the cleavage points suggest that monomers of PrP^{Sc} are multi-rung solenoids that stack along the protofilament, in a similar way that the architecture adopted by the fungal prion HET-s (Figure 3.1).

The results described in this chapter have shown a destruction of the fiber architecture while the amount of aggregates was increased. This result is in agreement with the idea that PrP^{Sc} is coiled itself into a ß-sheet rungs where once the N-terminal half was unfolded and digested with PK, stacking of subunits could not be supported and fibers were disassembled in aggregates.

B) PIRIBS model (2): According to this model, thePrP^{Sc} fiber does not contain two identical protofilaments, rather, PrP^{Sc} fibers consist of a single molecule, ~10 nm wide, and each monomer arranges into a single monolayer of ß-sheets packed by laterally pleating. ß-sheets are connected by loops and hairpins in the same plane or "flat". The glycan cleft, located in the middle of two hairpins (127-161 and 179-214) could collect stain when the fibers are negative stained to be visualized by TEM, giving the misleading visual impression of two protofilaments. Each monomer stacks in register with an intermolecular spacing of 4,8 Å indicating that the ß-sheets are parallel alignment along the fibril axis (Figure 3.2A). The stacking of each monomer forms an individual protofilament in similar way than a half pipe where the negative stain is located in the glycans cleft.

In the study described in this chapter, recombinant PrP fibers were used due to its similar architecture than PIRIBS. The proteolytic digestion with different ratios of PK resulted in a digestion of its N-terminal half, leaving the C-terminus intact. This result is in agreement with what observed when the infectious and purified GPI-anchorless PrP^{Sc} were digested with PK under partial unfolding (Figure 3.4). However the resulting PK resistant architecture is greatly different; while the rPrP fibers retain its fibrilar status, no fibers were found in samples after PK digestion in partial unfolding GPI-anchorless PrP^{Sc} fibers.

In conclusion, although the results shown in this chapter cannot define the PrP^{Sc} structure, they provide new evidence in support of the hypothesis that the fibers of PrP^{Sc} are formed by stacking of multilayered, instead of monolayered subunits, that stack parallel in register.

References.

1. Vázquez-Fernández E, V. M., Cebey L, Renault L, Sevillano AM, Peters PJ, Fernández JL, Young H, Wille H, Requena JR. (2014) Recent advances towards an understanding of the structure of PrP^{Sc}. *International Prion Congress 2014* (Chernoff, Y. O. ed., Landes Bioscience, Trieste

2. Groveman, B. R., Dolan, M. A., Taubner, L. M., Kraus, A., Wickner, R. B. and Caughey, B. (2014) Parallel in-register intermolecular beta-sheet architectures for prion-seeded prion protein (PrP) amyloids. *J Biol Chem* 289, 24129-24142

3. Kocisko, D. A., Lansbury, P. T., Jr. and Caughey, B. (1996) Partial unfolding and refolding of scrapie-associated prion protein: evidence for a critical 16-kDa C-terminal domain. *Biochemistry* 35, 13434-13442

4. Prusiner, S. B. (1998) Prions. *Proc Natl Acad Sci U S A* 95, 13363-13383

5. Aguzzi, A. and Polymenidou, M. (2004) Mammalian prion biology: one century of evolving concepts. *Cell* 116, 313-327

6. Diaz-Espinoza, R. and Soto, C. (2012) High-resolution structure of infectious prion protein: the final frontier. *Nat Struct Mol Biol* 19, 370-377

7. Requena, J. R. and Wille, H. (2014) The structure of the infectious prion protein: experimental data and molecular models. *Prion* 8, 60-66

8. Wille, H., Bian, W., McDonald, M., Kendall, A., Colby, D. W., Bloch, L., Ollesch, J., Borovinskiy, A. L., Cohen, F. E., Prusiner, S. B. and Stubbs, G. (2009) Natural and synthetic prion structure from X-ray fiber diffraction. *Proc Natl Acad Sci U S A* 106, 16990-16995

9. Baron, G. S., Hughson, A. G., Raymond, G. J., Offerdahl, D. K., Barton, K. A., Raymond, L. D., Dorward, D. W. and Caughey, B. (2011) Effect of glycans and the glycophosphatidylinositol anchor on strain dependent conformations of scrapie prion protein: improved purifications and infrared spectra. *Biochemistry* 50, 4479-4490

10. Smirnovas, V., Baron, G. S., Offerdahl, D. K., Raymond, G. J., Caughey, B. and Surewicz, W. K. (2011) Structural organization of brain-derived

mammalian prions examined by hydrogen-deuterium exchange. *Nat Struct Mol Biol* 18, 504-506

11. Sim, V. L. and Caughey, B. (2009) Ultrastructures and strain comparison of under-glycosylated scrapie prion fibrils. *Neurobiol Aging* 30, 2031-2042

12. Tycko, R., Savtchenko, R., Ostapchenko, V. G., Makarava, N. and Baskakov, I. V. (2010) The α-helical C-terminal domain of full-length recombinant PrP converts to an in-register parallel beta-sheet structure in PrP fibrils: evidence from solid state nuclear magnetic resonance. *Biochemistry* 49, 9488-9497

13. Amenitsch, H., Benetti, F., Ramos, A., Legname, G. and Requena, J. R. (2013) SAXS structural study of PrP(Sc) reveals ~11 nm diameter of basic double intertwined fibers. *Prion* 7, 496-500

14. Wille, H., Michelitsch, M. D., Guenebaut, V., Supattapone, S., Serban, A., Cohen, F. E., Agard, D. A. and Prusiner, S. B. (2002) Structural studies of the scrapie prion protein by electron crystallography. *Proc Natl Acad Sci U S A* 99, 3563-3568

15. Wasmer, C., Lange, A., Van Melckebeke, H., Siemer, A. B., Riek, R. and Meier, B. H. (2008) Amyloid fibrils of the HET-s(218-289) prion form a beta solenoid with a triangular hydrophobic core. *Science* 319, 1523-1526

16. Sajnani, G., Pastrana, M. A., Dynin, I., Onisko, B. and Requena, J. R. (2008) Scrapie prion protein structural constraints obtained by limited proteolysis and mass spectrometry. *J Mol Biol* 382, 88-98

17. Vazquez-Fernandez, E., Alonso, J., Pastrana, M. A., Ramos, A., Stitz, L., Vidal, E., Dynin, I., Petsch, B., Silva, C. J. and Requena, J. R. (2012) Structural organization of mammalian prions as probed by limited proteolysis. *PLoS One* 7, e50111

18. Rogers, M., Yehiely, F., Scott, M. and Prusiner, S. B. (1993) Conversion of truncated and elongated prion proteins into the scrapie isoform in cultured cells. *Proc Natl Acad Sci U S A* 90, 3182-3186

19. Walmsley, A. R., Zeng, F. and Hooper, N. M. (2001) Membrane topology influences N-glycosylation of the prion protein. *EMBO J* 20, 703-712

20. Chesebro, B., Race, B., Meade-White, K., Lacasse, R., Race, R., Klingeborn, M., Striebel, J., Dorward, D., McGovern, G. and Jeffrey, M. (2010) Fatal transmissible amyloid encephalopathy: a new type of prion disease associated with lack of prion protein membrane anchoring. *PLoS Pathog* 6, e1000800

21. Bett, C., Kurt, T. D., Lucero, M., Trejo, M., Rozemuller, A. J., Kong, Q., Nilsson, K. P., Masliah, E., Oldstone, M. B. and Sigurdson, C. J. (2013) Defining the conformational features of anchorless, poorly neuroinvasive prions. *PLoS Pathog* 9, e1003280

22. Vazquez-Fernandez, E. (2012) Structural studies of PrP^{Sc}. PhD, Universidad Santiago de Compostela

23. Giorgi, A., Di Francesco, L., Principe, S., Mignogna, G., Sennels, L., Mancone, C., Alonzi, T., Sbriccoli, M., De Pascalis, A., Rappsilber, J., Cardone, F., Pocchiari, M., Maras, B. and Schinina, M. E. (2009) Proteomic profiling of PrP27-30-enriched preparations extracted from the brain of hamsters with experimental scrapie. *Proteomics* 9, 3802-3814

24. Safar, J., Wille, H., Itri, V., Groth, D., Serban, H., Torchia, M., Cohen, F. E. and Prusiner, S. B. (1998) Eight prion strains have PrP(Sc) molecules with different conformations. *Nat Med* 4, 1157-1165

25. Sajnani, G., Silva, C. J., Ramos, A., Pastrana, M. A., Onisko, B. C., Erickson, M. L., Antaki, E. M., Dynin, I., Vazquez-Fernandez, E., Sigurdson, C. J., Carter, J. M. and Requena, J. R. (2012) PK-sensitive PrP is infectious and shares basic structural features with PK-resistant PrP. *PLoS Pathog* 8, e1002547

26. Gabizon, R., McKinley, M. P. and Prusiner, S. B. (1987) Purified prion proteins and scrapie infectivity copartition into liposomes. *Proc Natl Acad Sci U S A* 84, 4017-4021

27. Silveira, J. R., Raymond, G. J., Hughson, A. G., Race, R. E., Sim, V. L., Hayes, S. F. and Caughey, B. (2005) The most infectious prion protein particles. *Nature* 437, 257-261

28. Cobb, N. J., Apostol, M. I., Chen, S., Smirnovas, V. and Surewicz, W. K. (2014) Conformational stability of mammalian prion protein amyloid fibrils

is dictated by a packing polymorphism within the core region. *J Biol Chem* 289, 2643-2650

29. Bocharova, O. V., Breydo, L., Salnikov, V. V., Gill, A. C. and Baskakov, I. V. (2005) Synthetic prions generated *in vitro* are similar to a newly identified subpopulation of PrP^{Sc} from sporadic Creutzfeldt-Jakob Disease. *Protein Sci* 14, 1222-1232

30. Novitskaya, V., Makarava, N., Bellon, A., Bocharova, O. V., Bronstein, I. B., Williamson, R. A. and Baskakov, I. V. (2006) Probing the conformation of the prion protein within a single amyloid fibril using a novel immunoconformational assay. *J Biol Chem* 281, 15536-15545

31. Anderson, M., Bocharova, O. V., Makarava, N., Breydo, L., Salnikov, V. V. and Baskakov, I. V. (2006) Polymorphism and ultrastructural organization of prion protein amyloid fibrils: an insight from high resolution atomic force microscopy. *J Mol Biol* 358, 580-596

32. Baskakov, I. V. and Bocharova, O. V. (2005) *In vitro* conversion of mammalian prion protein into amyloid fibrils displays unusual features. *Biochemistry* 44, 2339-2348

33. Nguyen, J. T., Inouye, H., Baldwin, M. A., Fletterick, R. J., Cohen, F. E., Prusiner, S. B. and Kirschner, D. A. (1995) X-ray diffraction of scrapie prion rods and PrP peptides. *J Mol Biol* 252, 412-422

Expanded Materials and methods.

Generation of transgenic homozygous anchorless PrP mice, tg44+/+.

Ester Vázquez- Fernández performed different intercrossing to create the homozygous GPI anchorless PrP line during her thesis (1).

Transgenic heterozygous GPI-anchorless mice (tg44+/-) (generously provided by Buce Chesebro, from the Rocky Mountain Laboratories, NIH, Montana, USA) were crossed with wild-type PrP (+/+) on the C57BL/10 background (F0) followed by serial intercrossing (Figure E3.1A) until transgenic homozygous GPI-anchorless mice (tg44+/+) were generated (Figure E3.1A, F3). Mice were genotyped by DNA PCR test on tail DNA (Figure E3.1B).

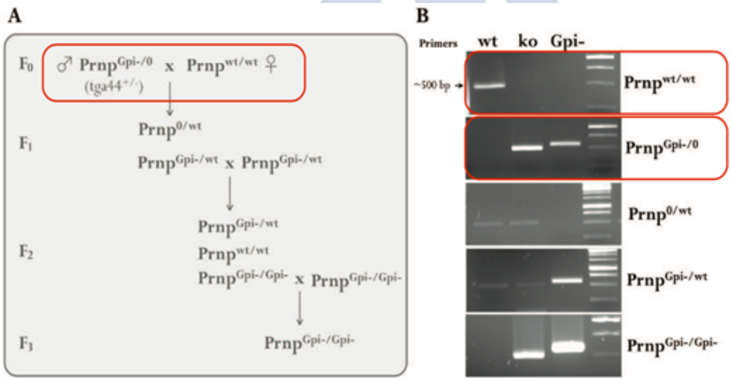

Figure E3.1. A) Family tree of GPI-anchorless transgenic mice B) PCR genotyping was done using three sets of primers. Images taken from Ester Vázquez Fernández´s Thesis.(1).

Mice tail excision was done as indicated by manufacturer´s protocol (REALPURE DNA extraction kit, Durviz, s.l.u. Valencia, Spain). Polymerase Chain Reaction, PCR, was performed using 200 µM as final concentration of forward and reverse oligonucleotide primers, 10 ng/µl of DNA and 0,025 U/µl of PrimeSTAR HS DNA polymerase Takara (Bio Inc. Otsu, Japan). Temperature and number of cycles used in the PCR reaction, as well as the oligonucleotide sequence used is indicate in the Table E3-I. Offspring genotyping was carried out by PCR using a set of primers; for normal anchored mouse PrP allele (WT), null allele (KO) and anchorless PrP transgene allele (GPI-anchorless) (1-2) indicated in Table E3-I.

Table E3-1. **Temperature, time and cycles of PCR.**

Temperature (ºC)	Time (sec)	
94	30	
94	60	27 cycles
60	30	
72	60	
72	300	
4	∞	

WT: F2057—> 5´CCAAGGAGGGGGTACCCAT3´ (1)
R2038—> 5´TCCCACGATCAGGAAGATGAG3´ (2)
PrPnullallele. KO. F1179—> 5´GATGGATTGCACGCAGGTTC3´ (3)
R1180—> 5´TTGAGCCTGGCGAACAGTTC3. (4)
GPIlesstg: F624—> 5´AACCGTTACCCACCTCAGGGT3´ (5)
R2037—> 5´CAGGGCGCCTCGAGACGCGTCA3´(6)

Mouse GPI-anchorless PrP^{Sc} isolation

Purification of GPI-anchorless PrP^{Sc} was performed according to a previously reported protocol by Baron *et al.* (2) with small changes.

RML-infected, GPI-anchorless mice, tg44$^{+/+}$, were humanly euthanized after 365 days post inoculation. No clinical signs of prion diseases were observed. Brains were harvested and stored at -80ºC until use.

Three and a half brains were placed in a Petri-dish and rinsed with PBS previously filtered with 0,45 µm filters (Merck Millipore, Billerica, MA, USA) to remove residual blood and hairs. Brains were cut with a scalpel into small pieces to enhance the homogenization. Brain homogenazation was carried out with 15 ml of PBS using a 50ml WHEATON® homogenizer^{+} (WHEATON industries Inc, NJ, USA). Brain homogenates (BH) was placed in two 50 ml conical tubes (Vertex technics S.L., Barcelona, Spain) (8 ml per tube). In each tube, the sample was adjusted to contain 50 mM Tris-HCl (pH8.0 at RT), 137 mM NaCl and 2% sarkosyl to a final volume of 24 ml. The mixture was incubated at room temperature (RT) for 20 minutes. Sample was mixed several times by inversion. Nucleic acids, were digested by addition of 25 U/ml of Benzonase (Sigma-Aldrich, St Louis, MO, USA) and incubation at 37ºC for 30 minutes*. Sample was then transferred to a 26 ml ultracentrifuge tube (Beckman Coulter, Brea, CA, USA). Ultracentrifugation was carried out at 18198 g for 24 min at 20ºC in a Beckman Type 70 Ti rotor. Carefully, the supernatant was discarded. The resulting pellet consisted of a white core surrounded by a brown ring layer that, based on the observation in previous procedures carried out by our group and indications of Gerald Baron (personal communication) contained hairs and impurities. To increase the quality of the purification, the brown ring was separated and discarded using a Pasteur pipette. The white part of the pellet was rinsed with 50 mM Tris-HCl (pH8.0 at RT), 137 mM NaCl and 2% sarkosyl solution and stored at +4ºC O/N. The next morning, the white pellet was resuspended in 10 of 50 mM Tris-HCl (pH8.0 at RT), 137 mM NaCl and 2% sarkosyl, and was homogenized using a 15ml WHEATON® homogenizer**+. The homogenized sample was then digested with Proteinase K (PK) at a concentration of 10 µg/ml at 37ªC for 1 hour. PK digestion was quenched by the addition of Pefabloc to 2 mM for 15 minutes on ice**. EDTA added to a final concentration of to 30 mM (650 µl from 0.5 M stock solution) and the sample was incubated for 5 minutes at RT. After mixing by repeated inversion, NaCl was added to a final concentration of 1.7M (5.61 ml from 5M stock solution) and mixing by inversion repeated. The mixture was incubated 10 min at RT **.

The sample was then transferred to 26 ml ultracentrifuge tubes.

Carefully, 7ml of a sucrose cushion (1 M sucrose, 100 mM NaCl, 0,5% sulfobetaine 3-14,10 mM Tris-HCl (pH 7.4) was layered onto each tube under the sample using a syringe with a cannula.

Centrifugation was carried at the same conditions described above, 18198 g, 24min 20ºC in a Beckman Type 70 Ti rotor.

The supernatant, formed by two lipid layers, was discarded with extreme care with the help of a cannula attached to a syringe. Once lipids and intermediate layers were discarded, the floating pellet was “fished” with a pipette and transferred into a conical 1,5 ml tube.

The floating pellet was sedimented by centrifugation at 20.238 rpm for 20 minutes at RT (Microfuge 5424, Eppendorf Hamburg, Germany).

The supernatant was discarded and the resulting pellet resuspended in 1ml of 0,5% PBS-Zwittergent 3-14 and sonicated with 1 pulse at 50% of amplitude with a probe sonicator (4710 series, Cole Palmer, Venon Hills, IL, USA). The sonicated sample was incubated at 30ºC and shaking for 30 minutes at 900rpm. Sedimentation of GPI-anchorless PrP^{Sc} was carried out by centrifugation at the same conditions mentioned above. The supernatant was discarded and the resulting pellet was resuspended in 500 µl of sterilized H_2O (B. Braun, Rubí, Barcelona, Spain). This step was repeated twice to guarantee a complete detergent elimination. The last resulting pellet was resuspended in 100 µl of sterilized-H_2O.

To guarantee a proper dispersion of GPI-anchorless PrP^{Sc} fibers, the sample was sonicated by 3 pulses at 50% amplitude.

To avoid bacterial growth,1% of azide was added and stored at 4ºC until used. For bioassay studies, the sample was stored at -20ºC.

+I could observe that in many purifications samples contained impurities such as hairs. These impurities can affect at good yield of purification. The impurities were removed by "fishing" using plastic pipets.

**Alternative to fishing, impurities were removed by aspiration once they deposited by gravity.*

***Samples were transferred into two 50ml tubes with the exception of the 500 µl residual sample, where hair and other impurities were settled by gravity.*

Note; all buffers were prepared freshly and filtered with 0,45 µm filter (Merck Millipore, Billerica, MA, USA).

SDS-PAGE of isolated GPI-anchorless PrP^{Sc}.

Purified GPI-anchorless PrP^{Sc} was analyzed by Coomassie and Sypro Ruby (Invitrogen, Thermofisher, Walthan, MS, USA). For both analyses, 5 µl of sample were loaded in 15% SDS-PAGE gels. Electrophoresis was carried out at 200V for 50 minutes (Figure 3.8). After electrophoresis the gel was washed two times with MiliQ-H_2O for 10 minutes. For Sypro Ruby staining, proteins were fixed with solution of 10% methanol and 7% acetic acid in MiliQ-H_2O for 1 hour, then the gel was washed two times with H_2O and was incubated ON at RT with Sypro Ruby. For Coomassie staining, the gel was incubated with a Coomassie solution; 50% methanol, 10% acetic acid, 0,005% Brilliant Blue R Coomassie (Sigma-Aldrich, St Louis, MO, USA) for 30 minutes at RT. The gel was destined with 30% methanol, 10% acetic acid.

Fiber digestion after partial unfolding.

Purified GPI-anchorless PrP^{Sc} fibers were treated with 0, 1, 2, 3 and 4 M of Gn/HCl and incubated at 37ºC with shaking at 600 rpm for 2 hours. Samples from Gn/HCl treatment were either directly negatively stained for Transmission Electron Microscopy analysis, or digested with PK (Figure 3.10). To digest GPI-anchorless PrP^{Sc} fibers, Gn/HCl concentration was reduced to 0,4M by adding MilliQ-H_2O, and subsequently, fibers were digested with 50µg/ml of PK at 37ºC for 1 hour. Specific volume of sample is described in Table E3-III.

Table E3-III. Detailed amount of purified GPI-anchorless PrP^{Sc} subjected to treatment with Gn/HCl and subsequent PK digestion.

Sample	Vol. Sample (µl)	Gn/HCl (M)	Vol. Gn/HCl (from 6M)	Vol. H_2O (µl)	Vol. Final (µl)	Vol. H_2O (µl)	Gn/HCl (M)	Vol. Final (µl)	PK (µg/ml)
G26	22,5	0	0	45	67,5	607,5	0	675	50
G26	22,5	1	11,25	33,75	67,5	607,5	0,1	675	50
G26	22,5	2	22,5	22,5	67,5	607,5	0,2	675	50
G26	22,5	3	33,75	11,25	67,5	607,5	0,3	675	50
G26	22,5	4	45	0	67,5	607,5	0,4	675	50

GPI-anchorless PrPSc suspension in super-pure H2O, was mixed with the equivalent volume of 6M Gn/HCl to attain the desired final guanidine concentration. Gn/HCl was 10 fold diluted in order to digest the GPI-anchorless PrP^{Sc} fibers.

Electrophoresis and immunoblotting.

Purified GPI-anchorless PrP^{Sc}, directly after isolation from mouse brains, was analyzed by Coomassie and Sypro Ruby. For both analyses, 5 µl of sample were loaded in 15% SDS-PAGE gels. Electrophoresis was carried out at 200V for 50 minutes (Figure 3.8). For immunoblotting, purified GPI-anchorless PrP^{Sc} was precipitated with ice-cold 85% methanol and pelleted by 1 hour centrifugation at 18.000 g at 4ºC. The pellets were resuspended in Laemli Buffer (Bio-Rad, Hercules, CA, USA), heated at 100ºC for 10 minutes and loaded to gels of 15% SDS-PAGE. After electrophoresis, gels were transferred to Immobilion$^{(R)}$-P Transfer membranes PVDF-0,45 µm (Merk-Millipore, Billerica, MA, USA) by wet electroblotting at 80V for 90 minutes (Figure 3.9A; Figure 3.11), (Mini Trans-Blot$^{(R)}$ Electrophoresis Transfer Cell, BioRad, Hercules, CA, USA) or at 15V for 45 minutes in semi-dry system (Figure

3.9D) (Trans-Blot(R) SD Semi-Dry Electrophoresis Transfer Cell, BioRad, Hercules, CA, USA).

To estimate the amount of purified GPI-anchorless PrP^{Sc} suitable for inoculation (Figure 3.9A) and from Gn/HCl- PK treatment (Figure 3.11), samples were probed with R1 antibody, whose epitope is 225-230. Peroxidase-labeled anti- human antibody (Thermo Fisher Scientific, Rockford, IL, USA) was used as secondary antibody. Both antibodies were diluted at 1:5000.

To analyze the presence of PrP^{Sc} in brain from mice inoculated with the purified GPI-anchorless PrP^{Sc} (Figure 3.9D), immunoblotting was probed with 3F10 antibody, whose epitope is 137-151 (generously provided by Joaquín Castilla, CIC-BioGUNE, Derio, Basque Country, Spain). Peroxidase-labeled anti-mouse antibody (GE Healthcare Life Science) was used as secondary antibody. Both antibodies were used at 1:5000 dilution.

Immunohistochemistry.

For histopathology, the other half brains was fixed in 10% formaldehyde and shipped to Enric Vidal for histopathology study (CReSA, Barcelona, Spain). Samples were sliced into four transversal sections by cutting the brain caudally and rostrally to the midbrain and at the level of the basal nuclei. The sections were dehydrated by immersion in solutions of progressively higher ethanol concentration and, finally, with xylene before being embedded in paraffin. Hematoxylin-eosin was used to stain the 4 µm thick sections. Additional sections were mounted on 3-triethoxysilyl-propylamine-coated glass slides for immunehistochemical (IHC) studies.

IHC for the detection of PrP^{Sc} was performed. Deparaffinized sections were subjected to epitope unmasking treatments: Immersed in formic acid and boiled at low pH (6.15) in a pressure cooker and pre-treated with proteinase K. Endogenous peroxidases were blocked by immersion in a 3% H_2O_2 in methanol. Then, the sections were incubated overnight with anti-PrPMAb 2G11 primary antibody (1:100, kindly supplied by Dr. Eoin Monks, University College Dublin, Ireland) and subsequently visualized using the DakoEnVision system K400111/0 (Dako, Glostrup, Denmark) and 3,3'diaminobenzidine as the chromogenic substrate. Additional sections were incubated with a rabbit polyclonal antibody against glial fibrillary acidic protein (Dako, Glostrup, Denmark, Z0334, 1:600) to visualize astrocytic activation. For the glial fibrillary acidic protein detection epitope unmasking treatments were omitted, but the same visualization system was used. As a background control, the incubation with the primary antibodies was omitted.

Transmission Electron Microscopy.

GPI-anchorless PrP^{Sc} samples were adsorbed to freshly glow-discharged carbon-coated 400 mesh gold grids (Electron Microscopy Science, Hatfield, PA, USA) by floating an inverted grid on a 10 µl droplet of sample. After 2 minute incubation at RT, grids were wicked dry with filter paper and washed in two successive droplets of water, followed by staining for 1 minute on a freshly prepared and filtered 2% solution of uranyl acetate. Excess stain was wicked on filter paper and the grid allowed to dry overnight at RT. The grids were imaged in a JEOL JEM 2010 transmission electron microscope at 120 KV.

References

1. Vazquez-Fernandez, E. (2012) Structural studies of PrP^{Sc}. PhD, Universidad Santiago de Compostela

2. Chesebro, B., Trifilo, M., Race, R., Meade-White, K., Teng, C., LaCasse, R., Raymond, L., Favara, C., Baron, G., Priola, S., Caughey, B., Masliah, E. and Oldstone, M. (2005) Anchorless prion protein results in infectious amyloid disease without clinical scrapie. Science 308, 1435-1439

3. Baron, G. S., Hughson, A. G., Raymond, G. J., Offerdahl, D. K., Barton, K. A., Raymond, L. D., Dorward, D. W. and Caughey, B. (2011) Effect of glycans and the glycophosphatidylinositol anchor on strain dependent conformations of scrapie prion protein: improved purifications and infrared spectra. Biochemistry 50, 4479-4490

Chapter 4

Generation of recombinant prions

Since the development of a method that allows the generation of prions in vitro, some studies that are focusing on the understanding of molecular conversion mechanism of PrP^{C} to PrP^{Sc}, go through the use of synthetic PrP^{C}, in which the introduction of all kind of modifications can help to explain the molecular mechanism that governs the conversion into PrP^{Sc}. In this context, one of the most important events in the prion field was the development of a recPMCA, in which the production of the recombinant amyloid generated under sonication cycles recapitulates the nature of wild type prions.

The main goal of the study described in this chapter is the generation of $recPrP^{Sc}$ that recapitulates the nature of the PrP^{Sc} and to use this synthetic prion for structural studies. For that purpose, the recombinant mouse $PrP_{23\text{-}230}$ was bacterially expressed and then purified using a HisTrap Column. During the purification, the immobilized protein was refolded and then eluted using a gradient of imidazole. The refolded $recPrP_{23\text{-}230}$ was collected in different fractions and subsequently each fraction was submitted to several rounds of recPMCA for the conversion into a misfolded $recPrP^{Sc}$. Due to the fact that the misfolded recPrP shows different infectivity rates (non infectious or infectious) to probe the infectivity of the different misfolded PrP23-230, a bioassay was performed using a set of transgenic mice. Mice were inoculated with different misfolded PrP23-230. Only one of the misfolded $PrP_{23\text{-}230}$ generated by recPMCA resulted infectious in all the mice inoculated. This $recPrP^{Sc}$ was used for structural studies (chapter 5).

Introduction

The central event of the prion diseases is the conformation conversion of PrP^{C} into the pathogenic isoform PrP^{Sc}. The mechanism in which the structural conformation changes, promotes the protein-only hypothesis postulated to explain that the unique agent responsible for the prion diseases is the PrP^{Sc}. Elucidating the molecular mechanism that governs this structural transformation is an important event for the understanding of the prion diseases. In this context, one of the milestones in the prion field was the development of a method that achieves the conversion process of the PrP^{C} into the PrP^{Sc} *in vitro* (1). This method, the Protein Misfolded Cycling Amplification or PMCA, opened a new strategy on the generation of recombinant PrP^{Sc} (2). Recombinant prions generated under PMCA (recPMCA) confirmed that the PrP^{Sc} is the essential agent of the TSE, providing a definitive evidence to confirm the protein-only hypothesis (2).

The earliest initiative to understand the prion conversion was described in the1990's. Kocisko and collaborators tried to reproduce the PrP^{Sc} conversion *in vitro*, mixing purified PrP^{C} with PrP^{Sc} from a brain homogenate from a sick hamster, which developed clinical signs of prion diseases after being inoculated with PrP^{Sc} (3). The resulting PrP misfolded protein recapitulated some of the hallmarks of PrP^{Sc} protein (PK-resistant PrP molecules, PK-res PrP, insolubility and the formation of large aggregates). However, the hamster inoculated with this misfolded recPrP did not show any clinical signs of prion diseases, indicating that this misfolded recPrP lacked the infectious nature of prions (4). Nevertheless, in these studies, the misfolded form of the recPrP recapitulated many features related to the prion transmission *in vitro,* suggesting that the central event of the PrP^{C} conversion is the direct interaction between PrP^C and PrP^{Sc} (4). Another implication of the protein-only hypothesis is the generation *de novo* of the PrP^{Sc} without earlier PrP^{Sc} molecules that template the conversion. In this context, many studies have been focused in generating PrP^{Sc} *de novo* using physico-chemical approaches.

In 2002, Baskakov and collaborators, using the $recPrP_{89\text{-}231}$, generated a set of misfolded PK-res PrP that resulted in condition-depended (pH, Urea), demonstrating that the lag phase (time that the recPrP amyloid fibrils are formed) was reduced when a pre-misfolded PrP was incubated with $recPrP_{89\text{-}231}$ (5). Later on, PK-res PrP was generated and proved its infectivity in transgenic mice that overexpress around 16-32 times the $PrP_{89\text{-}231}$ form than the normal PrP^C. These mice were culled after more than 600 dpi when some signs of disease were observed. Due to that, the authors interpreted the PK-res PrP as infectious (6). However, given the extended time of the inoculation time, it remains unclear if that the clinical signs were due to prion diseases or due to the overexpression of the PrP protein, as previously observed in mice that overexpress the normal PrP^C (7, 8).

Another strategy for the preparation of the PrP^{Sc} was applied in the earliest years of the 2000's. Saborio and coworkers developed a method in which the PrP^{Sc} was amplified, under several sonication cycles, by the incubation of the brain homogenate (BH)-PrP^C with BH from a hamster inoculated with PrP^{Sc} (1). In this new method, named Protein Misfolding Cycling Amplification or PMCA, the PrP^{Sc} is incubated with PrP^C and the resulting aggregates are disrupted by sonication cycles to create several units for the constant formation of PrP^{Sc}, and finally, after several cycles, the PrP^{Sc} was amplified (Figure 4.1).

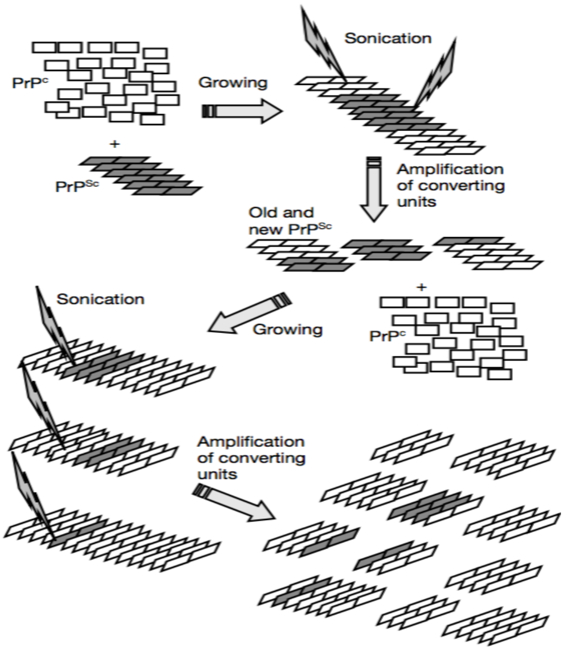

Figure 4.1. **Schematic representation of the PMCA procedure**. Amplification is based on the incubation of PrP^{C} with PrP^{Sc} under multiple sonication cycles. Images adapted from Saborio *et al.*(16)

In this context, Castilla *et al.* were able to amplify the PrP^{Sc} after several rounds of PMCA using as the seed of the PMCA a serial dilution of a PrP^{Sc} from the BH of a hamster inoculated with PrP^{Sc} (9). They demonstrated that the PMCA achieves the conversion of the PrP^{C} into PrP^{Sc}. The resulting PK-resistant PrP shares similar biochemical and structural features with the PrP^{Sc} from BH of an inoculated hamster. The hamsters inoculated with the PK-res PrP generated after PMCA develop the scrapie disease with the same clinical signs and histopathology profiles as the ones inoculated with the wild type PrP^{Sc}, demonstrating that prions can be generated *in vitro*.

Subsequently, regarding the PMCA, Barria *et al.* performed an experiment in which normal PrP^{C} was subjected to PMCA under similar conditions than the previously used (9) without the presence of the seed PrP^{Sc} (10). After a greater a number of sonication cycles, PrP^{Sc} was generated *de novo* (10). Although all of these PrP^{Sc} recapitulated all the hallmarks of the prionic nature of the PrP^{Sc}, the contribution of the cellular factors to the infectivity remains unclear.

An important step forward in the study of prion replication derived from the studies of the influence of different cofactors.

In this context, recently Wang *et al.* (2) generated for the first time a recombinant mouse PrP^{Sc} ($recMoPrP^{Sc}$) *de novo*, that fulfills the prionic nature of the wild type PrP^{Sc} (79). The authors found that the use of RNA and synthetic lipids as cofactors for the misfolding of the PrP^{C} into PrP^{Sc} result essential in the recPMCA. Later on, the same group demonstrated the reproducibility of *de novo* generation of the $recPrP^{Sc}$ (11).

On the other hand, it has been recently reported another method to obtain a misfolded form of the recPrP. This method, named QUIC (QUaking Induced Conversion) replaces the sonications by simple agitation. Although this method can detect a large number of prion strains and can monitor the formation of amyloid fibers, the major disadvantage against QUIC is the lack of infectivity of the recPrP amyloid that is produced by QUIC (12).

According to this, the generation of synthetic prions is an attractive tool for the understanding of the nature of the PrP and opens a new strategy for prion research. The development of a method that generates recombinant prions and allows the introduction all kind of modifications and facilitates the understanding of the transmission process (13). In addition to this, the isotopically labeled amyloid recPrP has been used for the structural studies using different NMR conditions (14, 15) or crystallography approaches (16).

The aim of the study described in this chapter was to generate recPrP^{Sc} by recPMCA in order to obtain a sufficient amount of protein for structural studies. The recombinant mouse PrP$_{23\text{-}230}$ expressed in *E. coli.* and purified in HisTrap column, was mixed with the cofactors POPG and RNA and subjected to PMCA, as indicated previously (2), in the presence of the seed recPrP^{Sc}. This seed derived from the amplification of the recPrP^{Sc} by PMCA. This recPrP^{Sc} was kindly provided by Jiyan Ma (Van Andel Research Institute, Grand Rapids (MI), USA) and was termed in this study as Ma-PrP^{Sc} to distinguish it from other recPrP^{Sc}. Due to the fact that the misfolded recPrP obtained after recPMCA shows different infectivity rates (non infectious or infectious) (11), to test the infectivity of the misfolded forms of recPrP$_{23\text{-}230}$ from the PMCA, a bioassay was performed using a set of transgenic mice overexpressing the normal PrP^{C}, named tga20 (17). Tga20 mice were intracranially inoculated with the different misfolded recPrP forms from the recPMCA. Only one of set of the misfolded recPrP generated by recPMCA resulted infectious.

Generation of recombinant PrP$_{23\text{-}230}$.

The recombinant PrP$_{23\text{-}230}$ generation is indicated in the Expanded Materials and Methods section (EM&M).

Protein purification and refolding process were performed using the His-trap 5ml (HisTrap FF crude 5ml, GE Healthcare Amersham) columns for its binding capacity between the histidines from the octarepeats of the PrP sequence and the pre-packed Ni from the column matrix (*In column refolding*).

In column refolding.

In order to obtain a protein refolded correctly, purification and refolding of recPrP$_{23\text{-}230}$ were performed according to the previously described method with small changes (18). The column was adapted to HPLC system in order to the possibility of the gradient mode. Firstly, to be purified, HPLC tubes were cleaned by adding 60 ml of MiliQ-H_2O at the flow of 5 ml/min. Once all tubes were cleaned, buffer B (EM&M) was used to feed every tube. The HisTrap column was adapted to the HPLC and was pre-equilibrated with the buffer B by the addition of 25 ml with a flow of 5 ml/min. The sample was loaded in the column and incubated at room temperature for 30 min. Column was washed with 20 ml of buffer B at 5ml/min. The pressure should not exceed 128 bar. To recPrP$_{23\text{-}230}$ refold gradient was applied at 2 m/min for 100 min following the Table 4-I.

Table 4-I. Gradient applied for the recombinant PrP$_{23\text{-}230}$ refolding.

Time (min)	0	100
Buffer B%	100	0
Buffer A%	0	100

According to the possibility of the presence of several misfolded and aggregates formed during the refolding process of the recPrP$_{23\text{-}230}$ (19), protein was eluted using a step gradient of imidazole (Buffer C) as indicated in the Table 4-II at 2 ml/min in order to collect fractions with the recPrP$_{23\text{-}230}$ correctly refolded.

Table 4-II. Gradient of Imidazole used during the purification

Fration	Imidazol (M)	Volume (ml)
1	50	6
2	50	5
3	50	25
4	100	5
5	100	25
6	150	5
7	150	25
8	200	5
9	200	25

Fraction number indicates the number of the tube where the factions were collected. The first 5-6 ml correspond with the residual volume of the previous buffer remaining in the column. The 25 ml correspond with the 5 times of the column volume used to elute the protein.

It is worth to mention that somehow recPrP$_{23\text{-}230}$ did not elute in the same fraction among the different purifications, e.g., protein was eluted with 50 mM and 100 mM of imidazole in the purification 1 (Figure 4.2A). However, the recPrP$_{23\text{-}230}$ was not detected when 50 mM of imidazole were used to elute the protein (Figure 4.2B) in the purification 2. For this reason, in each purification, only the fraction where the refolded recPrP$_{23\text{-}230}$ protein was detected, was subjected to dialysis. (Slide-A-Lyzer Dialysis Cassette 10K MWCO, Thermo Scientific) Eluted fractions were dialyzed three times against buffer E (appendix) and subsequently dialyzed three times with MiliQ-H_2O. After dialysis, eluted fraction that contained the recPrP$_{23\text{-}230}$, was concentrated 10 times under the manufacture´s recommendations (Amicon Ultra-15 10 KDa Centrifugal filter unit, Millipore). The protein was stored at -20ºC until being subjected to recPMCA.

Considering the possibility of a different recPrP$_{23-230}$ being generated during the in-column refolding (19), protein eluted in different fractions was used to generate misfolded recPrP$_{23-230}$ by recPMCA.

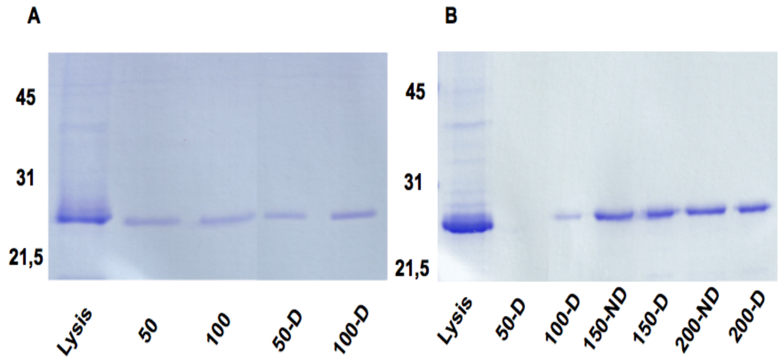

Figure 4.2. Recovery of purified recPrP$_{23-230}$ in different fractions of imidazole elution. To test the amount of protein that was recovered, 10µl of sample from each fraction were loaded into 12% SDS-PAGE. Electrophoresis was carried out for 35 minutes at 200V (BioRad) and stained by Comassie. In pruficiation 1, the recPrP$^{23-230}$ was recovery with 50 and 100 mM of imidazole **(A)**. In purification 2, recPrP$^{23-230}$ was recovery with 150 and 200 mM of imidazole **(B)**.

Generation of recPrP^{Sc}

Among all the methods used to generate recPrP^{Sc} (*vide supra*) recPMCA was the one selected, due to its efficiency to generate a recPrP^{Sc} that recapitulates the features of the prionic nature of PrP^{Sc} (2)

In a first attempt, the recombinant PrP^{Sc} generated in the laboratory of Jiyan Ma, the Ma-PrP^{Sc} (Van Andel Research Institute, Grand Rapids, MI, USA, (2)) was incubated with the recombinant PrP$_{23-230}$ in order to prove the efficiency of the recPMCA for the generation of the recombinant PrP^{Sc}. The misfolded recombinant PrP obtained in this first attempt resulted infectious in the tga20 mice and signs of prion diseases were observed after 101 days post-inoculation (20). The Histopathology and biochemistry from the BH of these mice demonstrated the prion nature of the recPrP^{Sc}-Ma, amplified after the incubation of Ma-PrP^{Sc} and recPrP$_{23-230}$ in the recPMCA (17). Due to that, in order to generate a high amount of recPrP^{Sc}, the recPrP^{Sc}-Ma was used to seed the recPMCA reaction where the refolded proteins recPrP$_{23\text{-}230}$ were mixed with 750 µg of RNA (purified from mouse liver by RNAZol, Sigma-Aldrich) and 112 µg of POPG (1-palmitoil-2-oleil-sn-glycero-3-phospho-(1´-sn-glycerol)) (Avanti Polar Lipids) according to the conditions described by Wang *et al*. (2) (Figure 4.3).

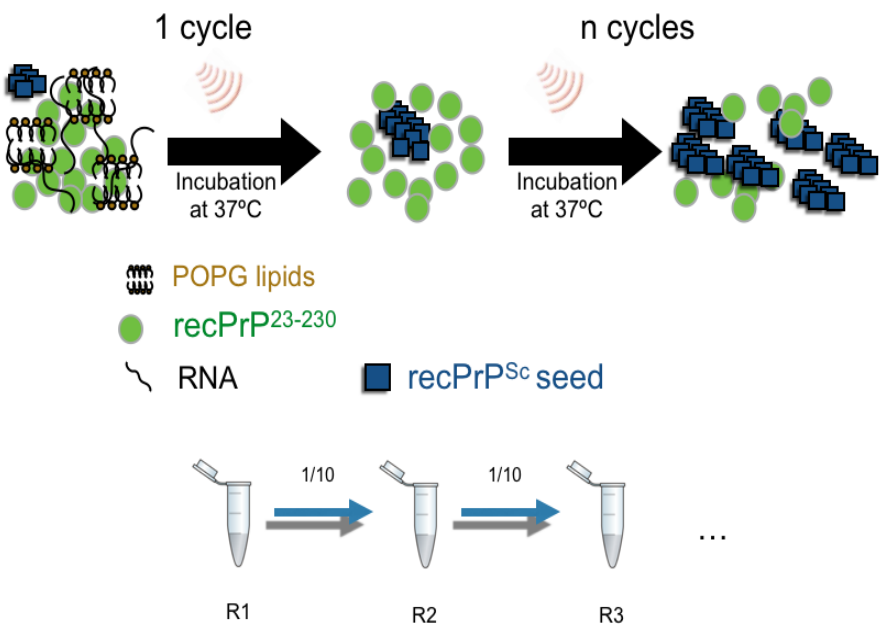

Figure 4.3. recPMCA. Scheme representation of the recPMCA rounds. In each round, the aggregates have grown and are broken under sonication cycles forming multiple nuclei for the templating of the PrP^{Sc} formation.

After several rounds of recPMCA, the $recPrP_{23\text{-}230}$ likely was amplified into the misfolded form $recPrP^{Sc}$. The presence of the misfolded forms of the $recPrP_{23\text{-}230}$ was confirmed by the resistance to PK degradation of the PMCA products (PK-res recPrP) (Figure 4.4).

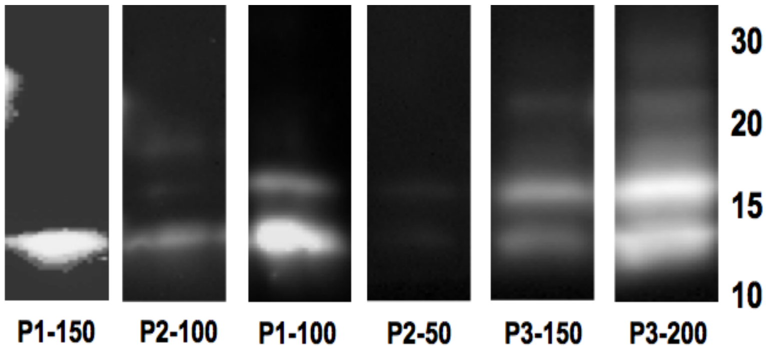

Figure 4.4. Western Blot of the PMCA products. Substrate that contains the $recPrP_{23\text{-}230}$ was subjected to different rounds of PMCA for PrP conversion into misfolded isoforms. The final product was digested with 10 µg/ml of PK for 30 minutes at 37°C to prove the presence of the PrP-res. Each lane is labelled with the number of purification and the imidazole concentration (mM) used to elute each recPrP23-230. Antibody: SAF-84 (1:400).

Bioassay

Due to the fact that the misfolded recPrP shows different infectivity rates (non infectious or infectious (11)) to verify the infectivity of these misfolded forms of the recPrP, a bioassay was performed using a set of tga20 mice, kindly provided by Joaquin Castilla (CIC-BioGune, Derio, Vizcaya, Basque Country) that overexpress the normal PrP^C (17). The selection of these mice was based on the absence of any pathological signs due to the aging commonly observed in other transgenic mice that overexpress the PrP^C (7, 8). Mice were intra-cerebrally (IC) inoculated at the age of 2-3 months with 20 µl of the misfolded recPrP (Table 4-III).

Table 4-III. Inocula names based on the fraction of the recPrP23-230 eluted

Purification	Imidazol (M)	Inoculum
1	100	947
2	50	948
	100	944
3	150	949
	200	950

Refolded recPrP23-230 eluted with different concentration of imidazole were used to propagate and generate new recPrP^{Sc}. To generate the inocula the products of the recPMCA were diluted 1/10 in PBS.

To date, only the 950 recPrP$_{23\text{-}230}$ result infectious in 11 of the 12 inoculated mice (Table 4-IV), and animals inoculated with this recPrP^{Sc} were culled after the development of signs of prion diseases, characterized by motor impairment (ataxia), tremor and kyphosis (Figure 4.5). Brains were extracted and stored as well as described in the Chapter 3.

Table 4-IV. Recombinant misfolded PrP23-230 used as inocula.

Name of the inoculum	Incubation time ± SD (dpi)	Attack rate
Ma-PrP^{Sc}	115 ± 11	4/4**
recPrP^{Sc}-Ma	101 ± 10	6/6^{+}
944	>240 ± 56	1/5*
947	>307	0/6
948	263 ± 108	2/8*
949	260 ± 68	1/5*
950	194 ± 47	11/12***

idicates that animals are still alive without any signs of prion diseases. indicates that this is the original inoculum obtained by Wang et al. (9) and was used first to seed the recPMCA reaction to obtain recPrP^{Sc}-Ma.*** indicates that the mouse of this group that is still alive and have started to develop clinical signs of prion diseases at 170 dpi. $^{+}$ indicates that these recPrP^{Sc}-Ma was obtained by the incubation of recPrP23-230 with Ma-PrP^{Sc} in order to prove the recPMCA conditions to further generate hight amount of recPrP^{Sc} during this study. The recPrP^{Sc}-Ma was generated by Saioa Rodriguez Elezgarai (28)*

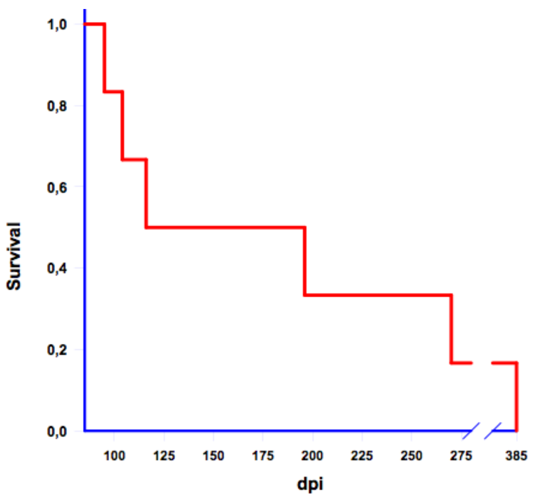

Figure 4.5. Kaplan-Mier curve plot surivial of tga20 mice inoculated with 950-recPrP^{Sc} (mice were culled out at 89, 95, 104, 114, 114, 114 , 116, 177, 196, 270 and 385 dpi) (194±46) (n=11 Breslow-Wilcoson test)

For immunohistochemistry and lesion profile studies, brains were fixed in formalin and shipped to Enric Vidal (CReSA, Barcelona, Spain) Brains were sliced and treated as described in EM&M of Chapter 3. Only brains from mice inoculated with recPrP^{Sc} showed spongiosis (Figure 4.6C) and PK-res PrP deposits (Figure 4.6D), hallmarks of prion diseases.

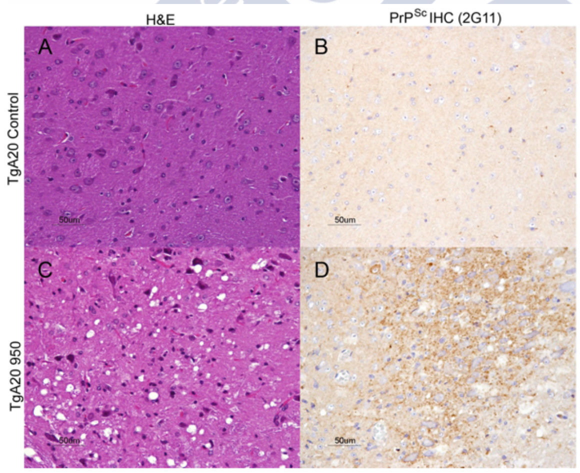

Figure 4.4. **Histopathology of the brains from tga20 that were inoculated with 950-recPrP^{Sc} and PBS**. One section was stained with hematoxylin and eosin (H&E, left), two others were analyzed via immunohistochemistry (IHC) using the anti-PrP antibody 2G11 . Control Tga20 mice (**A-B**).Tga20 inoculated with recPrP^{Sc} (**C-D).** Tga20 mice inoculated with recPrP^{Sc} show spongiform change, PrP^{Sc} deposition characteristic of a prion disease

The presence of PK-resistant PrP fragments were tested by immunoblotting in the brain homogenates of these mice (Figure 4.7).

Clinical sings of a prion disease, biochemistry and histopathology data confirmed the prionic nature of the $recPrP^{Sc}$ generated by recPMCA. (Figures 4.5; 4.6 and 4.7).

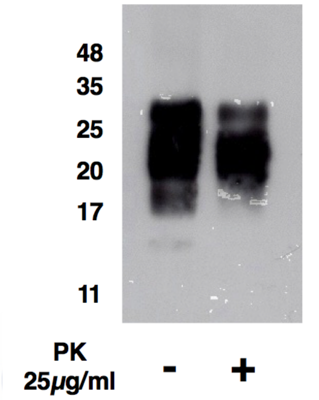

Figure 4.7. Western blot of brain homogenates from tga20 mice inoculated with $recPrP^{Sc}$. $recPrP^{Sc}$ was digested with 25 µg/ml for 1 hour at 37°C. The use of the primary antibody 3F10 (1:5000) revealed the presence of PK-resistant PrP.

Conclusion

During this study, the misfolded recombinant mouse $PrP_{23\text{-}230}$ was misfolded in the presence of $recPrP^{Sc}$ by recPMCA. This study was useful to observe that the refolding process (in column refolding) and the conditions of the propagation (rounds of PMCA, seed) generate a set of recombinant prion strains with different infectivity degrees, determined by the incubation times in concordance with the previously observed (20). The inoculum named 950 was the unique to be infectious in tga20 mice. The biochemistry and the histopathology of the brains from animals inoculated with this $recPrP^{Sc}$ showed typical features of prion infection, which confirm the prionic nature of this recPrP^{Sc}. For this reason, this recombinant mouse PrP^{Sc} was selected for structural studies.

References.

1. Saborio, G. P., Permanne, B. and Soto, C. (2001) Sensitive detection of pathological prion protein by cyclic amplification of protein misfolding. Nature 411, 810-813

2. Wang, F., Wang, X., Yuan, C. G. and Ma, J. (2010) Generating a prion with bacterially expressed recombinant prion protein. Science 327, 1132-1135

3. Kocisko, D. A., Come, J. H., Priola, S. A., Chesebro, B., Raymond, G. J., Lansbury, P. T. and Caughey, B. (1994) Cell-free formation of protease-resistant prion protein. Nature 370, 471-474

4. Hill, A. F., Antoniou, M. and Collinge, J. (1999) Protease-resistant prion protein produced *in vitro* lacks detectable infectivity. J Gen Virol 80 (Pt 1), 11-14

5. Baskakov, I. V., Legname, G., Baldwin, M. A., Prusiner, S. B. and Cohen, F. E. (2002) Pathway complexity of prion protein assembly into amyloid. J Biol Chem 277, 21140-21148

6. Legname, G., Baskakov, I. V., Nguyen, H. O., Riesner, D., Cohen, F. E., DeArmond, S. J. and Prusiner, S. B. (2004) Synthetic mammalian prions. Science 305, 673-676

7. Westaway, D., DeArmond, S. J., Cayetano-Canlas, J., Groth, D., Foster, D., Yang, S. L., Torchia, M., Carlson, G. A. and Prusiner, S. B. (1994) Degeneration of skeletal muscle, peripheral nerves, and the central nervous system in transgenic mice overexpressing wild-type prion proteins. Cell 76, 117-129

8. Castilla, J., Gutierrez-Adan, A., Brun, A., Doyle, D., Pintado, B., Ramirez, M. A., Salguero, F. J., Parra, B., Segundo, F. D., Sanchez-Vizcaino, J. M., Rogers, M. and Torres, J. M. (2004) Subclinical bovine spongiform encephalopathy infection in transgenic mice expressing porcine prion protein. J Neurosci 24, 5063-5069

9. Castilla, J., Saa, P., Hetz, C. and Soto, C. (2005) *In vitro* generation of infectious scrapie prions. Cell 121, 195-206

10. Barria, M. A., Mukherjee, A., Gonzalez-Romero, D., Morales, R. and Soto, C. (2009) *De novo* generation of infectious prions *in vitro* produces a new disease phenotype. PLoS Pathog 5, e1000421

11. Zhang, Z., Zhang, Y., Wang, F., Wang, X., Xu, Y., Yang, H., Yu, G., Yuan, C. and Ma, J. (2013) *de novo* generation of infectious prions with bacterially expressed recombinant prion protein. FASEB J 27, 4768-4775

12. Orru, C. D., Wilham, J. M., Vascellari, S., Hughson, A. G. and Caughey, B. (2012) New generation QuIC assays for prion seeding activity. Prion 6, 147-152

13. Castilla, J., Morales, R., Saa, P., Barria, M., Gambetti, P. and Soto, C. (2008) Cell-free propagation of prion strains. EMBO J 27, 2557-2566

14. Smirnovas, V., Baron, G. S., Offerdahl, D. K., Raymond, G. J., Caughey, B. and Surewicz, W. K. (2011) Structural organization of brain-derived mammalian prions examined by hydrogen-deuterium exchange. Nat Struct Mol Biol 18, 504-506

15. Skora, L., Fonseca-Ornelas, L., Hofele, R. V., Riedel, D., Giller, K., Watzlawik, J., Schulz-Schaeffer, W. J., Urlaub, H., Becker, S. and Zweckstetter, M. (2013) Burial of the polymorphic residue 129 in amyloid fibrils of prion stop mutants. J Biol Chem 288, 2994-3002

16. Apostol, M. I., Perry, K. and Surewicz, W. K. (2013) Crystal structure of a human prion protein fragment reveals a motif for oligomer formation. J Am Chem Soc 135, 10202-10205

17. Fischer, M., Rulicke, T., Raeber, A., Sailer, A., Moser, M., Oesch, B., Brandner, S., Aguzzi, A. and Weissmann, C. (1996) Prion protein (PrP) with amino-proximal deletions restoring susceptibility of PrP knockout mice to scrapie. EMBO J 15, 1255-1264

18. Zahn, R., von Schroetter, C. and Wuthrich, K. (1997) Human prion proteins expressed in Escherichia coli and purified by high-affinity column refolding. FEBS Lett 417, 400-404

19. Hutchinson, M. H. and Chase, H. A. (2006) Adsorptive refolding of histidine-tagged glutathione S-transferase using metal affinity chromatography. J Chromatogr A 1128, 125-132

20. Elezgarai, S. R. (2014) Priones recombinantes. Una novedosa estrategia para el estudio de las Encefalopatias Espongiformes Transmisible., Universidad del País Vasco. España.

Expanded Materials and Methods

Minimal 9 Media Recipe.

Minimal Media 9 10X

Na_2HPO_4	60 g
KH_2PO_4	30g
NaCl	5g
MilliQ H_2O	to 1L
pH	7.0

Autoclave and stored at RT.

Minimal 9 Media 1X.

For 1 L of Minimal 9 media 1x it was autoclaved 100 mL of M9-10X and mixed with 900 mL of autoclaved MilliQ H_2O. Then, under sterilize condition it was added the further reagents.

NH_4Cl	1g/1L
Glucose	3g/1L
[1]$MgSO_4$ 1M	1mL/L
[2]$CaCl_2$ 1M	1mL/L
Tiamine (from the stock solution 10mg/mL)	1mL/L
[4]Biotine (from the stock solution10mg/mL)	1mL/L
Ampicillin	20µg/ml

[1,2] should be freshly filtered through 0,22 µm filters.

[4] Biotine only was resuspended in M9 1x.

Generation of recombinant $PrP_{23\text{-}230}$

Vector plasmid DNA that contain the sequence to codify mouse $PrP_{23\text{-}230}$ (pOPIN E, Oxford Protein Production Facility UK) was performed in Joaquin Castilla´s laboratory (CIC-BioGune, Derio, Vizcaya, Basque Country). Plasmid DNA was freshly transformed into E. coli RosettaTM (DE3) (Novagen, Millipore). Rosetta cells were grown on agar plates supplemented with 50 µg/ml of ampicillin and incubated at 37ºC. The next day a single colony was picked from the plate and incubated at 37ºC for 16h at 225 rpm with 50 ml of M9 medium supplied with 20 µg/ml of Ampicillin.

After 16h, the OD should be around 0.9-1.1, cells were pelleted at 3000 x g, 4°C for 10 minutes (JA17 rotor, Beckmann Router) and resuspended in freshly 1L of M9 minimal medium. Recombinant $MoPrP_{23\text{-}230}$ protein (from here to ahead $recPrP_{23\text{-}230}$) expression was induced by the addition 1 mM of IPTG (Sigma-Aldrich) and incubated at 30ºC for 16 h at 225 rpm. Cells were pelleted at 6000 g for 10 min at 4ºC (JA10 rotor, Beckman Router). Supernatant was discarded and pellet were stored at -20ºC overnight. The bacterial pellet was resuspended in 30 ml of Lysis buffer (50 mM Tris-HCl pH8, 5 mM EDTA, 1% Triton X-100, 1 mM PMSF, 100 µg/mL lysozyme) incubated for 30 minutes at room temperature at 50 rpm. DNA were degraded by adding 20 mM $MgCl_2$, 5 µg/mL (100 U/mL) DNaseI and incubated another 30 minutes at room temperature at 250 rpm. Inclusion bodies were pelleted by centrifugation at 20.000 g for 20 minutes at 4ºC (JA17 rotor, Beckman Router). Supernatant was discarded and the resulted pellet was washed twice with a solution that contained 20 mM Tris-HCl pH, 150 mM NaCl,1 mM EDTA, 1% sarkosyl. Sample was centrifuged at 20000 g for 20 minutes at 4ºC in a beckman JA17 rotor. The supernatant was discarded and the resulting pellet was washed with MiliQ H_2O. The pellet was resuspended in the a solubilization buffer, 6M GdnHCl, 10 mM Tris-HCl, 100 mM NaPO4, 10 mM βME, pH8.0) and incubated O/N at 37 ºC at 250 rpm. Cellular debris were pelleted by centrifugation at 20.000 g for 20 minutes at 4ºC (Beckman rotor JA17). Supernatant that contained the $recMoPrP_{23\text{-}230}$ was transferred into new tubes and filtered through 0.45 µm filter (Millipore, Billerica, MS, USA). To check the expression and the amount of $recPrP_{23\text{-}230}$ recovered after filter, 1,5 µl of sample was precipitated with 85% MeOH (mix 1,5 µl of sample with 100% MeOH to final 85%, incubate at -20ºC for 30 minutes and centrifuge 18000 g for 30 minutes at 4ºC) and loaded in 12% SDS-PAGE gel (Figure E4.1)

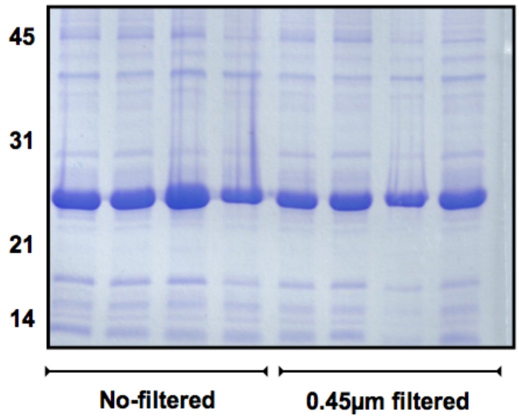

Figure E4.1. Comassie-Blue staining of recPrP$_{23-230}$. After inclusion bodies solubilization, cellular debris was pellet by centrifugation. Supernatant was filtered through 0.45 µm filter. The presence of the recPrP$_{23-230}$ was probed by blue Comassie staining in a 12% SDS-PAGE gel. Each lane corresponds to precipitate 1,5 µl from 250 ml of M9.

In column refolding.

The adsorptive refolding method is based on the immobilization of the protein during the refolding process to avoid protein-protein interaction. Despite the immobilization of the protein during the refolding, decreasing yield are observed at elevated concentration of protein given the closer proximity of proteins (1-3). Gradient of imidazole concentration was applied to elute the recPrP$_{23-230}$ from HisTrap Columns (Table E4-I). After elution with 200 mM of imidazole there was not additional recPrP$_{23-230}$ recovered by further increasing imidazole concentration. The misfolded and aggregated forms of recPrP$_{23-230}$ that were retained in the column throughout elution step (4). To recover these proteins, 500 mM of imidazole and 2M of Gn/HCl were required.

Buffers used to purify and refold the recPrP$_{23-230}$.

A: 10 mM Tris-HCl, 100 mM $NaPO_4$, pH 8.0

B: 6M Gn/HCl, 10 mM Tris-HCl, 100 mM $NaPO_4$, 10 mM βME, pH 8.0

C: ***CI***: 10 mM Tris-HCl, 100 mM $NaPO_4$, 50 mM imidazole, pH 8.0

CII: 10 mM Tris-HCl, 100 mM $NaPO_4$, 100 mM imidazole, pH 8.0

CIII: 10 mM Tris-HCl, 100 mM $NaPO_4$, 150 mM imidazole, pH 8.0

CIV: 10 mM Tris-HCl, 100 mM $NaPO_4$, 200 mM imidazole, pH 8.0

CV: 10 mM Tris-HCl, 100 mM $NaPO_4$, 250 mM imidazole, pH 8.0

CVI: 10 mM Tris-HCl, 100 mM $NaPO_4$, 300 mM imidazole, pH 8.0

CVII: 10 mM Tris-HCl, 100 mM $NaPO_4$, 350 mM imidazole, pH 8.0

CVIII: 10 mM Tris-HCl, 100 mM $NaPO_4$, 400 mM imidazole, pH 8.0

CIX: 10 mM Tris-HCl, 100 mM $NaPO_4$, 500 mM imidazole, pH 8.0

EB: (Elution buffer) 20 mM Tris-HCl, 500 mM NaCl, 500 mM imidazole 2M Gn/HCl. pH 8.0.

Dialyze Buffer (Buffer E): 10 mM $NaPO_4$, pH 5.8.

Dialysis was performed by buffer exchange for 30 minutes at 4ºC. After the third exchange, dialysis was repeated with MiliQ-H_2O.

Table E4-I. Imadozole gradient used in each purification.

Fraction	Imizadol (M)	Volume eluted (ml)	
1	50	6	
2	50	5	
3	50	25	
4	100	5	
5	100	25	
6	150	5	
7	150	25	
8	200	5	
9	200	25	
10	250	5	
11	250	25	
12	300	5	
13	300	25	
14	350	5	
15	350	25	
16	400	5	
17	400	25	
18	450	5	
19	450	25	
20	500	5	
21	500	25	
22	500 +2M Gn/HCl	30	Elution Buffer

After protein elution with 200 mM imidazole, it was not able to recover protein in the following fractions. To recover the protein adsorbed in the column, it was applied 500 mM of imidazole and 2M of Gn/HCl according with the manufactures recommendation (HisTrap FF crude 5 ml, GE Healthcare Amersham)

Electrophoresis and Coomassie staining.

Electrophoresis was carried out for 35 minutes at 200V (BioRad, CA, USA). Gel was separated from the electrophoresis cassette and incubated with Coomassie solution (50% methanol, 10% acetic acid and 0,005% brilliant blue Coomassie) during 45 minutes and destained by incubation during 30 minutes with a solution containing 30% methanol, 10% acetic acid. This buffer was exchanged 5 times.

Ethics statement

Animal experiments were carried out in accordance with the European Union Council Directive 86/609/EEC. The procedures and animal care were governed by a protocol that was approved by the Institutional Ethics Committee of the University of Santiago de Compostela. All efforts were made to minimize the suffering of the animals.

References

1. Stempfer, G., Holl-Neugebauer, B. and Rudolph, R. (1996) Improved refolding of an immobilized fusion protein. *Nat Biotechnol* 14, 329-334

2. Langenhof, M., Leong, S. S., Pattenden, L. K. and Middelberg, A. P. (2005) Controlled oxidative protein refolding using an ion-exchange column. *J Chromatogr A* 1069, 195-201

3. Hutchinson, M. H. (2006) Ph.D. Thesis, University of Cambridge

4. Hutchinson, M. H. and Chase, H. A. (2006) Adsorptive refolding of histidine-tagged glutathione S-transferase using metal affinity chromatography. *J Chromatogr A* 1128, 125-132

Chapter 5

Recombinant PrP^{Sc} shares structural features with brain-derived GPI-anchorless PrP^{Sc}

Substantial evidence suggests that PrP^{Sc} is a 4-rung β-solenoid, and that individual PrP^{Sc} subunits stack to form amyloid fibers. Recently limited proteolysis was used to map the β-strands and connecting loops that conform the PrP^{Sc} solenoid. Using high resolution SDS-PAGE followed by epitope mapping, and mass spectrometry, it was possible to identify positions ~116/118, 133-134, 141, 152-153, 162, 169 and 179 (murine numbering) as Proteinase K (PK) cleavage sites in PrP^{Sc}. Such sites define loops and/or borders of β-strands, and help to define the threading of the β-solenoid.

In the studies described in this chapter, this approach was extended to recombinant PrP^{Sc} (recPrP^{Sc}). The term recPrP^{Sc} was applied to bona fide recombinant prions prepared by PMCA, exhibiting infectious properties with attack rates of ~100%.

Limited proteolysis of mouse recPrP^{Sc} yields N-terminally truncated PK-resistant fragments similar to those seen in brain-derived PrP^{Sc}. Along with these, doubly N- and C-terminally truncated fragments, in particular ~89/97-152, were detected; similar fragments are characteristic of atypical strains of brain-derived PrP^{Sc}. Resistance to PK of recPrP^{Sc} was lower than that of "classic" PrP^{Sc} and more akin to that of atypical PrP^{Sc} strains. These results suggest that the architecture of *recPrP^{Sc} is similar to that of brain-derived PrP^{Sc}. The presence of a mixture of PK-resistant fragments that are characteristic of both "classic" and "atypical" PrP^{Sc} suggests nuances in threading that are specific of recPrP^{Sc}, resulting in biochemical properties that are somewhat intermediate between these two PrP^{Sc} types.*

Recombinant PrP^{Sc} offers exciting opportunities for structural studies not possible to date with brain-derived PrP^{Sc}

To understand the molecular mechanism that governs the conversion and the subsequent propagation of the PrP^{Sc} it is essential to elucidate the conformational structure of the PrP^{Sc}. This effort has been a central issue and challenge since this infectious agent was discovered (1).

In this respect, it is important to note that all known prions, including PrP^{Sc}, are amyloids (2-4). Therefore, the main force driving and modulating prion propagation must be templating of an incoming partially or totally unfolded prion precursor protein molecule by the upper and lower surfaces of the amyloid, which contain “sticky” ß-strands ready to form an array of hydrogen bonds with a newly-formed ß-strand-rich layer, thus promoting growth of the amyloid filament in the direction of its axis. The simplest possible version of amyloid propagation is the so-called “in-register stacking”. In register stacking involves superposition of ß-strands in which each amino acid residue of the upper and lower protein molecule are exactly one on top of the other. However, very substantial evidence suggests that PrP^{Sc} does not consist in flat subunits stacked in-register; rather, the experimental evidence suggests that PrP^{Sc} is a ß-solenoid. Thus, fiber X-ray diffraction studies showed that while PrP^{Sc} fiber spectra contain the characteristic meridional 4.8 Å reflection, a telltale for ß-strands stacked along the fiber axis, they lack the equatorial ~10 Å reflection that is characteristic of classic, in-register stacked amyloids, and correspond to the separation between two opposing ß-strands (5). Instead, the equator of PrP^{Sc} spectra contains a variety of reflections that are typically seen in spectra of ß-solenoids (5). Besides the mentioned 4.8Å reflection, the equator contains additional reflections that can be interpreted, as a set, as corresponding to secondary and tertiary reflections of a 4 rung unit along the fiber axis, *i.e.*, a 4-rung ß-solenoid (5). SAXS-based measurements also agree with a coiling PrP^{Sc} molecule whose diameter is considerably smaller than it would be if it extended horizontally in a single-rung β-strand rich structure, as required by the in-register stacking (6). Furthermore, data obtained from analysis of PrP^{Sc} 2D crystals also support a ß-solenoidal cross-section for PrP^{Sc} (7). It should be note that the fungal prion HET-S, whose architecture has been solved by means of solid state NMR, is a stack of ß-solenoids (8). Besides, new evidences support the ß-solenoid conformation of the PrP^{Sc}. Furthermore, in chapter 3 of this thesis, purified GPI-anchorless PrP^{Sc} fibers underwent a complete disassembling after being partially unfolded and subjected to PK digestion whereas the recombinant PrP amyloid (recPrP) maintained its fibrilar architecture. We concluded that our results support a multi-rung architecture rather than the single floor from which the recPrP are made (Chapter 3).

A multi-rung ß-solenoidal structure can propagate by the same basic mechanism as flat, in-register stacked amyloid, although only the upper and lower rungs participate in inter-molecular hydrogen bonding. Besides, intra-molecular hydrogen bonds must be formed in association to coiling, and stacking of dissimilar amino acid residues must necessarily take place. It is therefore obvious that identification of the specific amino acid residues that participate in the templating interfaces and/or posing steric hindrances to matching between pre-formed and nascent PrP^{Sc} molecules is critical to understand the details of PrP^{Sc} propagation, and, critically, to understand transmission barriers. In other words, while we are beginning to understand how prions propagate, we will need a more detailed structural model of PrP^{Sc}. Unfortunately, given the intractable nature of PrP^{Sc}, an understanding of its structure at a high resolution is unlikely to happen soon (4).

Alternatively to high resolution techniques for the structural studies for PrP^{Sc} (5, 8-10) indirect techniques, like limited proteolysis, have been used to elucidate structural characteristics of PrP^{Sc} (11, 12).

Biological systems use the limited proteolysis for activating a large range of proteins, where the proteolysis of the immature forms of proteins lead/drive the final active forms. The name "limited proteolysis" emerged from several ways to limit the proteolytic digestion such as the addition of protease inhibitors or the alteration of the reaction conditions (temperature, pH, time). This limitation is essential for structural studies because provides information about the peptide bonds regarding the fold of the protein. The tertiary structure of a protein is generally formed by the secondary structures; α-helices and ß-sheets connected by loops and turns. In this context, proteases would digest, under limited conditions, those elements that are more exposed to the solvent and more flexible, such as turns and loops, that are usually occupying the surface of the protein providing information on the location of particular peptide bond respecting to the overall fold of the protein.

Proteinase K (PK), has been used for a long time in the study of prions. PK is a serine protease that has been found for the first time in the fungus *Engyodontium album* and was found to digest keratin (13). Due to the persistence of PrP^{Sc} to be fully digested by PK (1, 14), PK has been used to detect PrP^{Sc} in the presence of PrP^{C}, that is completely degraded.

Whereas PK has been depicted as a highly non-specific protease for a long time (13), it was demonstrated that PK has preference for cleavages on the side chain of specific amino-acids (15-17). Computer simulation, based on experimental procedures of PK cleavage on mouse sequence of the PrP GPI-anchorless, predicts around 70 cleavage sites. Nevertheless, the cleavages site predicted *in silico* have not been found *in vitro*. The absence of some of the predicted PK cleavages indicate that these cleavages site predicted *in silico* are placed forming a secondary structure *in vivo* that holds in a conformation that is resistant to PK digestion, thus, this implies that the identification of the PK digestion products may be useful to map the secondary structure of PrP^{Sc}.

Regarding the nature of the PrP^{Sc}, the presence of α-helix was surmised from FTIR studies (18, 19), however in a recent experimental acquisition by the FTIR, the absorption peak at 1660 cm^{-1} attributed to α-helices, was reinterpreted when the same signal was obtained in a recPrP sample that is conformed by ß-sheets and random coil (20). This finding implies that the existence of α-helices in PrP^{Sc} conformation can not longer be supported by the means of FTIR. Indeed this new reinterpretation of the FTIR signal indicates that the only secondary structure remaining after PK digestion is ß-sheet and random coil conformation (loops connecting β-strands).

In this context, a study of $recPrP^{Sc}$ that resulted highly infectious in tga20 mice (see chapter 4), was performed by the use of limited proteolysis. Using a PK as protease to digest the more accessible and flexible stretches, would provide a set of peptides that will be resistant to the proteolytic digestion providing information of the location of putative loops and/or the borders of the ß-strands. The peptides from the protease digestion were monitored by electrophoresis. The use of a system that allows the separation of peptides smaller that 20 KDa with high resolution, such as tricine SDS-PAGE electrophoresis, allows the identification of a higher number of peptides than that observed with a glycine SDS-PAGE. To resolve the peptides, a set of antibodies with different epitopes was used. To resolve the peptides, a set of antibodies with different epitopes was used. To get the exact masses and unequivocally identification of the PK-resistant peptides is important the use of the mass spectrometry (MS) technique.

Given that the ESI-TOF provides an high mass accuracy, it was used to analyze the PK-resistant peptides. However, due to limitations in the amount of sample available and the presence of a high concentration of guanidine that could not be easily removed and suppressed the signal, only three peaks could be identified with exact molecular masses. As an alternatively, MALDI-TOF was used to identify the rest of the PK-resistant peptides observed after tricine SDS-PAGE electrophoresis (Figure 5.1). Together, MS (ESI-TOF and MALDI-TOF) in combination with epitope mapping after tricine SDS-PAGE electrophoresis allowed identification of the PK cleavage sites in the sequence of the recPrP^{Sc}, allowing in turn the identification of the loops/turns and

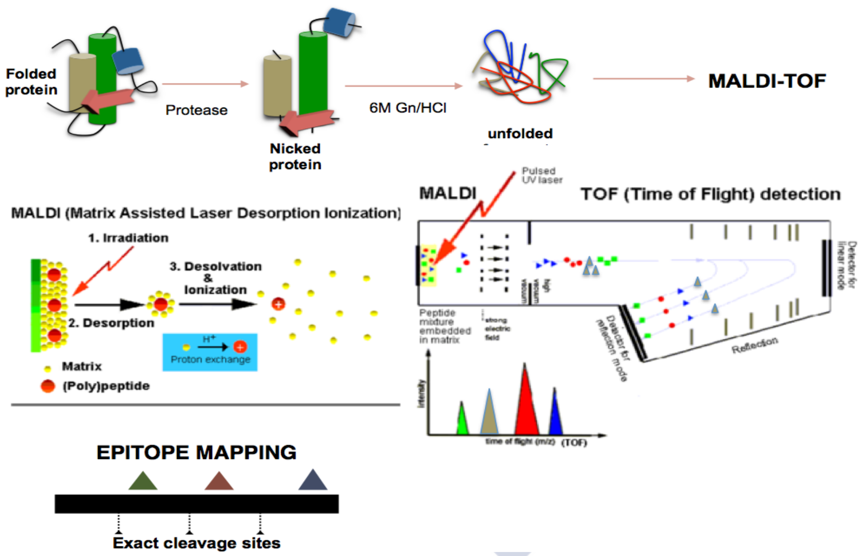

Figure 5.1. Scheme of the limited proteolysis coupled with mass spectopmetry and epitope mapping. Protease would digest the most exposed and flexible determinant of a protein. Peptides from the proteolytic digestion would be analyzed by MALDI-TOF. A set of peaks with the masses of the peptides would be identified with the use of three antibodies that recognized different epitopes of the protein. Finally, exact cleavage site would be identified and allow to define the most flexible stretches of the protein. Scheme of MALDI-TOF process was obtained from the Radbound University website: (http://www.ru.nl/science/gi/facilities/other-devices/maldi-tof/)

putative ß-strands.

Previously, limited proteolysis was used to probe the structural features of the PrP^{Sc}, in an attempt to identify sequential stretches that participate in ß-strands vs. loops/turns of the PrP^{Sc} (12). Using two analytical approaches, mass spectrometry combined with high resolution tricine SDS-PAGE electrophoresis and epitope mapping allowed the identification of several PK cleavages in the brain-derived GPI-anchorless PrP^{Sc}; 116/118, 133-134, 141, 152-153, 162, 169 and 179 (moPrP). These results have been used to identify the more accessible, flexible stretches connecting the ß-strand components in PrP^{Sc}, which define the loops and/or borders of the β-strands within the PrP^{Sc}, and reinforced the hypothesis that the structure of PrP^{Sc} consists of a series of short highly PK-resistant ß-sheet strands connected by short flexible loops and turns that exhibit high sensitive to PK digestion. These data, combined with physical constraints imposed by spectroscopic results, were used to propose a qualitative model for the structure of PrP^{Sc} (5). Assuming

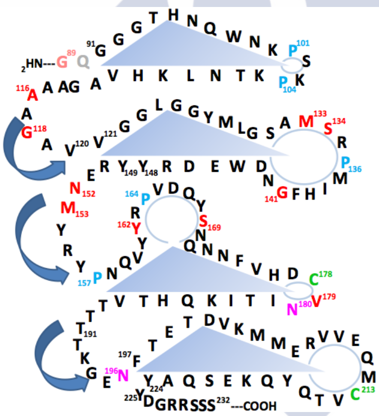

Figure 5.2. The threading model for the structure of mouse PrP^{Sc}. Qualitative model based on the combination of the data from limited proteolysis of mouse GPI-anchorless PrP^{Sc} and spectroscopical constraints (21). The restrains given under experimental procedure make the proline (blue) and PK cleavage sites (red) located in the loops connecting ß-strands. Ragged terminuses are indicated by faint colors. The disulfide bridge between the two cysteine amino acids are indicated in green color. Pink amino acids are the N-glycosilation sites N180 and N196. (21).

that PrP^{Sc} is a four rung -solenoid, the PrP sequence was threaded to satisfy the PK proteolysis data and other experimental constraints (21) (Figure 5.2).
In this context, recPrP^{Sc} appears as a very attractive tool for structural studies, because it should allow the introduction of all kinds of sequence variations, labels and isotopically labelled amino acid residues for selected NMR studies. It is worth to mention that many studies fail to generate a recPrP that recapitulate all the hallmarks that define a PrP^{Sc} as a prion (22). Recently, Wang *et al.* generated recPrP^{Sc} exhibiting incubation times similar to those of brain-derived PrP^{Sc} of the same sequence (23). While the incubation times should be considered very cautiously, given that a long incubation time can be the result of low titer but also of a transmission barrier, the study carried out by Wang *et al.* led to the definitive acceptance that bona fide, highly infectious recPrP^{Sc} can be generated *in vitro*. As a corollary, the possibility to use the versatile recPrP^{Sc} as a convenient model for structural elucidation of the structure of PrP^{Sc} in general was opened.
For structural analysis, the infectious recPrP^{Sc} was subjected to limited proteolysis. To identified the exact masses of the PK-resistant peptides of the recPrP^{Sc}, ESI-TOF and MALDI-TOF were used; furthermore, the resulting PK-digestion fragments were solved by epitope mapping. The exact masses of the PK-resistant fragments in combination with epitope mapping were applied to placed the cleavage points where the PK nicks into the sequence of recPrP^{Sc}. Finally, mouse recPrP^{Sc} species, yield an N-terminally truncated PK-resistant fragments very similar to those seen in brain-derived PrP^{Sc}, indicative of an overall similar architecture of both prion types.

To address the architecture of this recombinant prion, a sample from recPMCA that contained the recPrP^{Sc}, was subjected to limited proteolysis using 10 μg/ml of PK for 30 minutes at 37 ºC (see Expanded Material and Methods, EM&M). Under these conditions, an array of PK-resistant fragments were obtained. Most of the peptides that arose from the cleavage of the PK could be observed by Sypro Ruby staining after separation by tricine SDS-PAGE electrophoresis (Figure 5.3A).

Among these, a ~16 kDa fragment was seen, roughly corresponding to the size of full-length MoPrP minus the ~23-90 stretch classically cleaved by PK off brain-derived PrP^{Sc}, to yield PrP27-30 (1, 12, 24, 25). However, there were other smaller PK-resistant fragments with MWs between ~15 and ~4 kDa (Figure 5.3A).

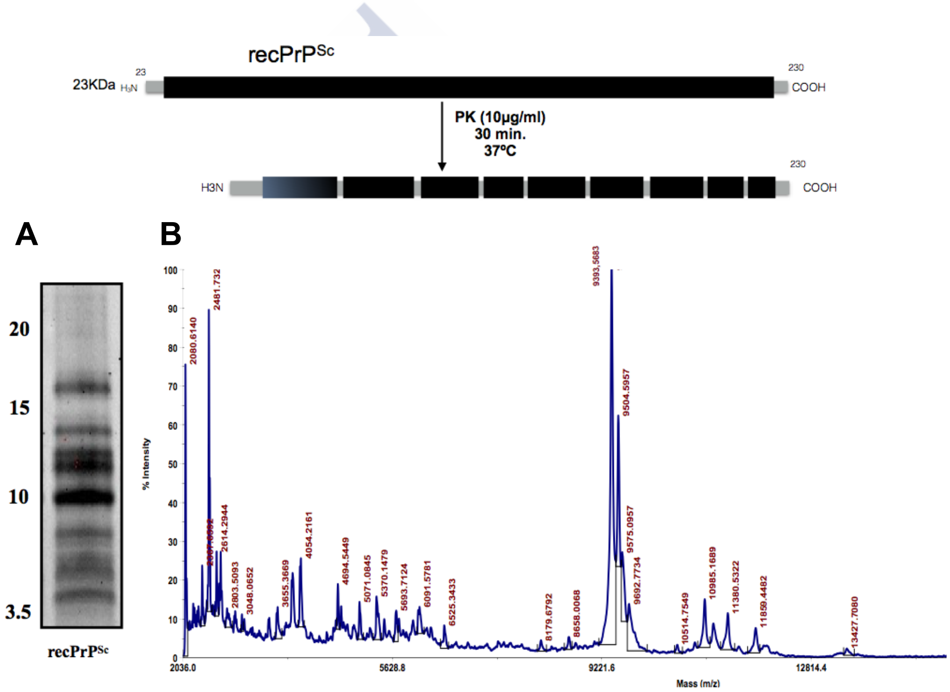

Figure 5.3. Fragmentation pattern of $recPrP^{Sc}$. The Sample was digested with 10 μg/ml for 30 minutes at 37ºC and the PK-resistant fragments were electrophoretically separated by tricine SDS-PAGE; to asses the global fragmentation pattern Sypro Ruby staining was used (A). MALDI-TOF spectrum of the peptides from the proteolytic digestion of the PK in the $recPrP^{Sc}$ (B)

To assess the exact mass, peptides from the proteolytic digestion of PK in the $recPrP^{Sc}$, were firstly subjected to ESI-TOF analysis. As a consequence of limitations in the amount of sample available for analysis, only three peaks with the masses 9513, 9399, 8184 Da were observed. Due to the fact of the need to analyze the rest of the PK-resistant peptides, sample was subjected to MALDI-TOF analysis. (Figure 5.3B).

Several peaks were observed that might correspond to the masses of the peptides from the PK digestion.

In parallel, the sample after PK digestion was subjected to epitope mapping by western blotting using antibodies that recognizes N-terminal (#51: 92-100, a gift from Lothar Stitz, Friedrich Loeffler Institut, Tübingen, Germany, (12) (Figure 5.4A), central (3F10: 137-151, (26), a kindly provided by Joaquín Castilla) (Figure 5.4B), and C-terminal (R1: 225-230, (27)) (Figure 5.4C) and compared to the brain derived GPI-anchorless PrP^{Sc} (see EM&M). The comparison of the PK-resistant fragmentation pattern of the $recPrP^{Sc}$ with the PK-resistant fragmentation pattern of the GPI-anchorless PrP^{Sc} (12), may help to elucidate the structural features of the $recPrP^{Sc}$. The 92-100 epitope is considered N-terminal given the generalized loss under all conditions tested of the labile ~23-90 amino-terminal stretch.

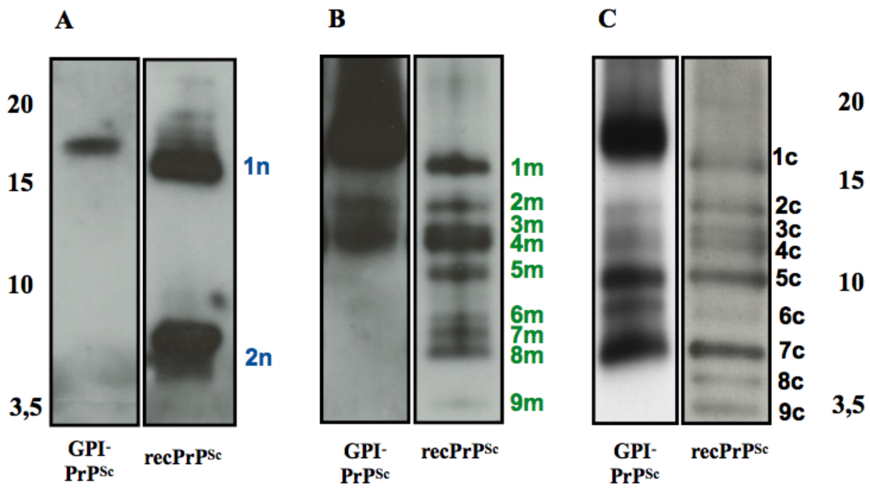

Figure 5.4. Immunoblotting of recPrP^{Sc} that was probed with three antibodies after limited proteolysis. PK-resistant fragments were electrophoretically separated by tricine SDS-PAGE and probed with antibodies that recognized different epitopes of the moPrP sequence. PK resistant fragments were observed by **(A)** #51 (undiluted, 92-100) **(B)** 3F10 (1:5000, 137-151) **(C)** and R1 (1:5000, 225-230)

The pattern of bands detected by the C-terminal antibody R1 was very similar in the GPI-anchorless PrP^{Sc} and recPrP^{Sc} samples, except that the uppermost band was, as mentioned ~16 kDa, with a slightly lower apparent MW than the ~17 kDa band seen in GPI-anchorless PrP^{Sc} (Figure 5.4). This difference is reminiscent of the difference between Drowsy vs. Hyper or CJD type I vs. type II major PK-resistant PrP^{Sc} fragments (28, 29). This suggests that cleavage of the N-terminal flexible tail by PK leaves a peptide with "ragged termini" (30) centered around a position C-terminal with respect to those of GPI-anchorless PrP^{Sc}, *i.e.*, G81/G89, presumably, around G92/W98 (28, 29). The recPrP^{Sc} sample contained bands migrating to the same positions as the ~14.6, ~13, ~12,~10.2, ~8 and ~6.7 kDa bands of GPI-anchorless PrP^{Sc} (Figure 5.4C, bands 2c to 7c and Vázquez-Fernández *et al.*). Considering the extreme C-terminal position of the R1 epitope, which leaves virtually no leeway for alternative sequence combinations leading to a given apparent

MW, it was concluded that there is a coincidence in the identity of these bands between both samples.

Such preliminary conclusion was confirmed by means of mass spectrometry (Figure 5.5 and Table 5-I).

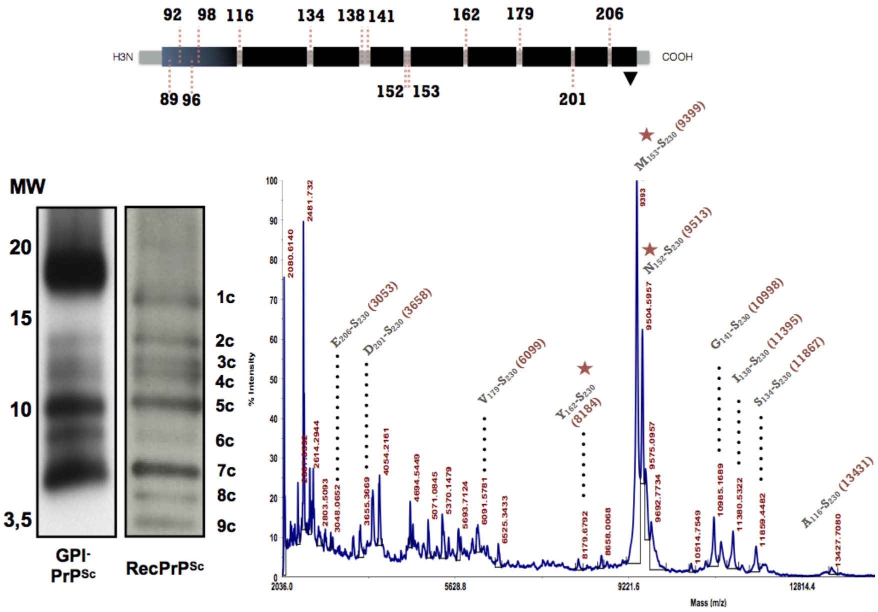

Figure 5.5. Immunoblotting of recPrP^{Sc} and MALDI-TOF spectrum of PK-treated recPrP^{Sc}. A) PK resistant fragments were solved by R1 (1:5000, 225-230). **B)** Sample after PK digestion was sedimented and the resulting pellet was resuspended in 20 µl of 6M Gn/HCl. To analysis by MALDI-TOF, 1 µl of the sample resuspended in Gn/HCl was mixed 49µl of sinapinic acid as matrix (see EM&M). Numbering into brackets indicate the theoretical Mass (KDa) of the peptides calculated by the GPMAW software (Lighthouse, Odense, Denmark). Marked peaks was found in ESI-TOF analysis and used to calculate a correction factor (EM&M)

As shown in the Figure 5.5 and summarized in the Table 5-I, several peaks were observed that might correspond to the masses of the peptides from the PK digestion. The PK-resistant peptides masses obtained by the means of the peaks 13427, 11859, 10985, 9504, 9393, 8179, 6091, might correspond to peptides equivalent to those observed in the GPI-anchorless PrP^{Sc} after PK digestion and whose masses are: 13606, 12041, 11171, 9687, 9573, 8358, 6274 (12), suggesting that the peptides from the PK cleavage in the recPrP^{Sc}

would be formed by cleavage at the same cleavages site that those observed in the GPI-anchorless PrP^{Sc}. The difference between the masses of the GPI-anchorless PrP^{Sc} peptides with its “analog” recPrP^{Sc} (23-230) is given by the two extra amino acids in the Ct of the GPI-anchorless PrP^{Sc} sequence (23-232) and minor differences in the sequences. ESI-TOF and epitope mapping analysis of the sample identified three C-terminal PK-resistant peptides, namely, 152-230, 153-230 and 162-230. In addition to this, MALDI-TOF and epitope mapping analysis of the sample, identified a number of C-terminal PK-resistant peptides, namely, 116-230, 134-230, 138-230, 141-230, 152-230, 153-230, 162-230,179-230. Such peptides coincide quite well with the apparent MWs of C-terminal peptides detected by antibody R1 (Figure 5.4C, Figure 5.5 and Table 5-I). Also, in agreement with the results obtained with epitope mapping, these peptides are very similar to those obtained after PK treatment of GPI-anchorless PrP^{Sc} (12) with the additional cleavage at positions 201 and 206 that their theoretical masses match quite well with the observed in the MALDI spectrum 3658 and 3050 (Figure 5.5 and table I), which also were observed in the western blotting after probing with the R1 antibody. Unfortunately, it was impossible to match the theoretical molecular weight of peptides ~92/98-230 by the means of the MALDI-TOF analysis, due to the fact that the ionization of peptides with high molecular weight is less efficient than those peptides with lower mass (31, 32).

Despite all these coincidences, some important differences are also evident when the PK digestion patterns from recPrP^{Sc} and GPI-anchorless PrP^{Sc} are compared. First, the relative intensities of these bands were different: in the GPI-anchorless PrP^{Sc} sample the ~17 kDa band, corresponding to G_{81}/G_{89}-S_{232} is absolutely predominant over the other ones, whose abundances are much lower (12), while in the $recPrP^{Sc}$ sample, a number of bands exhibit comparable intensities (Figure 5.5). Finally, the $recPrP^{Sc}$ sample contains two small size PK-resistant bands, with apparent MWs of ~4 and ~3,5 kDa which were absent in GPI-anchorless PrP^{Sc} (Figure 5.5 and Vázquez-Fernández *et al.*). These bands would correspond to putative PK-res PrP fragments with N-termini around D_{201} and E_{206}, respectively.

The N-terminal antibody, #51(92-100), revealed a much simpler pattern of PK-resistant bands in both $recPrP^{Sc}$ and GPI-anchorless PrP^{Sc} (Figure 5.4A). In the latter, only the ~17 kDa band (81/89-232) was recognized, in agreement with previous studies (21). In the $recPrP^{Sc}$ sample, two bands were detected. On the one hand, the ~16 kDa band, also recognized by the R1 antibody (*vide supra*). The fact that this antibody recognizes the band means that some of its ragged termini reach position G_{92}. Besides band 1n, a broad band of ~6.7 and -4 kDa appeared, 2n. Considering its apparent MW, it can be concluded that this band necessarily corresponds to doubly N- and C-truncated PK-resistant fragments (Figure 5.4 and 5.6), and that its broad appearance presumably results from the co-existence of several fragments trimmed at slightly different positions by PK, or "ragged termini". MALDI spectra shows a group of peaks with masses ranging from ~4100 to 6500 (Figure 5.6). Theses masses should correspond with the peptides doubly truncated spanning ~89/98-134/152.

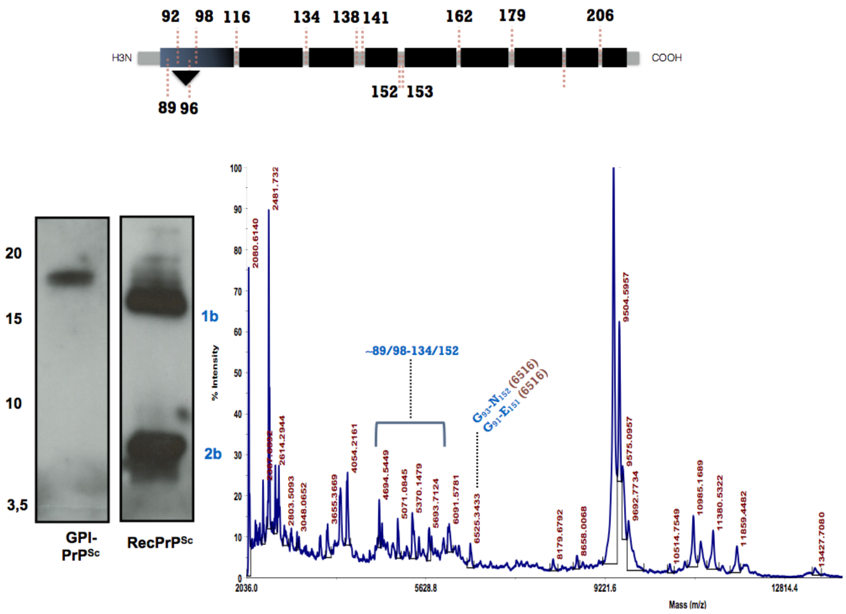

Figure 5.6. Immunoblotting of recPrP^{Sc} and MALDI-TOF spectrum of PK-treated recPrP^{Sc}. A) PK resistant fragments were observed by #51 (undiluted, 92-100) **B)** Sample after PK digestion was sedimented and the resulting pellets was resuspended in 20 µl of 6M Gn/HCl. To analysis by MALDI-TOF, 1 µl of the sample resuspended in Gn/HCl was mixed 49µl of sinapinic acid as matrix (see EM&M). Numbering into brackets indicate the theoretical Mass (KDa) of the peptides calculated by the GPMAW software (Lighthouse, Odense, Denmark).

Finally, the central antibody, 3F10 (137-151) detected 9 bands in the PK-treated recPrP^{Sc} sample, with apparent MWs of ~16, ~14.6, ~13, ~12, ~10.2, ~8, ~7 ~6.7 kDa and ~4 KDa, identified as 1m to 9m (from "middle") in the Figure 5.7. Considering the epitopes recognized by R1 and 3F10, and the apparent MW of "c" (C-terminal fragments recognized by R1), and "m" bands, it necessarily follows that some of the bands in the two blots must correspond to the same PK-res PrP fragments, recognized by both antibodies (Figures 5.4B and 5.4C). The ~16, ~14.6, and ~13, kDa bands recognized by R1 (Figure 5.4C, bands 1c, 2c, and 3c, respectively) putatively correspond, based on their analogy with similar bands in the GPI-anchorless sample, to PK-resistant fragments ~98-230, 116-230, and 134-230. Such fragments must be also recognized by 3F10, yielding bands 1m, 2m and 3m (Figure 5.7). Of the fragments identified by mass spectrometry and putatively contributing to band 4c (138-230 and 141-230), the second would not be recognized by antibody 3F10, but it is not certain whether the first would or would not, as it lacks just one residue of the epitope. Therefore it cannot be concluded whether 4m is the same as 4c or represents a different, doubly truncated fragment (Figures 5.4B-C and 5.7). One way or the other, it is clear that all smaller fragments spanning to the C-terminus (~152-230, ~162-230 and ~169/179-230), which lack the 3F10 epitope, would not be recognized by this antibody. Therefore, bands 5m to 8m are not the same as 5c to 7c PK-res fragments; rather, they must correspond to doubly N- and C-terminally truncated PK-res fragments (Figures 5.4 and 5.11). Furthermore, given that antibody #51 did not recognize any band of an apparent MW higher than ~7 kDa, 3F10 bands 4m, 5m, and 6m, running at higher positions, must feature an N-terminus beyond residue G_{92}, likely, around W_{98} (Figure 5.4A-B). On the other hand, bands 7m and 8m may or may not contain the #51 epitope, given that they run at positions that overlap with bands recognized by this antibody (Figure 5.4).

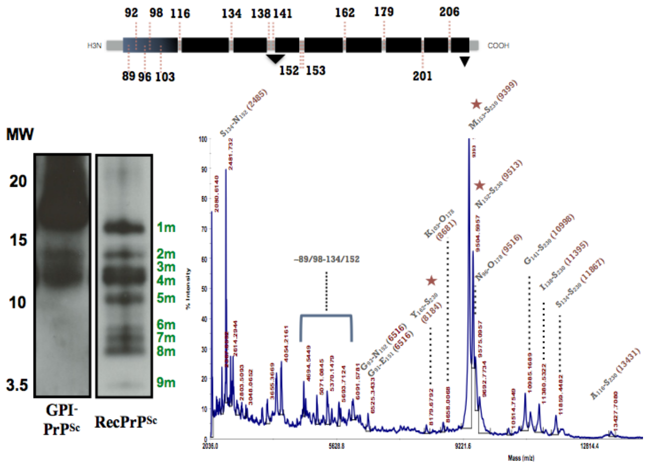

Figure 5.7. Immunoblotting of recPrP^{Sc} and MALDI-TOF spectrum of PK-treated recPrP^{Sc}. A) PK resistant fragments were observed by 3F10 (1:5000, 137-151) **B)** Sample after Pk digestion was sedimented and the resulting pellets was resuspended in 20 µl of 6M Gn/HCl. To analysis by MALDI-TOF, 1 µl of the sample resuspended in Gn/HCl was mixed 49µl of sinapinic acid as matrix (see EM&M). Numbering into brackets indicate the theoretical Mass (KDa) of the peptides calculated by the GPMAW software (Lighthouse, Odense, Denmark). Marked peaks was found in ESI-TOF analysis and used to calculate a correction factor (EM&M)

Considering all this, the most parsimonious conclusion is that bands 7m and 8m might correspond to PK-res fragments spanning from ~G_{91}/W_{98} to a position near N_{152}; 6m, lacking the #51 epitope, would span from ~K_{103} to 178; and 5m, from ~N_{96} to ~178. Peaks with masses of 6525, 8658, and 9510, in MALDI spectra might correspond to 7m /8m ($G_{91/93}$-E_{151}), 6m (K_{103}-O_{178}) and 5m (N_{96}-O_{178}) respectively (Figure 5.10). However, it is worth to mention that the peak observed at 6525, is relative bigger that the theoretical mass of the peptide G_{91}-E_{151}, the interpretation of these peptides was based on the epitope antibody analysis and further studies have to be conducted to identified unambiguously this PK-resistant. The presence of the doubly truncated band 9m, was confirmed by the peak with the mass of 2481 observed in the MALDI-TOF spectrum, and might correspond to the peptide S_{134}-N_{152} (Figure 5.7).

In conclusion, the limited proteolysis of these recPrP^{Sc} species generated a fragmentation pattern that containing a number of PK-resistant fragments that were the same as or equivalent to those obtained during limited proteolysis of GPI-anchorless MoPrP^{Sc} and wt SHaPrP^{Sc} (11, 12). In particular, mass spectrometry-based analysis revealed nicks at or positions 89/90, 116,134, 138, 141, 152/153 and 169 and 179 in GPI-anchorless MoPrP^{Sc} (12), whereas in this study nicks were observed at positions 89/96, 116, 134, 138, 141, 145, 152/153, 162 and 179 in the recPrP^{Sc}. (Figure 5.8 and Table 5-I). With the additional PK cleavages at 103, 201 and 206, that have not been identified before, that may define a new loop within the lowermost rung. Indeed, the identification of the cleavages site at 103, confirmed the presence of a loop that was previously predicted (Figure 5.2).

Unambiguous identification of the doubly truncated fragments has not yet been achieved by means of mass spectrometry, but their approximate termini could be surmised from epitope mapping, in combination with consideration of their apparent MW. Thus, there is a group of PK-resistant fragments spanning from positions ~89/98 to positions ~134, ~152/153, ~162, and ~179 (Figure 5.8).

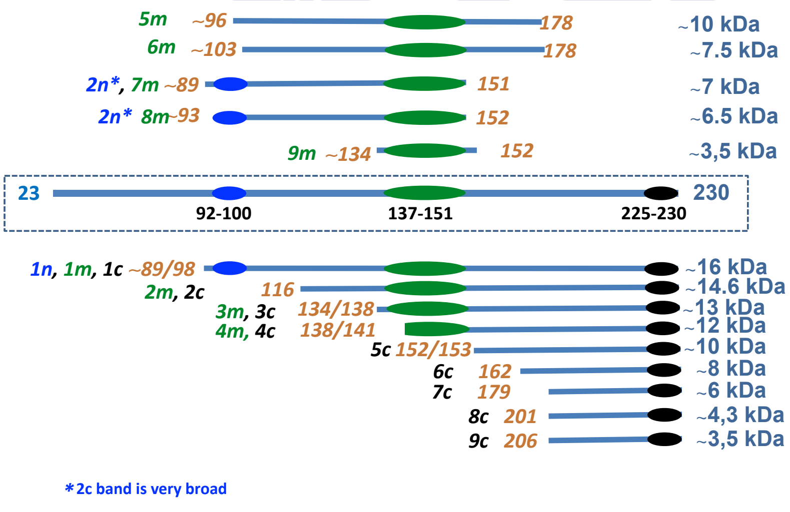

Figure 5.8. Scheme showing the location of cleavage sites in recPrP^{Sc} identified by the means of limited proteolysis, epitope mapping and MALDI-TOF

Therefore, such fragments might be, in fact the result of the action of PK at the described cleavage sites. Doubly truncated fragments have not been associated to the majority of "classic" brain derived prions, such as GPI-anchorless PrP^{Sc} (12), scrapie $MoPrP^{Sc}$, 263K and Dy $SHaPrP^{Sc}$ (11), or CJD PrP^{Sc} (30). In contrast, low MW bands corresponding to doubly truncated PK resistant fragments are very characteristic of "atypical" PrP^{Sc} strains, including Gertsmann-Streussler-Scheinker (GSS)- PrP^{Sc}, and atypical scrapie- -$OvPrP^{Sc}$ such as Nor98 PrP^{Sc} (30, 33). Thus, analysis of brain homogenates from GSS P102L patients showed the presence of two PK-res PrP fragments with apparent molecular masses of ~21 and ~8 kDa. The ~21 kDa fragment, similar to the PK-res PrP type 1 described in CJD (*i.e.*, the classic triad of PrP27-

30 fragments with variable glycosylation), is typically found in some cases, whereas the ~8 kDa fragment is found in all cases, and represents a pathognomonic characteristic of GSS (34). Mass spectrometry-based analysis of the ~8 kDa fragment revealed that it consists of a collection of peptides with ragged termini, spanning from 74/78/80/82 to 147/150/151/152/153 (huPrP) (34). Furthermore, the ~7 kDa PK-resistant fragment of PrP^{Sc} detected in A117V GSS cases was seen, using mass spectrometry analysis, to span from Gly_{88}/Gly_{90} to $Arg_{148}/Glu_{152}/Asn_{153}$ (huPrP) (35). As shown by Pirisinu *et al.*, this pattern is remarkably similar to that of Nor98 atypical PrP^{Sc}, treatment of which with PK yields a ~7 kDa resistant fragment whose sequence is 71/79-153 (30).

Table 5-I. PK-resistant fragments in recPrP^{S}

WB(Da)	MALDI Peaks (Da)	Corrected Peaks (Da)	Theoretical mass(Da)	Cleavage $\hat{}X_{123}$	Peptide	Antibody	Band
15			16197	G_{89}	G_{89}-S_{230}	51/3F10/R1	1n,1m,1c
	13428	13441	13431	A_{116}	A_{116}-S_{230}	R1/3F10	2c,2m
	11859	11871	11867	S_{134}	S_{134}-S_{230}	R1/3F10	3c,3m
	11380	11391	11395	I_{138}	I_{138}-S_{230}	R1/3F10	3c,3m
	10985	10996	10998	G_{141}	G_{141}-S_{230}	R1/3F10	4c, 4m
	10514	10524	10525	E_{145}	E_{145}-S_{230}	R1	4c
10	9510	9519	9516	N_{96}	N_{96}-O_{178}	3F10	5m
	9504	9514	9513	N_{152}	N_{152}-S_{230}	R1	5c
	9393	9402	9399	M_{153}	M_{153}-S_{230}	R1	5c
	8658	8666	8661	K_{103}	K_{103}-O_{178}	3F10	6m
	8179	8187	8184	Y_{162}	Y_{162}-S_{230}	R1	6c
	6525	6531	6516	G_{91}	G_{91}-E_{151}	51/3F10	2n/7m
	6092	6097	6103	V_{179}	V_{179}-S_{230}	R1	7c
3,5	3655	3659	3658	D_{201}	D_{201}-S_{230}	R1	8c
	3048	3051	3053	E_{206}	E_{206}-S_{230}	R1	9c
	2482	2484	2485	S_{134}	S_{134}-N_{152}	3F10	9m

Peaks observed in MALDI-TOF were corrected by the factor (1,0007-0,162, see EM&M). Peptides from the PK digestion was subjected to ESI-TOF analysis for its high accuracy. Only three peaks (9513; 9399 and 8184) were recorded. These peaks match very well with the theoretical MWs of peptides 153-230; 152-230; 169-230, respectively. These three peptides were used to build an internal calibration curve (EM&M)

Overall, Nor98 PrP^{Sc} is less PK-resistant than classic strains (30, 33, 36), and the 71/79-153 fragment is the most resistant part of it (30). In contrast, the most resistant part of PrP^{Sc} from classic strains is, precisely, the complementary sequence: a 152/153-232 fragment becomes prevalent with increasing treatment time with PK of GPI-anchorless PrP^{Sc} (12), and remains folded upon guanidine-induced partial unfolding of this prion (24). All of this suggests that the region around 152/153 marks a "hinge" that connects two stable sub-domains within PrP^{Sc}. It is noteworthy that this region signals two halves of the putatively folded region of PrP^{Sc} of comparable size; since the flexible loop likely spans to P_{157} (moPrP), as proline residues should be located in or at the borders of loops, it would connect two subdomains of ~62 and ~72 residues spanning N- and C-terminally with respect to it. If PrP^{Sc} is a four rung solenoid (5), higher resistance of either the ~152/153-230 half, typical of "classic" PrP^{Sc} strains (11, 12, 24) or of the ~80/90-152/153 half, characteristic of "atypical strains" (30, 34, 36) might reflect differences in the threading within these specific sub-domains, with differences in the relative content in ß-sheet secondary structure (longer or shorter ß-strands) and packing of the loops connecting them. Furthermore, the overall higher resistance to PK of "classic" *vs.* "atypical" and recombinant PrP^{Sc} might suggest that the overall structural "tightness"/packing is higher in the former. However, the fact that overall similar nicks are detected in all cases suggests that threading differences are not very large, and in general, the same elements of secondary structure, likely arranged in the same way, are characteristic of the structures of all three classes of PrP^{Sc}.

To study the relationship between fragments, a kinetic study of PK digestion was performed (EM&M) (Figure 5.9).

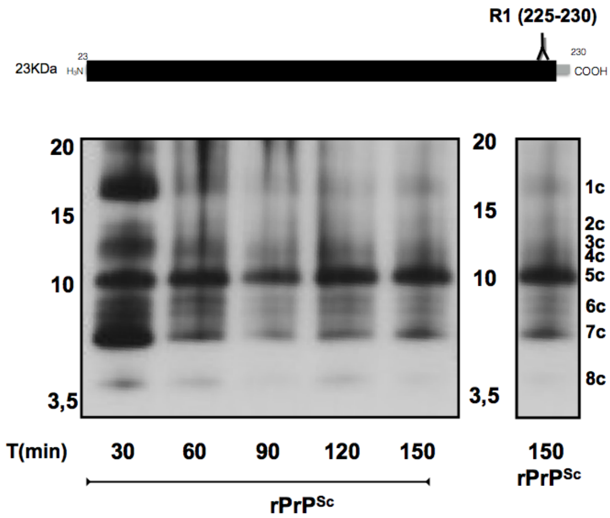

Figure 5.9. Kinetics of PK digestion on rPrP^{Sc}. Samples were digested with 10 µg/m of PK at 37°C for 30, 60, 90, 120, 150 minutes. Samples were analyzed to tricine SDS-PAGE and probed with R1 antibody.

As shown in Figure 5.9, the fragments resulting from the PK cleavages at 30 minutes, match very well with the observed before (Figure 5.4 and 5.5), with the exception of the additional band observed around 8 KDa (Figure 5.9, 6c). The observation of this band might be attributed to the existence of additional cleavages site around ~138 as well as observed in GPI-anchorless PrP^{Sc} (12). However, this band was detected somehow only in this experiment and was not observed in the previous tricine SDS-PAGE electrophoresis (Figure 5.4C), for that, this band has not been included as a definitively confirmed point of the PK cleavage (Figure 5.8, Table 5-I).

RecPrP^{Sc} sample from the recPMCA reaction was treated with 10 µg/ml at 37°C for 30, 60, 90, 120 and 150 minutes (EM&M). Gradual disappearance of all PK-resistant was observed with the exception of the 5c, 6c and 7c bands;

however, the kinetics of disappearance was different for different bands. The intensities of the 1c, 2c, 3c, 4c and 8c bands decreased steadily over time, with faster relative decreases of 1c and 2c bands. On the other hand, although, the 6c and 7c bands exhibited a faster decrease in intensity after at 60 minutes, then they resulted persistent after 150 of PK-digestion. The intensity of the band 5c was virtually similar after 150 minutes, indicating that the peptide 152/153-230 is highly resistant to PK digestion. Regarding GPI-anchorless PrP^{Sc}, the intensities of the 17, 14.6, 13, 12 and 6.7 kDa bands decreased steadily over time, this observation is in agreement with the decrease in the intensity observed in the bands 1c, 2c, 3c, 4c of $recPrP^{Sc}$. Although the intensity of the 6,7 KDa band (179-232, GPI-anchorless PrP^{Sc}) steadily decreased, it resulted highly persistent after 180 minutes. Similar persistence to PK digestion was observed in the 7c band after 150 minutes, whose peptide might span 179-230. After 240 minutes PK digestion, the intensities of the 17 and 10.2 kDa bands observed in the GPI-anchorless PrP^{Sc}, were nearly equal and by 360 minutes the intensity of the 17, 10.2 and 8 kDa bands were similar. However, in contrast to the GPI-anchorless PrP^{Sc}, the intensities of the 6c, 7c and 5c bands, observed in the $recPrP^{Sc}$, are different by 150 minutes, only the band 5c was virtually similar over the time-curse incubation. These results indicate that the band 5c (152/153-230 in $recPrP^{Sc}$ and 152/153-232 in GPI-anchorless PrP^{Sc}) is highly resistant by the time curse of the PK incubation.

This study also provides preliminary evidence of two additional, C-terminally located, PK cleavage sites not previously detected in brain-derived PrP^{Sc}. The strongest evidence of the existence of such cleavage sites was provided by a ~4.5 kDa band (band 9) in the Sypro Ruby stained gel of $recPrP^{Sc}$ (Figure

5.3A). A band with a similar apparent MW (band 8c) detected by the C-terminal antibody R1 (225-230), and no similar size bands detected by either #51 (92-100) or 3F10 (137-151), indicate that substantial PK-res fragment spans from a position around D_{201} to the C-terminus. Furthermore, band 9c detected by R1 (225-230), with an apparent MW of ~3.5, suggests the existence of a second C-terminal PK-res fragment, starting around position E_{206} and spanning to the C-terminus. The absence of a clear equivalent band in the Sypro Ruby-stained gel suggests that the relative abundance of this fragment might be relatively small. Recently, as commented before, a generic threading model of PrP^{Sc} was elaborated by distributing PK-cleavage sites, proline residues and other known structural constraints into a 4-rung solenoid (Figure 5.2) (21). A cleavage sites at D_{201} and E_{206} define a new loop located in the lowermost (C-terminal) rung that would somehow be in register with the predicted in the upper rung (Figure 5.2).

This is not the first structural study of recPrP^{Sc}. Recently, Noble *et al.* probed the structure of recPrP^{Sc} by deuterium/hydrogen exchange followed by pepsin digestion and mass spectrometric analysis (37). They found very substantial protection (*i.e.*, resistance to exchange) in a stretch spanning from position ~89 up to the C-terminus, suggestive of a ß-sheet-rich secondary structure. Short stretches exhibiting somewhat lower protection suggest the presence of loops/turns. In particular, the R_{150}-Y_{154} stretch stands out as the possible location of a loop. The furthermost C-terminal stretch Y_{224}-S_{230} also shows slightly decreased protection. These results are very similar to those reported by Smirnovas *et al.* in a similar analysis of GPI-anchorless PrP^{Sc} (20). These authors found substantial protection, indicative of compact, ß-sheet-rich structure, from G_{81} up to the C-terminus, with a lower protection from Y_{224} to the C-terminus. This coincidence supports the notion that the structure of the recPrP^{Sc} prepared by Noble *et al.* is similar to that of GPI-anchorless PrP^{Sc}, in agreement with the results reported here. In contrast, the pattern of exchange of a non-infectious recPrP amyloid sample was very different, with low exchange rates seen only beyond position ~160 (20).

In this respect, it is important to bear in mind that not all recombinant PrP amyloids are prions (38), and that the majority of recPrP amyloids have structures that are different from that of PrP^{Sc}. In particular, a subset of recombinant PrP amyloids has been shown to feature in-register stacking of its C-terminal domains by solid state NMR (39); such material is characteristically non-infectious, although it propagates in the brain of recipient animals. Upon second or third passage, this material evolves to an alternative form that shares biochemical properties with classic brain-derived PrP^{Sc} and becomes fully infectious and lethal (40, 41). Baskakov and collaborators have proposed that the initial recPrP amyloid undergoes a process of "deformed templating" through which this material adapts its structure to that of PrP^{Sc}. It is of note that this kind of PrP amyloid shares some PK cleavage sites with PrP^{Sc}, in particular, 141, 152 and 153 (42, 43). This suggests that the rung, in-register stacked recPrP amyloid and the 4-rungs solenoidal recPrP^{Sc} and brain-derived PrP^{Sc} share some similar stretches featuring ß-strand or flexible loop secondary structure, which are, however, organized in different tertiary structures. The presence of proline residues (P_{101}, P_{104}, $P_{136,}$ P_{157} and P_{164} moPrP) near PK cleavage sites likely sets constraints to the boundaries of ß-strands. In turn, certain ß-strand stretches in the floor PrP amyloid monomer might template, under certain circumstances and in the presence of brain cofactors with chaperoning properties, the generation of similar ß-strand stretches that might then extend by coiling into themselves rather than lying flat. This would result in a deformed templating. It is noteworthy that doubly truncated PK-res fragments have not been to date detected in recPrP amyloid preparations (42, 43), and likely represent a specific feature of $recPrP^{Sc}$, shared with atypical brain-derived PrP^{Sc} strains.

The treatment of $recPrP^{Sc}$ with PK for increased periods of time showed different kinetics for the different PK-resistant $recPrP^{Sc}$ fragments. The behavior of the bands 5c, 6c, and 7c (Figure 5.9) (152/152-, 162- and 179-230) is particularly relevant as their intensities at 150 minutes, that are the same intensity than at 30 minutes (5c) or less intensity (6c and 7c). These results are consistent with a progressive digestion of $recPrP^{Sc}$ from the N-terminus. This further suggests that different PK-resistant fragments are not from different subpopulation of the $recPrP^{Sc}$ emerged from recPMCA (44, 45) instead they are derived from a larger common $recPrP^{Sc}$, in agreement with previously reported in the GPI-anchorless PrP^{Sc} by Vázquez-Fernández *et al.* (12). Furthermore indicates that the most highly resistant PK-resistant sub-domain is located in the C-terminal of the $recPrP^{Sc}$ (152-230).

In summary, this study shows that a highly infectious mouse $recPrP^{Sc}$, generated with the concourse of recPMCA, exhibit biochemical properties that strongly suggest that they share the architecture of brain-derived PrP^{Sc}. Furthermore they seem to feature a mixture of structural properties of "classic" and "atypical" strains of brain PrP^{Sc}, although they also show some specific structural nuances.

References.

1. Prusiner, S. B. (1998) Prions. *Proc Natl Acad Sci U S A* 95, 13363-13383

2. Ross, E. D., Minton, A. and Wickner, R. B. (2005) Prion domains: sequences, structures and interactions. *Nat Cell Biol* 7, 1039-1044

3. Kraus, A., Groveman, B. R. and Caughey, B. (2013) Prions and the potential transmissibility of protein misfolding diseases. *Annu Rev Microbiol* 67, 543-564

4. Requena, J. R. and Wille, H. (2014) The structure of the infectious prion protein: experimental data and molecular models. *Prion* 8, 60-66

5. Wille, H., Bian, W., McDonald, M., Kendall, A., Colby, D. W., Bloch, L., Ollesch, J., Borovinskiy, A. L., Cohen, F. E., Prusiner, S. B. and Stubbs, G. (2009) Natural and synthetic prion structure from X-ray fiber diffraction. *Proc Natl Acad Sci U S A* 106, 16990-16995

6. Amenitsch, H., Benetti, F., Ramos, A., Legname, G. and Requena, J. R. (2013) SAXS structural study of PrP(Sc) reveals ~11 nm diameter of basic double intertwined fibers. *Prion* 7, 496-500

7. Govaerts, C., Wille, H., Prusiner, S. B. and Cohen, F. E. (2004) Evidence for assembly of prions with left-handed beta-helices into trimers. *Proc Natl Acad Sci U S A* 101, 8342-8347

8. Wasmer, C., Lange, A., Van Melckebeke, H., Siemer, A. B., Riek, R. and Meier, B. H. (2008) Amyloid fibrils of the HET-s(218-289) prion form a beta solenoid with a triangular hydrophobic core. *Science* 319, 1523-1526

9. Wille, H., Govaerts, C., Borovinskiy, A., Latawiec, D., Downing, K. H., Cohen, F. E. and Prusiner, S. B. (2007) Electron crystallography of the scrapie prion protein complexed with heavy metals. *Arch Biochem Biophys* 467, 239-248

10. Groveman, B. R., Dolan, M. A., Taubner, L. M., Kraus, A., Wickner, R. B. and Caughey, B. (2014) Parallel in-register intermolecular beta-sheet architectures for prion-seeded prion protein (PrP) amyloids. *J Biol Chem* 289, 24129-24142

11. Sajnani, G., Pastrana, M. A., Dynin, I., Onisko, B. and Requena, J. R. (2008) Scrapie prion protein structural constraints obtained by limited proteolysis and mass spectrometry. *J Mol Biol* 382, 88-98

12. Vazquez-Fernandez, E., Alonso, J., Pastrana, M. A., Ramos, A., Stitz, L., Vidal, E., Dynin, I., Petsch, B., Silva, C. J. and Requena, J. R. (2012) Structural organization of mammalian prions as probed by limited proteolysis. *PLoS One* 7, e50111

13. Ebeling, W., Hennrich, N., Klockow, M., Metz, H., Orth, H. D. and Lang, H. (1974) Proteinase K from Tritirachium album Limber. *Eur J Biochem* 47, 91-97

14. Prusiner, S. B., Bolton, D. C., Groth, D. F., Bowman, K. A., Cochran, S. P. and McKinley, M. P. (1982) Further purification and characterization of scrapie prions. *Biochemistry* 21, 6942-6950

15. Morihara, K., Tsuzuki, H., 1975. (1975) Specificity of proteinase K from Tritirachiumn album limber for synthetic peptides. *Agr. Biol. Chem.* 39, 1489-1492

16. Keil, B. i. (1992) Specificity of proteolysis, Springer-Verlag, Berlin ; New York

17. Saenger, W. (2013) proteinase K.in *Handbook of Proteolytic Enzymes* (Rawlings, N. D., Salvesen, G ed., Academic Press, San Diego

18. Baron, G. S. and Caughey, B. (2003) Effect of glycosylphosphatidylinositol anchor-dependent and -independent prion protein association with model raft membranes on conversion to the protease-resistant isoform. *J Biol Chem* 278, 14883-14892

19. Cobb, N. J., Sonnichsen, F. D., McHaourab, H. and Surewicz, W. K. (2007) Molecular architecture of human prion protein amyloid: a parallel, in-register beta-structure. *Proc Natl Acad Sci U S A* 104, 18946-18951

20. Smirnovas, V., Baron, G. S., Offerdahl, D. K., Raymond, G. J., Caughey, B. and Surewicz, W. K. (2011) Structural organization of brain-derived mammalian prions examined by hydrogen-deuterium exchange. *Nat Struct Mol Biol* 18, 504-506

21. Silva, C. J., Vazquez-Fernandez, E., Onisko, B. and Requena, J. R. (2015) Proteinase K and the structure of PrP^{Sc}: The good, the bad and the ugly. *Virus Res* 207, 120-126

22. Le, N. T., Narkiewicz, J., Aulic, S., Salzano, G., Tran, H. T., Scaini, D., Moda, F., Giachin, G. and Legname, G. (2015) Synthetic prions and other human neurodegenerative proteinopathies. *Virus Res* 207, 25-37

23. Wang, F., Wang, X., Yuan, C. G. and Ma, J. (2010) Generating a prion with bacterially expressed recombinant prion protein. *Science* 327, 1132-1135

24. Kocisko, D. A., Lansbury, P. T., Jr. and Caughey, B. (1996) Partial unfolding and refolding of scrapie-associated prion protein: evidence for a critical 16-kDa C-terminal domain. *Biochemistry* 35, 13434-13442

25. Aguzzi, A. and Calella, A. M. (2009) Prions: protein aggregation and infectious diseases. *Physiol Rev* 89, 1105-1152

26. Choi, J. K., Park, S. J., Jun, Y. C., Oh, J. M., Jeong, B. H., Lee, H. P., Park, S. N., Carp, R. I. and Kim, Y. S. (2006) Generation of monoclonal antibody recognized by the GXXXG motif (glycine zipper) of prion protein. *Hybridoma (Larchmt)* 25, 271-277

27. Williamson, R. A., Peretz, D., Pinilla, C., Ball, H., Bastidas, R. B., Rozenshteyn, R., Houghten, R. A., Prusiner, S. B. and Burton, D. R. (1998) Mapping the prion protein using recombinant antibodies. *J Virol* 72, 9413-9418

28. Bessen, R. A. and Marsh, R. F. (1992) Identification of two biologically distinct strains of transmissible mink encephalopathy in hamsters. *J Gen Virol* 73 (Pt 2), 329-334

29. Parchi, P., Zou, W., Wang, W., Brown, P., Capellari, S., Ghetti, B., Kopp, N., Schulz-Schaeffer, W. J., Kretzschmar, H. A., Head, M. W., Ironside, J. W., Gambetti, P. and Chen, S. G. (2000) Genetic influence on the structural variations of the abnormal prion protein. *Proc Natl Acad Sci U S A* 97, 10168-10172

30. Pirisinu, L., Nonno, R., Esposito, E., Benestad, S. L., Gambetti, P., Agrimi, U. and Zou, W. Q. (2013) Small ruminant nor98 prions share biochemical features with human gerstmann-straussler-scheinker disease and variably protease-sensitive prionopathy. *PLoS One* 8, e66405

31. Moyer, S. C., Cotter, R. J. and Woods, A. S. (2002) Fragmentation of phosphopeptides by atmospheric pressure MALDI and ESI/Ion trap mass spectrometry. *J Am Soc Mass Spectrom* 13, 274-283

32. Bodnar, W. M., Blackburn, R. K., Krise, J. M. and Moseley, M. A. (2003) Exploiting the complementary nature of LC/MALDI/MS/MS and LC/ESI/MS/MS for increased proteome coverage. *J Am Soc Mass Spectrom* 14, 971-979

33. Klingeborn, M., Wik, L., Simonsson, M., Renstrom, L. H., Ottinger, T. and Linne, T. (2006) Characterization of proteinase K-resistant N- and C-terminally truncated PrP in Nor98 atypical scrapie. *J Gen Virol* 87, 1751-1760

34. Parchi, P., Chen, S. G., Brown, P., Zou, W., Capellari, S., Budka, H., Hainfellner, J., Reyes, P. F., Golden, G. T., Hauw, J. J., Gajdusek, D. C. and Gambetti, P. (1998) Different patterns of truncated prion protein fragments correlate with distinct phenotypes in P102L Gerstmann-Straussler-Scheinker disease. *Proc Natl Acad Sci U S A* 95, 8322-8327

35. Tagliavini, F., Lievens, P. M., Tranchant, C., Warter, J. M., Mohr, M., Giaccone, G., Perini, F., Rossi, G., Salmona, M., Piccardo, P., Ghetti, B., Beavis, R. C., Bugiani, O., Frangione, B. and Prelli, F. (2001) A 7-kDa prion protein (PrP) fragment, an integral component of the PrP region required for infectivity, is the major amyloid protein in Gerstmann-Straussler-Scheinker disease A117V. *J Biol Chem* 276, 6009-6015

36. Benestad, S. L., Arsac, J. N., Goldmann, W. and Noremark, M. (2008) Atypical/Nor98 scrapie: properties of the agent, genetics, and epidemiology. *Vet Res* 39, 19

37. Noble, G. P., Wang, D. W., Walsh, D. J., Barone, J. R., Miller, M. B., Nishina, K. A., Li, S. and Supattapone, S. (2015) A Structural and Functional Comparison Between Infectious and Non-Infectious Autocatalytic Recombinant PrP Conformers. *PLoS Pathog* 11, e1005017

38. Klimova, N., Makarava, N. and Baskakov, I. V. (2015) The diversity and relationship of prion protein self-replicating states. *Virus Res* 207, 113-119

39. Tycko, R., Savtchenko, R., Ostapchenko, V. G., Makarava, N. and Baskakov, I. V. (2010) The α-helical C-terminal domain of full-length recombinant PrP converts to an in-register parallel beta-sheet structure in PrP fibrils: evidence from solid state nuclear magnetic resonance. *Biochemistry* 49, 9488-9497

40. Makarava, N., Kovacs, G. G., Bocharova, O., Savtchenko, R., Alexeeva, I., Budka, H., Rohwer, R. G. and Baskakov, I. V. (2010) Recombinant prion

protein induces a new transmissible prion disease in wild-type animals. *Acta Neuropathol* 119, 177-187

41. Makarava, N. and Baskakov, I. V. (2012) Genesis of tramsmissible protein states via deformed templating. *Prion* 6, 252-255

42. Bocharova, O. V., Breydo, L., Parfenov, A. S., Salnikov, V. V. and Baskakov, I. V. (2005) *In vitro* conversion of full-length mammalian prion protein produces amyloid form with physical properties of PrP(Sc). *J Mol Biol* 346, 645-659

43. Bocharova, O. V., Breydo, L., Salnikov, V. V., Gill, A. C. and Baskakov, I. V. (2005) Synthetic prions generated *in vitro* are similar to a newly identified subpopulation of PrP^{Sc} from sporadic Creutzfeldt-Jakob Disease. *Protein Sci* 14, 1222-1232

44. Zhang, Y., Wang, F., Wang, X., Zhang, Z., Xu, Y., Yu, G., Yuan, C. and Ma, J. (2014) Comparison of 2 synthetically generated recombinant prions. *Prion* 8

45. Fernandez-Borges, N. D. B., MA. Eraña, H. Vidal, E. Vanegas, V. Sevillano, AM. Elezgarai, SR. Prirsinu, L. Váquez-Fernández, E. Harrathi, C. Parra, B. D'Agostino, C. Espinosa, JC. Surewicz, W. Torres, JM. Mayoral, T. Agrimi, U. Requena, JR. Nonno, R. Castilla, J. (2015) Infectious recombinant prions: *In vitro* generation and propagation of different strains.in *International Prion Congress 2015*, Fort Collins

Expanded Material and Methods

Ethics statement

Animal experiments were carried out in accordance with the European Union Council Directive 86/609/EEC. The procedures and animal care were governed by a protocol that was approved by the Institutional Ethics Committee of the University of Santiago de Compostela. All efforts were made to minimize the suffering of the animals.

GPI-anchorless PrP^{Sc}

Transgenic homozygous GPI-anchorless (GPI-) PrP mice (tg44-/-), were obtained by crossing of (tg44(+/-) heterozygous (GPI anchorless) PrP mice (tg44-/-) (1), generously provided by Bruce Chesebro, Rocky Mountain Laboratories, NIH, Montana, USA (2). Female mice were intracerebrally inoculated at six weeks of age with 20 µl of a 2% RML-infected mouse brain homogenate, kindly provided by Juan María Torres, CISA, Madrid, Spainas well described in the Chapter 3.

After 365 days post inoculation, mice were euthanized, their brains surgically removed, rinsed in PBS, and stored at -80 °C until needed. A 10% w/v, brain homogenate was prepared in PBS, using a dounce homogenizer (Wheaton Industries Inc, NJ, USA), followed by one pulse of sonication to clarify the homogenate, with an ultrasonic homogenizer probe (Cole Parmer Instrument CO., Chicago IL, USA). Brain homogenated derived- PrP^{Sc} was treated with 25 µg/ml of PK for 1 hour at 37ºC. The final GPI-anchorless PrP^{Sc} was deglycosylated with PNGaseF (New England Biolabs) following the manufacturer´s instructions. Tga20 mice were kindly provided by Joaquin Castilla (CIC-BioGune, Derio, Vizcaya, Basque Country)

Limited proteolysis

RecPrP^{Sc} was treated with 10 µg/ml PK at 37ºC for 30 minutes. The digestion was quenched by adding 2 mM Pefabloc (Sigma-Aldrich) and incubating for 15 minutes on ice. PK-resistant fragments were then pelleted by centrifugation at 18.000 g at 4ºC for 1 hour (Microfuge$^{(R)}$ 22R Centrifuge Beckman Coulter). Under these conditions, all PK-resistant fragments were pelleted (Figure E5.1). Sample were resuspended in 6M Gn/HCl and stored at -20ºC until use.

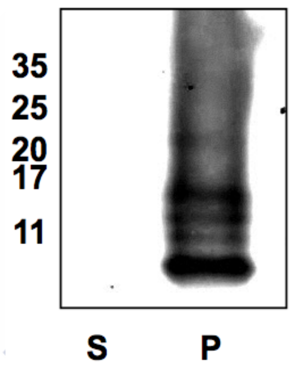

Figura E5.1 Western blot of the PK-resistant fragments that were sedimented after the digestion of recPrP^{Sc} with PK. All the fragments that persist to PK digestion were sedimented by centrifugation at 18.000 g for 1 hour at -4ºC. Pellets were resuspended in 20 µl of 6 M Gn/HCl. Previous to WB analysis ,sample was precipitated with 85% MeOH as indicated in chapter 3. Supernatant and pellets were subjected to western blot to analyze the location of ht PK-resistant fragment. Both samples was probed with the R1 antibody

Electrophoresis, Western blotting and epitope mapping

PK-resistant fragments were precipitated with ice-cold 85% MeOH. Pellets were resuspended in MiliQ H_2O and Trincine buffer in a ratio 1:2 (BioRad, Hercules, CA, USA). Reduction was carried out by adding β-mercatoethanol to 2% (v/v). Samples were boiled for 10 minutes. High resolution electrophoresis was carried as described by Vázquez-Fernández *et al.* After electrophoresis, gels were washed with miliQ H_2O and incubated with fixing solution (10% MeOH, 7% acetic acid) for 1 hour at room temperature. Sypro Ruby (Invitrogen) staining was then performed by incubation overnight at room temperature in the darkness as indicated in the EM&M of the chapter 3. Alternatively, the gels were transferred to Immobilion-P 0,45 μm PVDF membranes (Millipore), which were subsequently probed with the following antibodies: R1(1:5000), 3F10 (1:5000) and #51(undiluted); R1 was a generous gift from Anna Serban, Institute for Neurodegenerative Diseases, UCSF; #51 was kindly provided by Lothar Stitz, Fridrich Loeffler Institut, Insel Reims, Germany. Secondary antibodies were: Goat- antihuman and Goat anti-mouse to detect R1 and 3F10 and #51, respectively, both at a 1:5000 dilution.

Mass spectrometry

1 μL of the Gnd/HCl stock solution was mixed with 49 μL of sinapinic acid solution (SA) (10 μg/mL of SA dissolved in 30% ACN with 0.3% TFA) and analyzed by MALDI-TOF. One half μL aliquots were deposited using the dried-droplet method onto a 384 Opti-TOF MALDI plate (Applied Biosystems, Foster City, CA, USA). MALDI analysis was performed in a 4800

MALDI-TOF/TOF analyzer (Applied Biosystems, Foster City, CA, USA). MS spectra were acquired in linear mode (20 kV source) with a Nd:YAG, (355 nm) laser, and averaging 500 laser shots. Calibration was carried out using insulin (m/z = 5733), ribonuclease A (m/z = 13682) and lysozyme (m/z = 14305), (Sigma-Aldrich, St. Louis, MO) as internal standards. Masses were matched to PrP fragments with the help of GPMAW 6.0 software (Lighthouse, Odense, Denmark).

In parallel, 10 μl of the sample in-Gn/HCl stock solution was subjected to ESI-TOF analysis. The sample was injected to an Agilent 1100 HPLC system equipped with a Vydac C-18 column (Vydac®, W.R. Grace & Company, MD, USA). The following gradient was applied: Solution A (H_2O-FA) to solution B (ACN-FA) at a flow of 0,2 ml/min during 60 (for both solutions the concentration of the Formic Acid was at 0,1%) The effluent of the column was fed into a Bruker Microtof mass spectrometer (Bruker Co, Billerica, MS, USA). For the sample ionization, N_2 gas was applied at 2,5 bars at 200ºC.

This allowed identification, in spectra of recMoPrPSc samples, of peaks with m/z values of 9513, 9399, and 8184 as corresponding to fragments 152-, 153, 169-230, which were unambiguously identified with a mass error < 1 Da by ESI-TOF analysis of the same sample (vide infra). Subsequently, these three peptides were used to build an internal calibration curve: y= 1,001x - 0,162 (r=1), where x is the experimental value of the MALDI masses.

Kinetics of PK digestion.

Sample stored at -20ºC in PMCA conversion buffer, was digested with 10 μg/ml at 37ºC for 30; 60; 90; 120 and 150 minutes. After incubation, samples were precipitated with 85% ice MeOH as indicated in chapter 3.

Precipitated samples were diluted in tricine buffer in a ratio 1:2 and electrophoresis and immunoblotting with R1 antibody was followed as indicated above.

References

1. B. Chesebro, M. Trifilo, R. Race, K. Meade-White, C. Teng, R. LaCasse, L. Raymond, C. Favara, G. Baron, S. Priola, B. Caughey, E. Masliah, M. Oldstone, Anchorless prion protein results in infectious amyloid disease without clinical scrapie. *Science***308**, 1435-1439 (2005); published online EpubJun 3 (10.1126/science.1110837).

2. E. Vázquez-Fernández, J. Alonso, M. A. Pastrana, A. Ramos, L. Stitz, E. Vidal, I. Dynin, B. Petsch, C. J. Silva, J. R. Requena, Structural organization of mammalian prions as probed by limited proteolysis. *PloS one***7**, e50111 (2012)10.1371/journal.pone.0050111).

Chapter 6

General discussion

Finally, in this chapter, I have taken all the data from the different chapters to show the main conclusions and make a final common discussion. With this information, I believe that the results presented here support the notion that the structure of the PrP^{Sc} consist a multi-rungs ß-solenoid conformation. Another exciting challenge that I dealt, was to generate a synthetic prion. Unfortunately, only one of the set of the misfolded recPrPs, that were generated by recPMCA, resulted infectious in transgenic mice. Indeed, this $recPrP^{Sc}$ resulted very useful for structural studies. The data obtained from the limited proteolysis and MS analysis of the $recPrP^{Sc}$ showed structural features common with the GPI-anchorless PrP^{Sc}. Taken altogether, furthermore I believe that the results showed in this thesis demonstrate that the use of the synthetic prion is a good model to study the structure of the PrP^{Sc}.

Despite the difficulty to obtain substancial information on the structure of the PrP^{Sc}, in this thesis a large amount of experimental data were obtained, allowing to develop three final conclusions.

1. **PK-induced disassembly of partially unfolded PrP^{Sc} fibers supports a multi-rung architecture of PrP^{Sc} subunits.**
2. **The generation of recombinant prions by recPMCA recapitulates features of wild prions.**
3. **recPrPSc shares structural features than the brain-derived GPI-anchorless PrP^{Sc}.**

1) **PK-induced disassembly of partially unfolded PrP^{Sc} fibers supports a multi-rung architecture of PrP^{Sc} subunits**.

The PK digestion of the GPI-anchorless PrP^{Sc} after "partial unfolding" treatment, allowed to identify the inner "super-resistant" core (152-230) of GPI-anchorless PrP^{Sc}.

If the PrP^{Sc} adopts a conformation in which the ß-strands coil into a multi-rung structure, the digestion with PK after partial unfolding, would necessary result in a disassembling of the GPI-anchorless PrP^{Sc} fibers, due to the fact that destruction of the "base" N-terminal half of PrP^{Sc}. However, if PrP^{Sc} adopts a conformation in which the ß-strand coils itself into a single rung, and each molecule is stacking parallel in register along the fiber axes, the digestion of the PrP^{Sc} with PK will not affect to the fibrilar architecture. The images of the treated samples, after negative staining TEM, revealed that the Fibrilar architecture of the brain-derived GPI-anchorless PrP^{Sc} was disassembled. While the recPrP amyloid fibers were remained after the treatment with PK. This result indicates that the PrP^{Sc} conformation must not be represented by the PIRIBIS model, as a corollary, the conformation of PrP^{Sc} might adopt a multi-rung structure.

2) **The synthesis of recombinant prions by recPMCA recapitulate features of wild prions.**

The genesis of the recombinant PrP^{Sc} is one of the major challenges done in this work. For this purpose the recombinant PrP protein was firstly expressed and purified and then subjected to recPMCA conversion. From the set of the proteins that it were expressed and purified, only one of these proteins resulted infectious in the transgenic mice that overexpressing the PrP^{C}. It is uncertain why under the same purification procedure and conversion by recPMCA, only one of the proteins was converted to the misfolded infectious form $recPrP^{Sc}$. This fallibility may be attributed of the purification/refolding process or the recPMCA reaction. According to the purification/refolding process, it is worth to mention that somehow $recPrP_{23\text{-}230}$ did not elute in the same fraction among the different purifications. To explain this variability, some authors suggest that during the purification and refolding process, protein can adopt conformational structures different than the conformation of the wild-type protein. If this hypothesis takes place during the purification and refolding process of the protein, a pool of $recPrP_{23\text{-}230}$ may be formed within the column, with conformational differences that affects somehow to the binding of the Histidines with the Ni. The eluted proteins were subjected to recPMCA. Under the conditions of the recPMCA, all of these protein were converted to its misfolded form by seeding of the prion $recPrP^{Sc}$-Ma. After PMCA, it was observed that all of these misfolded proteins were resistant to PK, however the failure to be infectious could be explained by the fact that if the conformational refolding of the $recPrP_{23\text{-}230}$ was not the correct to be converted into the misfolded infectious form.

On the other hand, the possibility that the synthesis by recPMCA of misfolded form of recPrP that fail to infect wild-type mice have been reported in some studies. The authors suggest that the misfolded form of the recPrP, can adopt a non-infectious conformation by the stochastic process of the sonication cycles of the recPMCA. Whatever reason, either the synthesis of the correct refolded recPrP$_{23\text{-}230}$ or the stochastic process of the sonication cycles, it is important that both process should be fixed for reproducible future studies. Nevertheless the most important milestone was the generation of a synthetic PrP that reproduce the prion nature.

3) recPrP^{Sc} shares structural features than the brain-derived GPI-anchorless PrP^{Sc}.

The recPrP^{Sc} was subjected to structural analysis by proteolysis limited coupled to the MS analysis. The information emerging from this study indicates that the position 152/153 may represent a hinge between two halves of the recPrP^{Sc}. The identification of several PK nicks in the recPrP^{Sc} that are the same observed in the GPI-anchorless PrP^{Sc} indicate that the recPrP^{Sc} and the GPI-anchorless PrP^{Sc}, share a common structure. The finding of additional PK cleavage sites at the position 201 and 206 may represent the existence of a new loop or turns. The observation of doubly truncated peptides that only is observed in the atypical strains of PrP^{Sc} indicate that the recPrP^{Sc} share structural features with the atypical strains of prions. Therefore, such recPrP^{Sc} constitute an excellent tool for future additional structural studies, including those based on the use of NMR.

In summary, the data shown in this thesis support the notion that the PrP^{Sc} could not be represented by the PIRIBS model, as consequence, the ß-solenoid might be the most feasible model for the PrP^{Sc}. Keeping in mind this notion, we synthesized the recombinant PrP and was converted into the misfolded form by recPMCA reaction for structural studies. After recPMCA conversion, $recPrP^{Sc}$ was subjected to structural studies by limited proteolysis and MS, the results showed structural features similar than the brain-derived GPI-anchorless PrP^{Sc}, with a few naunces, as corollary the $recPrP^{Sc}$ might adopt a ß-solenoid conformation.

The results obtained in this study demonstrate that the recombinant prions generated by recPMCA, can be a good model for structural studies, furthermore for future studies, the use of recombinant PrP isotopically labeled and converted into the misfolded isoform $recPrP^{Sc}$ by recPMCA could be analyzed structurally by NMR. The high resolution data from NMR would be used for the construction of a good structure model of $recPrP^{Sc}$ and such have been showed in this study could be used for PrP^{Sc} model.

- Cryo-TEM: cryo-Transmission Electron Microscopy or electron cryomicroscopy.
- Cryo-ET: cryo-Electron Tomography.
- CWD: Chronic Wasting Disease.

D

- DNAsa: deoxyribonuclease
- Dy: Drowsy strain.

E

- EDTA: ethylenediaminetetraacetic acid.
- EM: Electron Microscopy.
- ESI-TOF: electron-spray ionization-time of flight.
- ET: Electron Tomography.
- E. coli: *Escherichia coli*.

F

- F: forward
- FFI: fatal familial insomnia.
- FFT: fast Fourier transform
- FTIR: Fourier transform infrared spectroscopy.
- FSE: feline spongiform encephalopathy

G

- Gn/HCl: guanidine hydricloride.
- GPI: Glycosylphophatidylinositol.
- GSS: Gerstmann-Sträussler Scheinker syndrome.
- g: centrifuge force.

H

- HE: haemotaxylin and eosin.
- HGH: human growth hormone.
- H/D: hydrogen-deuterium exchange.
- HPLC: high-performance liquid chromatography.
- Hy: Hyper prion strain.
- h: hours

I

- IHC: immunohistochemical.
- IR: infrared spectroscopy.

K

- KDa: kilodatlon.
- KO: knock out.

M

- MALDI-TOF: matrix-assisted laser desorption/ionization-time of flight.
- MBM: meat and bone meal
- MeOH: methanol.
- MS: mass spectrometry.
- MW: molecular weight.
- min: minutes.

N

- NA: nucleic acids.
- nano-LC-ESI Qq-TOF: electrospray ionization-double quadrupole-time of flight.
- NMR: nuclear magnetic resonance.
- NTCB: 2-nitro-5-thiocyanatobenzoic acid.
- dNTP: deoxynucleotide triphosphate.

P

- PBS: phosphate buffered saline.
- PCR: polymerase chain reaction.
- PK: proteinase K.
- PMCA: protein misfolding cyclic amplification.
- recPMCA: recombinant PMCA.
- PNGaseF: peptide-N-glycosidease F.
- PrP: prion protein.
- Prnp: prion protein gene.
- bPrP: bovine prion protein.
- BVolePrP: bank vole prion protein.
- huPrP: human prion protein.
- MoPrP: mouse prion protein.
- Nor98 PrP^{Sc}: prion strain
- PrP^{C}: cellular prion protein.
- PrP^{Sc}: scrapie prion protein or prion.
- PrP^{Sc} 106: mini prion.

- recPrP or rPrP: recombinant prion protein.
- $recPrP^{Sc}$: recombinant prion.
- Ma-$recPrP^{Sc}$: Ma strain recombinant prion.
- $recPrP^{Sc}$-Ma: new of $recPrP^{Sc}$ obtained by the seeding of Ma-$recPrP^{Sc}$
- $sPrP^{Sc}$: PK-sensitive prion.
- PrP27-30 or PK-res PrP: PK-resistant prion.
- $PrP_{23\text{-}230}$: recombinant prion protein 23-230.
- PMSF: phenylmethylsulfonyl fluoride.
- POPG: 1-palmitoil-2-oleil-sn-glycero-3-phospho-(1′-sn-glycerol).

O

- OR: octarepeats.
- ORF: open reading frame.

R

- R: reverse.
- R1: antibody R1.
- RML: Rocky Mountain Laboratory prion strain.
- mRNA: messenger RNA.
- rpm: revolutions per minutes.

S

- s: seconds.
- SA: sinapinic acid.
- SAFs: scrapie associated fibers.
- SAF83: antibody SAF83.

- SDS-PAGE: sodium dodecyl sulfate-polyacrylamide gel electrophoresis.
- SHaPrP: Syriam hamster prion protein.
- SP: signal peptide.

T

- TEM: transmission electron microscopy.
- TFA: tri-fluoroacetic acid.
- tg: transgenic mice.
- tg44$^{+/-}$: transgenic heterozygous GPI-anchorless PrP mice.
- tg44 $^{-/-}$: transgenic homozygous GPI-anchorless PrP mice.
- TNM: tetranitromethane.
- TSE: transmissible spongiform encephalopathy.
- TME: transmissible mink encephalopathy

V

- V: Volts.

W

- WB: Western blot.
- µg: micro-grams (10^{-6} g).
- µl: micro-liters (10^{-6} L).
- µm: micro-meter (10^{-6} m).
- Wt: wild-type mice.
- w/v: weight/volume.

List of publications

Dec-2015. **The architecture of recombinant prions is similar to that of brain-derived prions: insights from limited proteolysis.** Sevillano AM, Fernández- Borges N, Younas N, Vázquez-Fernández E, Nonno R, Castilla J, Requena JR. 4th Iberian Prion Congress 2015. Instituto Nacional de Investigação Agrária e Veterinária Lisbon. Portugal. (***Oral communication***)

May-2015. **PK-induced disassembly of partially unfolded PrP[Sc] fibers supports a multi-rung architecture of PrP[Sc] subunits.** Sevillano AM, Vos M, Baskakov IV, Requena JR. International Prion Conference 2015. University of Colorado State University, Fort Collins, Colorado. USA. (***Poster presentation***).

The architecture of recombinant prions is similar to that of brain-derived prions: insights from limited proteolysis. Sevillano AM, Fernández- Borges N, Younas N, Vázquez-Fernández E, Nonno R, Castilla J, Requena JR. International Prion Conference 2015. University of Colorado State University, Fort Collins, Colorado. USA. ***(Author***).

Infectious recombinant prions: *In vitro* generation and propagation of different strains. Fernandez-Borges N, Di Bari MA, Eraña1 H, Vidal E, Venegas V, Sevillano AM, Elezgarai1 SR, Pirisinu L, Vazquez-Fernandez E, Harrathi C, Parra B, D'Agostino C, Espinosa JC, Surewicz W, Torres JM, Mayoral T, Agrimi U, Requena JR, Nonno R, Castilla J. International Prion Conference 2015. University of Colorado State University, Fort Collins, Colorado. USA. (***Co-worker***)

Dec-2014. **Disassembling prion fibers using proteinase K digestion after partial unfolding: evidence against the PIRIBS model**. Sevillano AM, Baskakov IV, Requena JR, 3rd Iberian Prion Congress 2014, University of Zaragoza, Zaragoza, SPAIN. (***Oral communication***).

An update on progress towards elucidating the structure of mammalian prions. Requena JR, Vázquez-Fernández E, Vos M, Cebey L, Sevillano AM, Renault L, Young H, Wille H. 3rd Iberian Prion Congress 2014, University of Zaragoza, Zaragoza, SPAIN (***Co-worker)***.

May-2014. **Recent advances towards an understanding of the structure of PrP^{Sc}.** Ester Vázquez-Fernández, Matthijn Vos, Lino Cebey, Ludovic Renault, Alejandro M Sevillano, Peter J Peters, José Jesús Fernández, Howard Young, Holger Wille and Jesús R. Requena. International Prion conference 2014. International School of Advanced Studies. SISSA, Trieste, ITALY. (***Co-worker***).

Apr-2014. **Disassembling prion fibers using proteinase K digestion after partial unfolding.** Sevillano AM, Requena JR. Molecular Basis of Human Disease. Mérimée Joint Meeting, LÉcole Doctorale Biologie-Sante Nantes- Angers, Escola de Doutoramento Internacional da Universidade de Santiago de Compostela. (***Poster communication***).

Dec-2013 **Bexarotene as a possible drug for the treatment of prion disease**. Sevillano AM, Caamaño- Rodriguez I, Fernández-Borges N, Sanchez-Martín M, Castilla J, Requena JR. 2nd Iberian Prion Congress 2013, Center for molecular biotechnology and bioengineering, University of Algarve-Faro, PORTUGAL. (***Oral communication***)

Jun-2012. Bexarotene as a possible drug for the treatment of prion disease. Sevillano AM, Onisko B, Fernández-Borges N, Sanchez-Martín M, Castilla J, Requena JR. XII National Virology Congress. Astrobiology Center, University of Burgos, Burgos, SPAIN. (*Poster communication*) Award (200€)

UNIVERSIDADE
DE SANTIAGO
DE COMPOSTELA